INFORMATION TO USERS

This manuscript has been reproduced from the microfilm master. UMI films the text directly from the original or copy submitted. Thus, some thesis and dissertation copies are in typewriter face, while others may be from any type of computer printer.

The quality of this reproduction is dependent upon the quality of the copy submitted. Broken or indistinct print, colored or poor quality illustrations and photographs, print bleedthrough, substandard margins, and improper alignment can adversely affect reproduction.

In the unlikely event that the author did not send UMI a complete manuscript and there are missing pages, these will be noted. Also, if unauthorized copyright material had to be removed, a note will indicate the deletion.

Oversize materials (e.g., maps, drawings, charts) are reproduced by sectioning the original, beginning at the upper left-hand corner and continuing from left to right in equal sections with small overlaps.

Photographs included in the original manuscript have been reproduced xerographically in this copy. Higher quality 6" x 9" black and white photographic prints are available for any photographs or illustrations appearing in this copy for an additional charge. Contact UMI directly to order.

Bell & Howell Information and Learning
300 North Zeeb Road, Ann Arbor, MI 48106-1346 USA
800-521-0600

MODELLING AND COMPENSATION

OF ERRORS

IN FIVE-AXIS MACHINING

by

STEPHEN C. VELDHUIS, B. Eng. and Mgmt., M. Eng.

A Thesis

Submitted to the School of Graduate Studies

in Partial Fulfilment of the Requirements

for the Degree

Doctorate of Philosophy

McMaster University

MODELLING AND COMPENSATION OF ERRORS IN FIVE-AXIS MACHINING

DOCTORATE OF PHILOSOPHY (1998) McMASTER UNIVERSITY

(Mechanical Engineering) Hamilton, Ontario

TITLE: Modelling and Compensation of Errors in Five-Axis Machining

AUTHOR: Stephen C. Veldhuis, B. Eng. And Mgmt (McMaster University),
M. Eng. (Carnegie Mellon University)

SUPERVISOR: Professor M. A. Elbestawi

OF PAGES: xv, 214

ABSTRACT

This thesis outlines a modelling approach and compensation strategy for understanding and improving the accuracy of five-axis machining. The kinematic model of the machine was based on Homogeneous Transformation Matrices (HTM), which used small angle approximations to form shape and joint transformations. HTMs were chosen in this form because they allowed the kinematic model to include the geometric, kinematic, and thermal errors of the machine. These sources of error result in a significant loss of accuracy in the production of dies, molds, aircraft parts, and many other critical industrial components. The individual error terms in the HTM's formulation are difficult to measure on an assembled machine. Therefore, a test procedure was designed to isolate the error terms and an allocation strategy, using the kinematic model, was developed to associate the error measured in the work space to the error in each of the main components of the machine. The kinematic model of the machine was also used in calculating the compensation values to capture the interaction of the error components and all of the axis motions.

The compensation strategy was implemented by adjusting each axis in the motion code with offset values based on the expected error. The motion code was modified just before being sent to the machine tool for processing. Due to the difficulties in measuring the error continuously on-line, empirical models were used to estimate the errors. The empirical models related temperature distribution and various machine conditions to the error in the machine tool's components. The empirical models took advantage of *a priori* information

in the form of known physical relationships which described the deformation of the structures under thermal loading.

A multiple linear regression model was chosen as the empirical model for implementation in the compensation strategy. It was chosen because of its simplicity, robustness, and ease of implementation. Through the recasting of the linear model's parameters, nonlinearities could also be included in the model. The regression model was found to be able to interpolate within the experimental data set. Through the inclusion of physical relationships in the development of the model, it was found to provide reasonable estimates when extrapolating. A neural network model was also considered, but was not implemented in the final compensation strategy because of the model's limitations when extrapolating beyond the training set conditions.

A means of updating the error model on-line was included in the compensation strategy using measurements made from reference surfaces in the work space. This was done to account for any unmodelled variation not captured during off-line testing. Also, this includes any slowly varying changes which can occur to the machine over time due to wear and structural material instability.

Realistic cutting tests using light finishing cuts, high spindle speed and axis feed were conducted. These machining conditions are typical of the mold and die industry. The cutting tests showed that a reduction of dimensional error from 0.082 mm to 0.012 mm was possible using the proposed compensation strategy.

ACKNOWLEDGMENTS

The author would like to acknowledge his supervisory committee members for their help and suggestions throughout this work: Professors R. Judd, M. Sklad, P. Taylor, and in particular his thesis supervisor, Professor M. A. Elbestawi. Professor Elbestawi's constructive guidance, continuous encouragement, and support throughout the course of this study are greatly appreciated.

The author wishes to thank the Department of Mechanical Engineering, Intelligent Machines and Manufacturing Research Centre (IMMRC), Natural Sciences and Engineering Research Council (NSERC), International Order of the Daughters of the Empire (IODE), and Material Manufacturing of Ontario (MMO) for their financial backing which made this project possible. Also, many thanks go to the staff of the Mechanical Engineering Department, particularly R. Lodewyks, J. Mah, J. McLaren, B. Bedell-Ryc, D. Schick, J. Verhaeghe and A. Wenzowski for all of their advice and assistance.

It has been a pleasure working with the team which makes up the Intelligent Machines and Manufacturing Research Centre at McMaster. The support and encouragement was truly appreciated. The author also thanks his wife, Christine, and son, Nathan, for their patience and encouragement while this thesis was being completed.

To my dear wife, Christine

TABLE OF CONTENTS

LIST OF FIGURES

LIST OF TABLES

CHAPTER 1

INTRODUCTION

This research was motivated by the high accuracy requirements of the mold, die, and aerospace industries in Canada. These industries have invested considerable resources in five-axis machine tools and require technology to extend their machining capabilities without requiring extensive investments in new equipment. For this reason, the research approach taken in this thesis addresses a compensation strategy which can be implemented in a cost effective manner on existing machines, and does not necessarily address the design issues relevant at the construction stage. A compensation strategy which effectively improves the accuracy of a machine would significantly reduce the amount of rework and scrap parts produced. It would also eliminate the time consuming procedures used to stabilize the reference frame of a machine.

This research focused on five-axis machining because of the attention these machines are receiving in industry and the challenges associated with their operation. Their increase in popularity has been largely due to the improved control they offer over the tool's position and orientation with respect to the work piece. Some of the many benefits five-axis machining offers the user are:

- reduced fixturing
- ability to maximize use of cutter geometries
- higher metal removal rates
- improved surface finish
- ability to compensate for orientation errors

Reduced fixturing is possible given the ability to machine extensively on five of the six faces of a work piece by rotating the part. This saves time and reduces the errors associated with re-fixturing. By maximizing the use of cutter geometries, such as machining with a tapered end mill or by optimally using the circumference of a toroidal end mill, one can achieve higher metal removal rates and improve the surface finish. The additional rotational axes also provide the machine with the ability to compensate for orientation errors in the machine due to poor construction or thermal errors.

The five-axis machine tool used in this research is shown in Figure 1.1. It has three translational axes (X,Y and Z) and two rotational axes (A and B) mounted on the table. The presence of the rotational axes contributed additional sources of error and complicated the motion of the machine tool. This complication arose from the dependence of the tool position, with respect to the work piece, on both the rotary table's angles and the tool's

distance from the axes' centres of rotation. Thus, to maintain the same cutter contact point on a work piece while undergoing a rotation, the translation axes must move in a coordinated fashion to account for the effect of the contact point rotating through an arc. Another source of complication is that the second rotary axis B is dependant on the first angle of rotation A for its final orientation. This could align B with a singularity point. This occurs whenever the A axis is at 90° as this forces the B axis to align itself with the spindle's rotation allowing for an infinite number of configurations to exist.

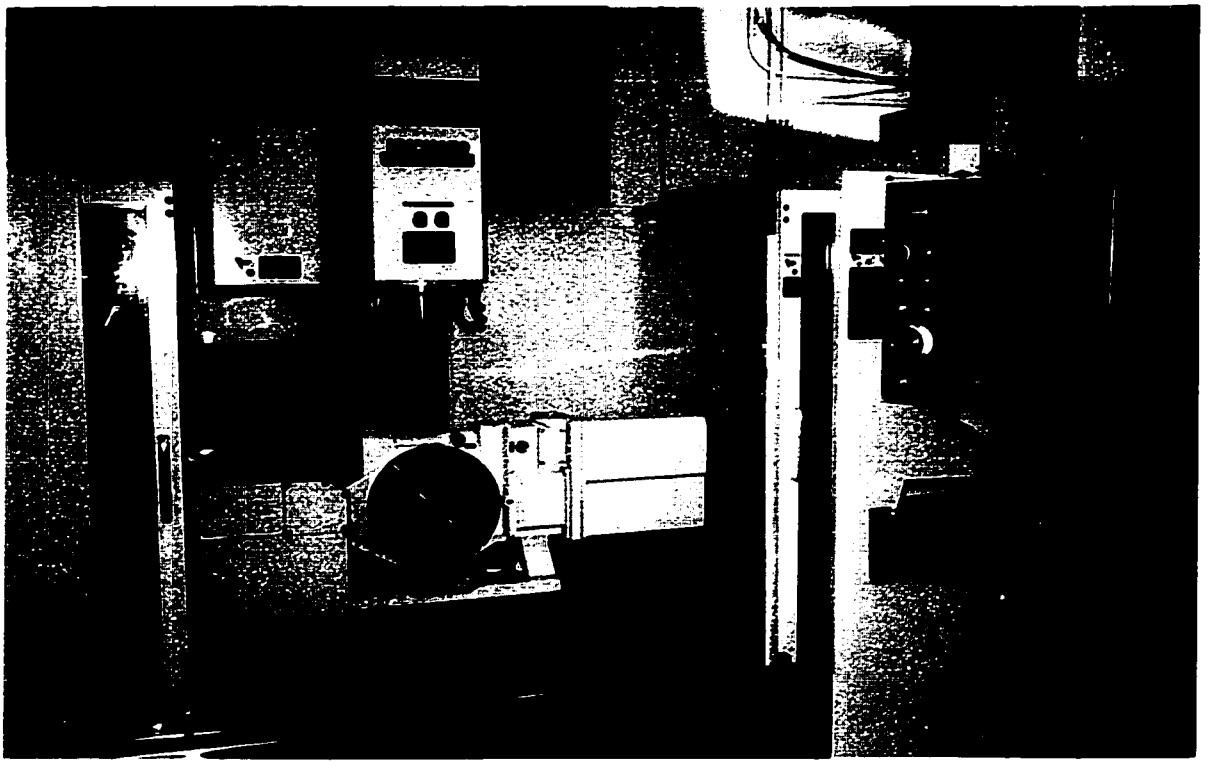

Figure 1.1 Five-Axis Machine Tool

Machine tool error has been defined as "the difference between the actual and anticipated response of the machine to a command issued according to the machine's accepted protocol" (Hocken, 1980). This difference in response is directly transferred onto the part during production as a machining error. The machining errors considered in this thesis can be broken down into three main areas. They are geometric, kinematic, and quasi-static thermal errors. Geometric errors are related to the structure of the machine. Kinematic errors arise from the motion controlling elements. Thermal errors are caused by temperature changes in the machine. Thermal errors are typically referred to as quasi-static because of their long time constants. Dynamic errors, such as those associated with high speed contouring and tool vibration are beyond the scope of this thesis due to their high frequency of response and the relatively low frequency compensation strategy that is being proposed.

Significant progress has been made in the areas of geometric and kinematic errors at the design stage. Improvements in geometric errors were accomplished through better quality control of part dimensions and material properties, improved assembly techniques and the implementation of recommendations from structural modelling. Also, improvements in the manufacturing of ballscrews and slides, together with precise motion control strategies and faster reacting motors and computers, have led to reductions in kinematic errors. Thermal errors in machine tools, however, remain significant and are generally difficult to avoid.

In a machine tool's design, the structural material's natural coefficient of thermal expansion, unavoidable internal heat sources, and uncontrolled environmental factors all contribute to thermal errors. Although materials with lower coefficients of thermal

expansion are available, cost, material damping, and other performance requirements typically lead machine tool designers to use grey cast iron. Sources of heat that are all difficult to avoid include: those generated by the cutting process; those mounted directly on the machine such as motors, bearings, gears, amplifiers, and electronics; and those that are integral to the machine tool's structure like sliding friction at joints. Additional external factors such as room temperature fluctuation, exposure to sunlight, and the use of coolant also effect the thermal state of the machine. The use of controlled cooling systems has reduced the problems associated with thermal loading, but often these systems are expensive and not easy to retrofit on an existing machine tool.

Recently, there has been an industry wide trend to move to higher speed machining operations to take advantage of the improved metal removal rates possible with new tooling materials and coatings. This machining practice creates further demands on the thermal stability of the machine tool because of the increased levels of heat generated by the higher spindle speeds and axis feeds typically used. These rapidly changing heat sources generate large thermal gradients in the structure of the machine in short periods of time which can lead to considerable errors in the work space. Thermal gradients are a significant problem due to the small amount of time required to induce them in a structure, and also due to their large impact on error through the coupling of angles with translations.

Due to the harsh environment in the work space caused by metal chips and coolant, no continuously on-line sensors are presently available which can provide an accurate measure of the error in the cutting zone. Typically, the motion in the work space is controlled using feedback from the ballscrews, gears, and motors. These measures of motion

include the errors such as backlash in the ballscrew nut and changes in dimensions of the ballscrew shaft due to thermal errors, and also any errors in their support structures. More expensive machines use additional motion sensors on the slides and rotary tables to eliminate the error associated with the ballscrew, gear train, or coupler devices. These motion sensors, however, are placed a distance from the work space for their own protection and also to avoid interference with the usable volume of the work space. This can result in an error accumulating between the measurement element and the work space as described by the Abbe Error Principle.

Typically, the operator measures the setup in the work space at a limited number of points before starting and adjusts the program offsets to account for any changes in the setup or machine that might have occurred since the last operation. Unfortunately, this does not account for the variation in the machine that takes place while cutting. Frequent updating would be required as significant machine variations can occur within 15 minutes of changes in the machine's condition. This is often impractical since sections of a program can take many hours to run. Given the expectation of most machine tool users to operate without significant supervision, little time is available to manually track the sources of error in a machine throughout a production cycle. Also, due to the complexity of modern Computer Numerical Control (CNC) code required to take full advantage of a five-axis machine, it is difficult for the operator to make meaningful changes to the code. Therefore, a strategy must be in place to automatically compensate for changes in the machine due to thermal errors.

The basic premise of the compensation strategy is to increase the machine's accuracy by using the repeatability of the errors measured and modelled off-line or periodically on-

line. This must be done in such a way so as to limit the interference to the machining process during production. The challenge is to empirically model the errors as functions of other more easily measured quantities on the machine. This was done by building an understanding of how the errors of the machine change with position, thermal profile, and machining condition. Special tests were performed which involved running the spindle at various RPMs and driving the axes at various feed rates for extended periods of time. The thermal profile of the machine was measured through the use of thermocouples mounted on the machine. Deciding on the optimal number and placement of the thermocouples was aided by a correlation analysis of their outputs. Through the use of a laser interferometer and reference surfaces, the work space errors were measured.

Two different off-line techniques were considered for the empirical model. The first was a neural network model and the second was a multiple linear regression model. The coefficients, often called weights and biases, of the neural network were trained using an iterative back propagation procedure, while the coefficients of the regression model were established using a stepwise regression technique. An on-line update feature was added to capture any unmodelled errors in the off-line model. This was done to account for the slow changes that the machine might experience over time, such as wear on motion controlling surfaces, and material instability.

To aid in the creation of an empirical model of machine tool errors, it was beneficial to use as much *a priori* information as possible on the nature of the errors and of the machine's structure. To this end, a kinematic model of a five-axis machine tool was used to build an understanding of the interaction of the structures and motions of the machine.

The model was based on Homogeneous Transformation Matrices which directly consider the shape and joint transformations for inaccurate links and joints using small angle approximations in place of using Denavit and Hartenberg transformations. This was done to provide a better relationship between the errors in the machine and the model. When completed, this model could relate the total volumetric error in the work space as a function of all possible errors in the links and joints. The kinematic model was simulated using realistic machine conditions to verify the compensation strategy and learn more about the interaction of the error terms. Through extensive testing and the use of the kinematic model, the error measured in the work space was allocated nearest to the component or region where it was generated on the machine. This aided the indirect modelling procedure as it was easier to model an error when it could be directly associated with a specific component or region on the machine. This also made it easier to include known physical relationships in the modelling process, thereby saving the model from having to learn the known relationships.

The underlying relationships between the error and the machine's condition are established by measuring all six motion errors for each degree of freedom while collecting temperature, position, feed rate, and spindle speed data. A total of thirty error data sets must be measured over extended periods of time under various conditions to characterize the error in all five axes on the machine. The error was measured in the work space using either a laser interferometer or through reference surfaces. These error measurement methods are discussed further in Chapter 5. Each test involved activating one group of heat sources, measuring the error in the work space, and allocating those errors to the individual components nearest the active heat sources. Effort was made to try to separate out the error

contributions and ensure that error was related to the correct region as much as physically possible, given the constraints of the machine's operation.

The compensation value for each axis that drives the error in the work space to zero was calculated on a PC using up-to-date sensor information and applied to the next batch of motion commands sent to the machine. The timing of the data transfer was important since the compensation values require relevant data while the machine must have a sufficient amount of data available to preprocess its path. This was necessary to allow it to blend its motion.

The following is a brief summary of the chapters. Chapter 2 provides a detailed literature survey on the areas of machine tool error modelling and compensation. The machine tool errors considered in this work are described in detail in Chapter 3. Chapter 4 covers the development and application of the kinematic model to the five-axis machine. The kinematic model was developed to include the error terms discussed in Chapter 3. A procedure for allocating the error measured in the work space to the individual components is also shown, as well as a method for calculating the compensation values. This chapter also provides a discussion on the simulation results of the compensation strategy, which used the kinematic model in place of the machine tool. The methods used to collect the error data is outlined in Chapter 5 along with the methods and setups used to calibrate the equipment. The technique used to select the thermocouple locations is also discussed. Some sample data is included in this chapter with the remainder placed in Appendix D. Chapter 6 deals with the empirical modelling of the error that is associated with every link and joint on the machine measured in Chapter 5. The proposed compensation control strategy and the issues

associated with its implementation are discussed in Chapter 7. This chapter also discusses the results of the cutting tests performed using the compensation strategy. Chapter 8 contains concluding remarks and some recommendations for the continuation of this area of research.

CHAPTER 2

LITERATURE SURVEY

2.1 Introduction

This chapter reviews the current literature related to error modelling and compensation in machine tools. Information on machine tool accuracy and factors affecting accuracy are discussed with special attention paid to thermal issues. The methods used to model the kinematics of machines, including the error terms are outlined. Procedures for measuring the volumetric error in the work space of a machine, as well as capturing the thermal profile of the machine are presented. Consideration is also given to the empirical methods and numerical algorithms researchers have used to describe the error in machine tools. Finally, the various compensation approaches used by others is reviewed.

2.2 Machine Tool Errors

The general literature on machine tool accuracy, repeatability, and resolution outlines the relationship between the errors in the final work piece and the errors in the structural components of a machine, its motion controlling elements, and their interaction (Hocken 1980). Slocum (1992) defines accuracy, related to machine tools, as the ability of a machine to position and orientate the tool in a desired manner in the work space. Repeatability is a measure of its ability to position and orientate over and over, while resolution is the smallest step in movement that can physically be performed by the machine. In general, compensation strategies strive to improve the performance of a machine by using the repeatability of the machine to enhance its accuracy. The practical limit of a compensation strategy is the resolution of the machine since that is the smallest motion that can be physically moved.

Errors affecting the accuracy of a machine are typically grouped together as geometric, kinematic, and thermal errors. Considerable progress has been made in improving geometric and kinematic errors. The main point of Bryan's 1990 CIRP keynote address, however, was that "in spite of some excellent research not much has changed in industry" with respect to thermal errors. He added that "thermal effects are still the largest single source of dimensional errors and apparent non-repeatability of equipment". He claimed that as much as 70% of dimensional errors in production parts can be directly attributed to thermal errors in machine tools. Other researchers support this including Weck et al. (1994), Slocum (1992), Hocken (1980), Tlusty and Mutch (1973), and Spur and Fischer

(1969).

Thermal errors in machined parts occur for two main reasons. The first occurs when the process is operating at a uniform temperature other than 20°C and there is a difference in the coefficient of thermal expansion between the part and the machine tool's components. The second occurs when there are thermal gradients present in the closed loop between the tool and the machine. From the first reason, it follows that if the machine and the part have the same coefficient of expansion and are at the same uniform temperature, then the closed loop of the machine and part will uniformly expand together and the part will be at the correct dimension when later measured at a uniform temperature of 20°C. Under realistic conditions, however, a machinist will need to machine a variety of materials possessing a range of coefficients of thermal expansion. Thermal gradients in a machine or work piece can cause bending which will lead to position and orientation errors between the tool and the work piece. The design of present day machines contains many potential sources of thermal gradients due to the practice of locating large heat sources directly on the structure. Also, the machines themselves are often assembled using components made with different materials, each with their own coefficients of expansion. This can account for significant errors within a machine (Bosch, 1995).

Thermal compensation for part dimension has proven to be difficult for large complex parts. The preference is to control the temperature of the part through soaking it or spraying it with coolant until the part has reached a uniform temperature of 20°C. More and more companies are making the considerable investment of air conditioning their machine shops in an effort to control temperature variations in their parts and machines. Controlling

the thermal errors in machines due to gradients and material properties is an issue that is addressed through both design and compensation strategies. It is generally agreed that every effort must be made at the design stage to remove as much potential for thermal error as possible, while only relying on error compensation as a follow-up strategy (Bosch, 1995).

An example of a machine in which thermal errors have been the focus of much design effort is the 84 inch diameter oil bathed diamond turning machine which was developed at the Lawrence Livermore Laboratory (Bryan, 1979). Unfortunately, this level of temperature control is not realistic for most manufacturing environments. However, other design strategies which make use of chilled bearings and ballscrew shafts are available. These strategies are expensive to install and even more expensive to retrofit on an existing machine. Other design approaches separate the motion driving element from the position measurement instrumentation. On linear axes, this can be accomplished with the addition of linear measurement scales directly on the axes. In this way, the components which are most susceptible to wear and thermal loading are separate from the precise position measurement functions. This feature is often available as an upgrade to a standard machine (Fadal, 1998).

Tanabe et al. (1986) discussed the impact of using an epoxy resin concrete material on thermal errors. The concretes are formed to make the main castings of the machine and are used because of their high damping coefficients and their ease of shaping. However, machines made from resin based concrete structures typically exhibit poor thermal stability. Their work showed that the lower thermal conductivity of the concrete materials may cause localized regions of high temperature in the structure. These large temperature gradients can generate significantly larger thermal errors, even though the material thermal coefficient of

expansion is similar to that of grey cast iron. Tanabe et al. proposed the selective use of epoxy concrete material as a structural component to separate heat sources from the main structure and as an insulator to isolate the machine from rapid room temperature variations. Insulating the machine from the room would increase its thermal time constant. If its time constant could be increased to the order of days, then the natural fluctuation in room temperature throughout the day would be averaged out, thus producing a more thermally stable machine. The other approach would be to use a material with a high thermal conductivity like aluminum to shorten the thermal time constant so that the machine would reach steady state faster. This has become popular on Coordinate Measuring Machines (CMMs) with the increasing use of aluminum in designs (Bosch, 1995).

In an effort to better understand the thermal effects on a machine, Venugopal (1985) analyzed a hypothetical machine by studying the problem of heat flow in a box made of thin plates. His results were then verified on a three-axis horizontal machine tool. This work provides useful insight into the complex nonlinear nature of the thermal error variation and provides evidence that thermal errors in a machine tool are predictable using only a limited amount of information on the temperature of the machine's components.

Attia and Kops (1979 and 1981) have also studied the thermoelastic behaviour of machine tools. They placed special emphasis on the importance of the thermoelastic reactions at the machine joints on the deformation behaviour of a machine tool. The reactions at the joints were identified as significant sources of nonlinearities in the thermal error relationships. They also identified surface asperities as another important nonlinear factor in the calculation of deformation of a structure. Recently, machine tool builders have

started using epoxy resin between fixed joints to fill voids at the interfaces, and thereby, eliminate some of the irregularities associated with the joints (Fadal, 1998).

Research done on thermal errors in a large gantry style machine revealed that dissimilar time constants of major structural components leads to significant thermal deformation. The thermal time constant of a structure is determined by its mass, dimensions, coefficient of thermal conduction, proximity to a heat source, and its interaction with the environment (Weck et al., 1994). This group selectively insulated different surfaces on a machine in an effort to equalize the thermal time constant and to balance the temperature rise between the two uprights of the gantry type machine. Although this did not eliminate the thermal drift completely, it did serve to significantly reduce it. This was done by reducing the difference in deformation between the two main uprights, thereby resulting in reduced angular errors in the spindle column. This example points out the importance of angular errors acting through long distances such as those associated with the long spindle column on a gantry machine.

2.3 Kinematic Modelling of Machine Tools

Direct error modelling techniques are used to relate the sources of error in the individual motion and structural components to the error in the work space, between the tool and the work piece. Love and Scarr (1973) applied analytical geometry using trigonometric functions to obtain the relationships for geometric errors in a machine tool. Hocken et al.

(1977) used vector representations to describe three dimensional metrology. Duffour and Groppetti (1981) used an error matrix method which stored the error vector components for different locations in the machine work space corresponding to different loading conditions and temperature distributions. Actual values were interpolated from this error matrix and applied to the machine. This matrix method requires that a considerable amount of data be collected and stored in the matrix form. The large amount of data is necessary due to the complexity of the thermal errors expected when operating under a wide range of conditions.

The error modelling approach which is now used by most researchers is the rigid body kinematics approach associated with Homogeneous Transformation Matrices (HTM). With this approach, one has the ability to model an arbitrary machine configuration using a simple formulation of matrix multiplications. Individual error terms are included in the modelling of each link and joint. These matrices are assembled together to form the representation of an entire machine (Eman et al., 1987). Donmez (1985) applied this technique to the study of the kinematic and geometric errors on a lathe. Kiridena and Ferreira (1994a and 1991) also used the method for representing the links and joints of a three-axis machine with matrices. Their model showed the effects of kinematic errors in machine axes on overall volumetric accuracy in the work space. Moriwaki et al. (1992) explored the same error relationship by using a similar mathematical model, but related the six components of the error directly to the final part accuracy for a typical end milling operation.

The majority of work reported in the literature is limited to three-axis machining; five-axis machining research is sparse. However, Lin (1989) studied a wide range of multi-

axis machines and made recommendations on how to analyze, measure, and compensate for certain errors. His work mainly focused on the geometric and kinematic errors in machines and not on the time varying thermal effects. When the investigation of thermal error is extended to five-axis machine tools, the complexity of the problem increases (Trankle, 1980). Extra sources of error due to the two rotational degrees of freedom and their interaction with the other axes complicates the problem.

Slocum (1992) provides an overview of the HTM model of a machine and how error terms can be added to the individual matrices which make up the machine tool. Dorndorf et al. (1994) have proposed that models of this form be used in the design of the machine for establishing the initial allocation of the manufacturing tolerances to the different structural components. This technique would prove helpful in controlling manufacturing costs when setting the specifications necessary for the fabrication of each part.

2.4 Measurement Methods

2.4.1 Machine Errors

Measurement methods designed to specifically study changes in errors over time can be broken down into two main categories. One is measuring the errors off-line before any real part production has begun. The other is to learn the errors while producing parts and to constantly update the error models with new estimates as they become available.

Early off-line methods for characterizing the machine errors over time monitored the

change in position of the centre of a hole drilled with increasingly larger diameters (Okushima et al., 1975). Knapp (1983 and 1980) probed a known circular profile mounted in different orientations in the work space to estimate the components of geometric and kinematic error of the machine. Kiridena and Ferreira (1991) built a special structure of metrolurgical balls and bars on the table and measured the locations of the balls with a custom designed proximity sensor probe. The objective of this work was to find a minimum number of points which could be used to characterize the kinematic error profile of a machine.

Hatamura et al. (1993 and 1992) used proximity sensors surrounding a bar of Super Invar mounted in the spindle to characterize the variation in position of the spindle as the machine warmed up. Super Invar is a material which is known to be far more dimensionally stable under temperature variations than cast iron. Riarh (1994) recommended the use of a ball bar mechanism for measuring the accuracy of a machine tool. This is a special off-line test which requires that a solid bar with balls mounted on both ends be put in the work space in place of the normal work piece, and that the machine's probing attachment be used to define the length of the bar under different orientations and positions in the work space. The ball bar is an excellent tool for finding positional errors in the machine as well as squareness errors. A telescoping ball bar or contisure system is similar to a regular ball bar except that its bar is a linear displacement sensor, the balls are kinematically coupled to the machine at the spindle and on the table by three matching balls, and it is held in place with a magnetic force. The measurement approach taken is to command the machine to move in a circular arc with a radius equal to the bar. Any deviations from the circle are measured as deflections

in the linear displacement sensor. This device is useful for finding scaling errors between axes, squareness errors, and backlash (Gull, 1990).

Venugopal and Barash (1986) used a He-Ne laser interferometer and a precision differential level to verify their analytical work on thermal errors in a three-axis machine. The laser was used to measure positional and some angular errors. A laser interferometer is a sensitive device, and when used properly, it gives the highest accuracy of any of the methods described. Hewlett Packard's application notes (1990a, 1990b, and 1988) provide details on the operation of the laser interferometer. Unfortunately, it is not possible to measure the roll error of a sliding axis using a laser interferometer as the laser beam is broken by the movement. This error was measured by Venugopal and Barash using a precision differential level.

Many of these direct methods of measuring error were not designed to function under normal machining conditions. The equipment used either takes the place of the work piece or tool, or at a minimum consumes some valuable area in the work space. Often these techniques are applied by companies as a way of acceptance testing the machines they purchase before taking delivery (Gull, 1990). Realistically, these techniques cannot provide real time error values during normal operations. At best, some of them can provide periodic values by interrupting the cutting process. However, frequent updating, such as that necessary to fully capture thermal variation, would be considered an excessive burden by industry.

Applications where on-line error measurement methods were applied include the work by Weck et al. (1994). They described a procedure used on a grinding machine to

measure the position of a point on the spindle housing. This required interrupting the grinding procedure to move the grinding head over to the proximity sensors and then update the machine's position based on a proximity sensor reading on the spindle bearing. Mou and Liu (1994a and 1994b) used a spindle mounted probe to measure the location of a metrolurgical block mounted in the work space and then went on to measure the variation in the part dimensions. The part dimension variation was measured by comparing the desired shape, as represented in the CAD model, to the machined part as measured on the machine and later by a CMM. This multiple stage measurement technique was necessary to separate the process errors, such as cutter deflection and wear, from the machine's errors.

The probing operation on the machine was done with a device made to withstand the harsh environment of the cutting process, thereby allowing it to be integrated in the production environment. A tool change operation, however, was required to replace the cutter with the probe before a measurement could be made. A typical measurement on a metrolurgical block would take approximately 20 seconds from the machining time and would need to be done frequently whenever the machine underwent a change in its operating conditions.

2.4.2 Temperature Measurement

Thermal errors on a machine have been found to be represented as first order lag functions in time. However, no time lag has been found between the temperature rise in a structure and its displacement (Okushima et al., 1975). This is significant since it indicates that an accurate measurement of temperature distribution provides a good indication of

thermal deformation. This is especially important when the deformation of a component cannot be exactly measured, such as on a rotating ballscrew. The key issues are to determine the optimal location and the minimum number of thermocouples required to provide sufficient information to predict the deformation of the machine within the desired accuracy range (Weck et al., 1994).

It is difficult to measure the exact temperature distribution inside of a structure without significantly impacting the integrity of the structure (Otter, 1968). Therefore, researchers use externally mounted thermocouples to measure surface temperature as an approximation of the structure's internal temperature distribution (Venugopal, 1985, Hardwick, 1992, and Fan et al., 1992). Much research as to the best thermocouple type and mounting condition for this application has been done by Attia and Kops (1993). Their recommendations regarding thermocouple type and mounting conditions have been followed in this work and are outlined in the temperature measurement section of this report.

2.4.3 Strain Measurement

Another method of estimating the error between the tool and the work piece is to measure the strain in the individual machine tool components. The strain measurements are then used to build an empirical model where the strain measurements are used much like the thermocouple values in the temperature measurement approach. Hatamura et al. (1993) and Moriwaki et al. (1997) developed special strain sensors suited to this application. Hatamura designed a large strain sensor which would act over an area large enough to avoid excessive sensitivity to localized strain. The localized strain can often be influenced by ribs, variations

in the casting, or surface asperities. Moriwaki paid special attention to designing a strain gauge setup that was not sensitive to temperature variations while being sensitive to thermal deformations. This was done by setting up a strain gauge network where the temperature component was canceled from the measurement. The results reported by the researchers using strain gauges are similar to those reported by the researchers using thermocouples as the basis for their empirical models. Unfortunately, it is not possible to place strain gauges on a surface like that of a rotating bearing or ballscrew shaft. Since these components contribute significantly to error, it is still necessary to estimate the errors in these regions using some other means.

2.5 Empirical and Numerical Algorithms for Modelling of Error

2.5.1 Linear Regression

Linear regression based error models relate some easily measurable quantity, like temperature or strain, to the error between the tool and the work piece. These basic relationships have been shown on simple cantilever beams by Kops and Bouzaniene (1992). Weck et al. (1994) showed that it is possible to model thermal deformations of a simple structure in terms of a few surface temperature measurements. Their results show that complete compensation is not possible. A reasonable level of accuracy, however, can be obtained when a manageable number of thermocouples are optimally placed.

Different modelling techniques have been used to represent the errors in motion on

three-axis machine tools. Ferreira and Liu (1986a, 1986b) developed a quadratic expression for geometric errors based on axis positions. Their model applied a linear relationship to the variation of geometric errors, but did not take thermal errors into account. Sata et al. (1977 and 1973) assumed a quadratic relationship between the kinematic and thermal errors in the work space to the coordinates of the tool and outputs from thermocouples. Kiridena and Ferreira (1994b, 1994c, 1993 and 1991) showed that it is possible to characterize and track the quasi-static errors of a machine in terms of a few measurements made in the work space on standardized components.

Mou and Liu (1993) developed a generalized error model describing the errors in motion on a vertical machining centre. Machine errors were measured by probing a standard part on a CMM after being machined. The difference between the measured dimensions and the desired dimensions was attributed to the machine. Care was taken to adequately separate the errors of interest on the part from the errors due to the machining process, such as tool deflection and tool wear.

Mou and Liu also used statistical tools to help identify the final model. To optimize the selection of inputs, they employed an analysis of variance technique to aid in selecting the most significant variables for inclusion in the model. The dynamics of the error variation were identified using a stepwise multiple linear regression technique with backward elimination to select significant independent variables. An adaptive approach, based on a state observer technique for machine tool error correction, was integrated with a process intermittent gauging technique to model the slowly varying thermal error component. This allowed their technique to update the model over time with the new information obtained

directly from the machine. The only drawback with this technique was the need to periodically stop the machining process and make measurements on a metrolurgical block located at the edge of the work space with the probe. Given that significant error variations can occur in fifteen minutes, their inspection process would need to be run frequently whenever the machine's condition changed dramatically. There is also some concern as to how stable a reference the metrolurgical block would be given the harshness of the machining environment and the chance that it might be hit while moving the part within the work space. If this problem were not detected, the compensation strategy would cause a permanent shift in the coordinates of the machine and produce a step in the surface of the machined part.

Mou and Liu (1994) went on to develop a probing strategy based on a predictive search algorithm which identified a minimum number of appropriate measurement points on an arbitrarily shaped manufactured part, to characterize the error. With this technique, the effort involved in the process intermittent probing used to update the error model was greatly reduced. However, they state that this technique would need to be repeated whenever the size or weight of the work piece changes significantly.

Mou et al. (1994a and 1994b) integrated information from a preprocessed characterization of the Computer Aided Design (CAD) model, a process intermittent probing operation, and a post process inspection on a CMM. This effort was necessary to separate the process related errors from the machine errors of interest. The difference between the CAD model and the CMM measurements are the total errors, assuming the CMM measurements are accurate. The errors measured during a process intermittent probing

operation, while the part was on the machine, provided a measure of the process related errors such as cutter deflection or tool wear. The difference between these two error measurements was the error arising in the machine structure.

Extending this technique to the use of form tools on complex surfaces or to a five-axis machining operation, requires that the exact tool path used to make the part be saved, along with the relevant machine conditions. This information is needed when calculating how best to compensate for an error measured on the surface, since any one spot on the part could be machined using a wide range of machine configurations.

Periodic updating of the models used for the estimation of error in the compensation techniques was recommended (Mou et al., 1994a). This is required to account for experimental uncertainties at the time the model was established, unavoidable changes in the assumptions used during modelling, and slow changes in the machine's accuracy. Over long periods of time, the relieving of internal stresses and material instability, as well as general wear and tear on the machine, can lead to changes in the machine's accuracy.

2.5.2 Neural Network Based Models

Srinivasa et al. (1992) used a multilayer feedforward neural network model to capture the geometric and kinematic errors associated with axis positioning, including reversal errors in a three-axis machine tool. The model was established using a back-propagation algorithm and was reported to be well suited to the application as the model was able to interpolate between the training points very effectively. Neural network models are known to interpolate well (Haykin, 1994), and since the machine has physical limits to its travel, its

inputs are bounded by the physical constraints of the machine.

Moriwaki and Zhoa (1992) and Hatamura et al. (1993) used a neural network model to capture the variation due to thermal errors, as well as kinematic and geometric errors. Temperature measurements from thermocouples distributed over the machine were included as inputs to the neural network. A neural network is ideally suited to modelling systems with a large number of inputs, so the number of sensors used does not pose any additional problems. The fact that the thermocouples were somewhat correlated, given the conductive properties of the structure, did not pose any serious problems in establishing the model. One potential problem that could occur if the inputs are highly correlated is that there might be a tendency for the coefficients (weights) associated with highly correlated inputs to grow very large compared to other terms. This winding up of the inputs could occur in the iterative search strategy for the minimum square error. Since the inputs are similar, the weights could become very large yet their combined effect on the model output could still be small. This would lead to a robustness problem, which would manifest itself, if one sensor varied to the point that the correlation relationship present during testing did not remain constant over long term use.

Another concern associated with the use of a neural network for thermal errors is that this modelling strategy is known to not perform well at extrapolating beyond the training data set. This feature would be required if the temperature distribution went beyond the range used during training. This can occur, given the possibility of room temperature fluctuations, changes in the heat generated by bearings due to wear, or due to motors operating under higher loads. In this event, the operator would need to be warned that the model was

operating beyond trained conditions and that the compensation strategy was no longer dependable. A certain amount of protection can be achieved by scaling the inputs and applying thresholding functions so that the inputs never go beyond the trained values. This would protect against problems associated with extrapolation. Unfortunately, it would also limit the range of compensation possible.

Chen et al. (1992 and 1991) used both multiple regression analysis and a neural network technique for predicting thermal errors from multiple temperature measurements. Both techniques performed equally well with the neural network reported as being slightly more robust to individual sensor failure. However, no additional logic was added to the regression technique to deal with the case of sensor failure in the regression model. This feature could be added to a regression model by using readings from the surrounding thermocouples. This is based on the fact that an individual thermocouple's output would be related to surrounding ones, given the conduction properties of the material and knowledge of the limited number of heat sources.

2.5.3 Finite Element Analysis (FEA)

Balsamo et al. (1990), Jedrzejewski et al. (1990), Okushima et al. (1975), and Sata et al. (1973) all used finite element analysis to predict the error between the tool and the work piece given information at the heat sources. The main research issues remaining with this technique involve the formulation of the finite element model at structural joints and across boundaries of moving components. Variations in the boundary conditions can be significant and highly nonlinear, as shown by Attia and Kops (1981, 1979). Variation due to the

intermittent presence of oil between surfaces and the tightness of a joint can all affect the boundary conditions. Also, for exposed surfaces, if forced air or coolant were intermittently flowing over a surface, the nature of heat transfer from the surface would be greatly affected. Modelling of the thermal profile of machines is further complicated by such factors as surface finish and coatings like paint. These aspects have a very small impact on the stress strain relationships predicted by Finite Element Analysis (FEA), yet they can have a significant impact on the thermal profile predicted by FEA.

In the comment section of Bryan's (1990) keynote paper, Professor G. Spur is quoted as saying:

> According to our experience, numerical algorithms such as finite element (FEA) or differential method, are suitable only for a qualitative description of the thermal behaviour of machine tools. Empirical equations have to be used for calculating the amount of thermal energy as well as the convective coefficients, as these values cannot be calculated using analytical methods.

Balsamo et al. (1990) extended the use of FEA by developing a model using a combination of FEA equations and "black box" empirical techniques to explain 80-85% of the deformations in a CMM. The FEA equations provide the basic form of the thermal error relationships, while the empirical techniques are used to account for uncertainty in the model due to variations in boundary conditions.

2.5.4 Generalized Modelling

Fraser et al. (1994) developed a thermal error model of a generic structure and used calibration coefficients to relate this model to an actual structure. The calibration coefficients were used to take into account the subtle differences in shape and boundary

conditions between the generic structure and the actual structure. This method required calibration data to establish the remaining coefficients used to define individual machines. The power of this technique was that it used thermal error models to help select the nature of the nonlinear functions used in the modelling process. Thus the generalized models would require less experimental data than a method with no *a priori* knowledge of the thermal relationships. This would save considerable time when building the models and enhance the model's ability to extrapolate beyond limited training conditions.

2.6 Compensation Strategies

When all practical efforts to improve a machine tool's accuracy through design and environmental control are exhausted, one can use the repeatability of the variation to further enhance the accuracy of the machine. The ability, to separate an error as random versus deterministic and to define the underlying variables, is key to this task (Bryan, 1990). To this end, various compensation techniques, done both in hardware and in software, have been used.

Hatamura et al. (1993) used direct heating and cooling of a section of the structure. The approach involves heating one side of a structure while cooling the opposite side to generate bending in a structural component. This is one way to compensate for angle errors on a three-axis machine, when no rotational degree of freedom is available in the desired direction. On a five-axis machine, there are typically two rotary degrees of freedom which

can be positioned to compensate for the angle errors.

Another approach involves heating the machine and maintaining its temperature profile during use (Sata, 1973). This entails turning special heat sources on and off to compensate for different amounts of heat generated under various operating conditions. The heat sources cycle on and off to maintain a predetermined temperature profile for which the accuracy of the machine is well known. The physical risk involved with this strategy is that uneven heating of bearings and sliding surfaces can occur which might damage them. Unfortunately, it is physically difficult to evenly heat or cool both the inner and outer races of a rotating bearing. However, this is necessary to simulate the heat generated under normal operation in which heat is generated in both inner and outer races of a bearing. This same risk exists when uneven cooling attempts are made around heat sources.

Chiappulini et al.(1991) used correction through software to implement a thermal calibration strategy involving the on-line correction of the Computer Numerical Control (CNC) code. This research also pointed out how difficult it was to manually adjust the CNC code to account for thermal errors. Before the heavy dependence on CNC technology, the operator would adjust the machine's offsets manually to account for variations in the thermal errors between each job. Now with extensive computer control, a machine will probe the location of a part and its features between major operations of the machining process and make adjustments to ensure a stable reference. Significant temperature gradients, however, can be generated in short periods of time, and thus, the probing process would need to be done frequently. Therefore, a major requirement of unsupervised machining is that the machine maintain a stable reference with which to coordinate all movements of the machine

throughout its production cycle (Lin, 1989). The difficulty of manual compensation of complex five-axis machine tool code is even further complicated given the difficulty in interpreting the errors on the part and compensating for them with appropriate machine offsets. This is due to the fact that the machining path on a five-axis machine used to create a feature on a part will have a large impact on how the compensation strategy should generate and apply the compensation values.

Okushima et al. (1975) demonstrated a software based coordinate system correction method. This system did not adjust the motion code sent to the machine, but rather adjusted the position of the machine's reference coordinate system. Typically, the compensation method chosen depends on the type of controller available on the machine tool and on one's ability to interface with it in real time. An open architecture controller would be ideally suited to the needs of compensation strategies such as these, given its flexibility and ease of interfacing with other external devices such as thermocouples, or additional processors (Teltz, 1998).

Balsamo et al. (1990), Belforte et al. (1987), and Zhang et al. (1985) outlined methods for correcting data from a CMM. Belforte focused on geometric and kinematic errors while Balsamo and Zhang focused on some thermal effects. CMMs differ from machine tools in that the magnitude of the heat sources and the number of degrees of freedom are typically greater in a five-axis machine tool than on a CMM. Also, due to the nature of a CMM's use as a gauge, the accuracy requirements are much higher and users are typically prepared to take additional measures to achieve the desired level of performance. The compensation values generated for a CMM can be applied either on-line to update the

position of the CMM, or through post processing of the collected data points. However, these two approaches do not always produce the same results due to the uncertainties associated with the probing process.

2.7 Summary

Much research has been done in the area of machine tool errors. The research outlined in this thesis report focuses on extending previous work to five-axis machine tools, with a specific emphasis on thermal errors. The kinematic modelling methods developed in the past will be extended to include the major errors in a five-axis machine. Methods for improving the empirical modelling of the machine are done by separating the effects of different heat sources through experimental design, and by allocating the error from the work space to the regions where the error is generated. The two methods of measuring error, both off-line and on-line, are combined with suitable regression equations to improve the overall accuracy of the compensation strategy.

CHAPTER 3

MACHINE TOOL ERRORS

3.1 Introduction

The machine tool errors relevant to this research are defined in this chapter. They have been loosely broken down into three main areas: geometric, kinematic, and thermal errors. The importance of angular errors on the volumetric error in the work space is also highlighted. Dynamic errors, such as vibration due to cutting, are not considered due to their high frequency of response and the relatively low speed compensation strategy proposed. Also, not considered are errors due to the deflection of the cutter or the deformation of the work piece as they are outside of the scope of this thesis.

3.2 Geometric Errors

Geometric errors relate to the structure of the machine tool and are often inherent in the manufacture of the machine's structural components. These errors include the manner in which the machine tool was assembled and installed on the factory floor for final use. For example, if the machine was not properly leveled or supported, the machine's slides can be bent, leading to excessive geometric errors. Geometric errors can also result from the deflection of structural components under the weight of the part or due to the part clamping force acting through the machine's table. A large portion of the geometric error component will be a constant for a given machine and setup. However, the change of the work piece weight and shift in position of a slide can generate an error component which varies with position and use. A simple case of varying geometric error is shown in Figure 3.1. In this example, the deformation of the Z column changes with the position of the spindle support arm for motion in the Z direction. This is due to the change in the application point of the moment generated by the weight of the spindle support arm on the Z column.

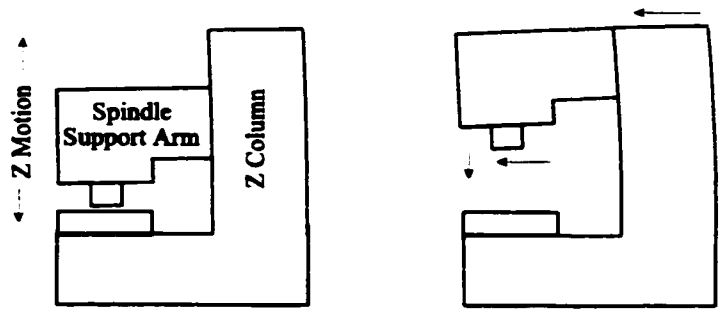

Figure 3.1 Example of a Gravity Induced Geometric Error

Other sources of geometric error in machines that are not considered separately in this thesis include: load induced errors, machine assembly errors, and material instability issues. However, the present state of the machine includes these errors as the initial starting point for the machine's configuration. Load induced errors relate to the effect of mounting different weighted work pieces in the work space. These errors are not included because this aspect of machine errors is typically addressed well by machine tool builders through detailed finite element analysis at the design stage. Furthermore, machine tool builders will only guarantee the stated accuracy of their machines to a certain work piece weight.

Machine assembly errors can result even if all of the components are machined accurately before assembly. For example, two structural components which are bolted together could experience assembly errors if some of the bolts were not equally preloaded. These errors are not considered because they are difficult to quantify without knowing the dimensions of all the components before assembly and the assembly details. Also, with good manufacturing practices these errors can be minimized.

Errors due to material instability and the relieving of internal stresses are not considered directly in the empirical modelling, but allowances have been made for their inclusion should they develop in the machine over time. The time constants associated with these errors are longer than the time frame used to measure the errors in this study. The longest time frame studied in this work was 70 hours, while material instability and internal stresses might take years to reveal themselves.

3.3 Kinematic Errors

In general, kinematic errors are defined by the interaction of the geometries under motion. They are a function of the position of the machine tool's slides, ballscrews, gears, couplers, motors, sensors, and their interaction through the motion controller. These errors are highly dependent on the geometries of the components involved, like the shape of sliding surfaces, ballscrew pitches, and gear teeth spacing. Kinematic errors also arise due to hysteresis or backlash in ballscrews, gears, and couplers, and hence, are a function of the direction of motion as well.

The six degrees of freedom of a body in space are typically constrained on a machine so that only one of them is free to move at a time. Often kinematic errors arise from axes that are over or under constrained. If an axis is over constrained, then the smallest geometric error in the components will cause it to deflect as it conforms to the conditions of the constraints. If the axis is under constrained, due to loose support conditions, then the axis will have extra degrees of freedom beyond the desired one. The errors associated with an over constrained axis will typically be more repeatable than the errors associated with an under constrained axis. However, problems associated with the constraints on an axis should first be addressed through mechanical adjustments of the axis before applying any compensation strategy. Examples of errors for the six degrees of freedom for both a translation and rotation joint are shown in Figures 3.2 and 3.3 respectively.

Errors in position are measured in the direction of travel and are directly attributable to the ballscrew, couplers, motors, sensors, and controller signals. Defects in the motion

controlling surfaces lead to errors in straightness. Straightness errors are perpendicular to the motion of travel. Errors in angle can result from bends in the motion controlling surfaces and are coupled to the position and straightness errors when allowed to act over a distance. For example, a Yaw error will generate straightness errors from side to side and a pitch error will generate up and down straightness errors. This coupling of angular errors and linear errors is discussed further in the section on the implications of angle errors.

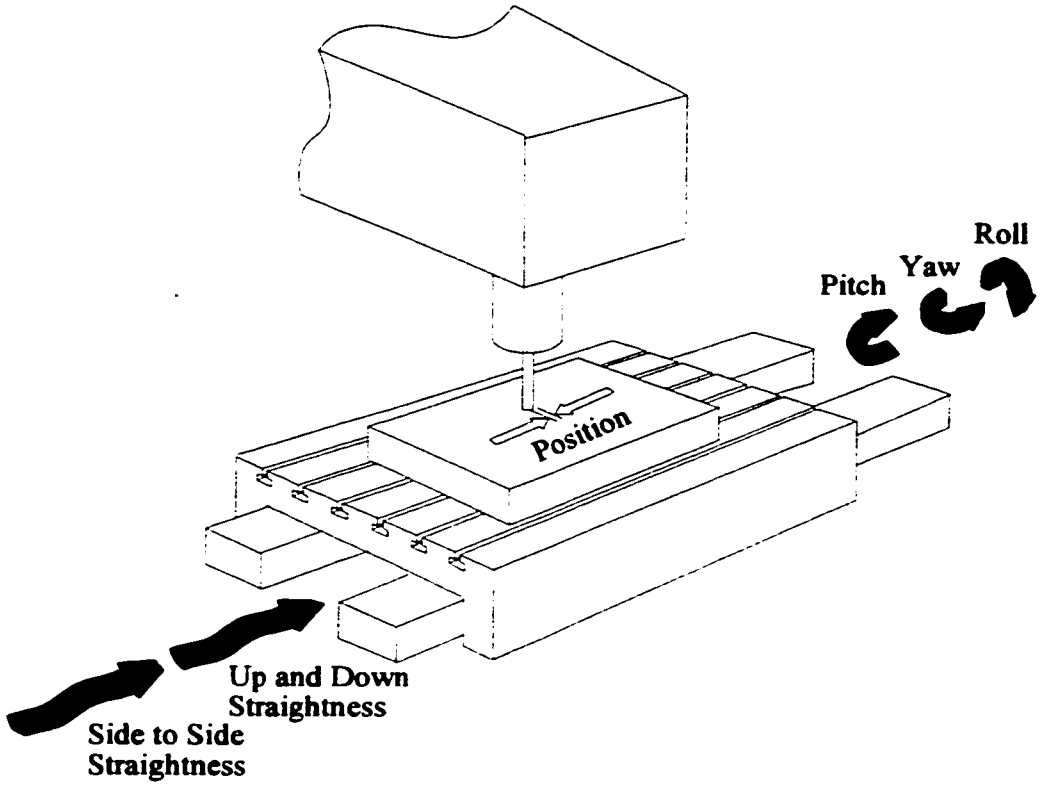

Figure 3.2 Example of Kinematic Error for Translational Motion

The angle error in the direction of rotation is defined by the accuracy of the gears, couplers, motors, sensors, and controller. Backlash in the gears and couplers results in reversal errors in the angle of rotation. Angle errors about the other two axes will result in tilt errors as the table rotates. Tilt errors are sometimes referred to as 'wobble' in a rotary table. When a tilt error acts through a distance it will also impact the positional accuracy in the work space. Errors in determining the position of the centre of rotation will impact the error in the work space in two ways: the first through the errors' stacked positional effect in the machine's chain of components, and the other through the angle component acting through a new critical distance.

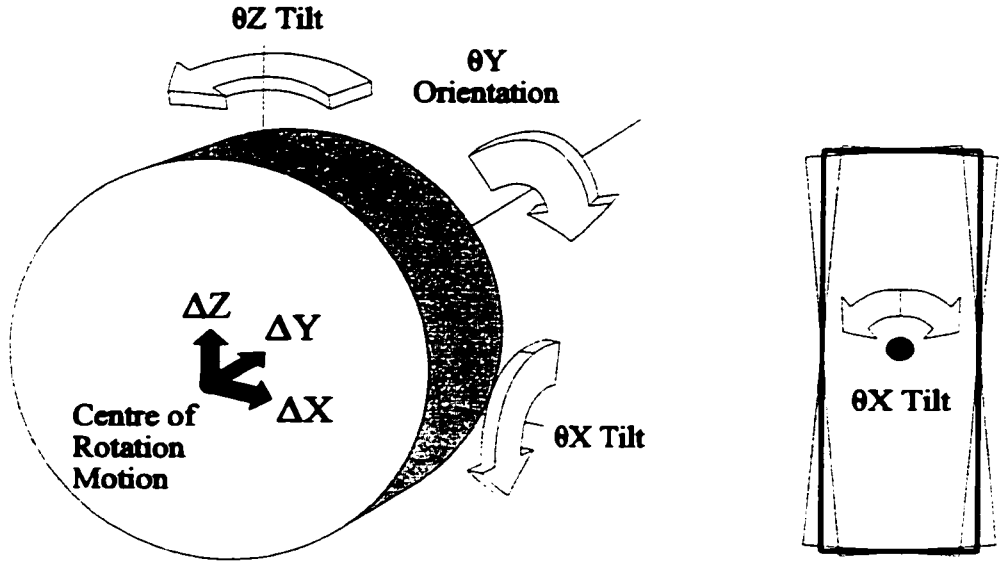

Figure 3.3 Example of Kinematic Errors for Rotary Motion

A large source of error in a machine can arise from non-orthogonality errors or squareness errors on a machine. These errors can be due to structural problems, which can occur when the axes are assembled incorrectly, or due to kinematic motion errors. An example of a squareness problem resulting from a kinematic motion error is the coordinated following between the two uprights on a gantry machine. A gantry machine supports the spindle on two parallel arms. If these arms do not follow each other perfectly during linear motion, a change in squareness will occur. This variation in squareness will be a function of the motion error between one column and the other as shown in Figure 3.4.

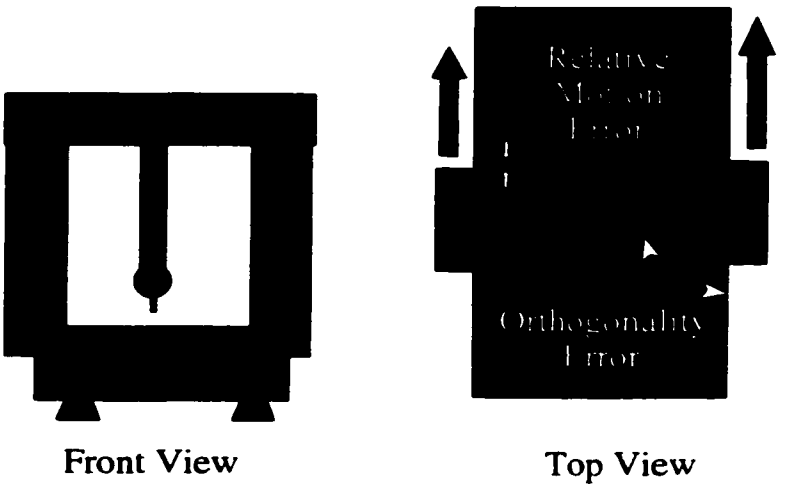

Figure 3.4 Orthogonality Errors on a Gantry Machine

3.4 Implications of Angle Errors

Angle errors, due to orthogonality problems for example, are very significant on large machines because of the relationship between angles and translations. Angular errors impact translation errors in two ways. An angular error can affect translation through a sine error or cause a translation measurement to be misread through a cosine error. A sine error results from an amplification of the error through a moment arm, while a cosine error results from measuring a distance along a length that is not parallel to the distance of interest.

The issue of angle errors in measuring systems is described in the Abbe error principle, which states that:

> The displacement measuring system should be in line with the functional point whose displacement is to be measured. If this is not possible either the slide ways that transfer the displacement must be free of angular motion or angular motion data must be used to calculate the consequence of the offset. (Bryan, 1979)

This principle is shown in Figure 3.5 for the measurement of a cylinder using Vernier calipers versus a more precise micrometer.

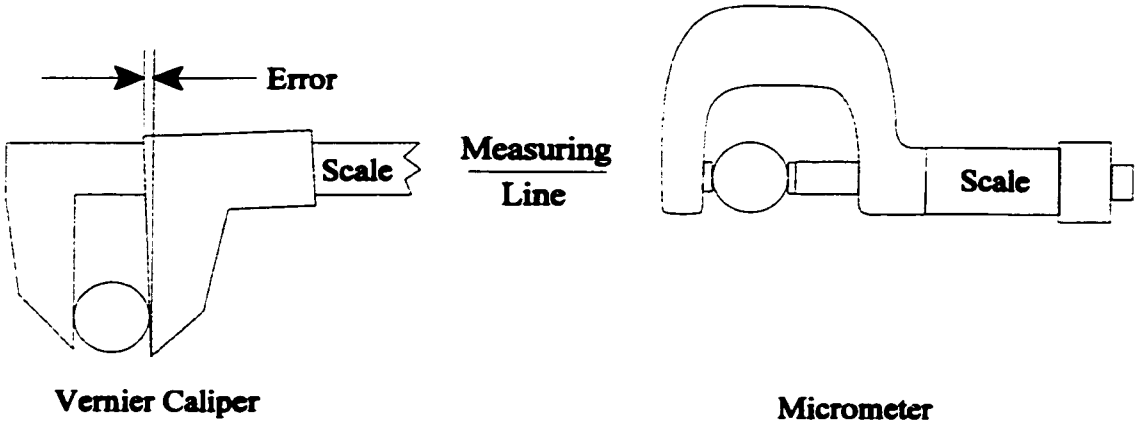

Figure 3.5 Measurement Error

Figure 3.6 shows the Abbe error principle applied to a bend in a motion control surface where the measuring system is offset from the line of interest. This offset is common on machine tools due to the size and harshness of the work space environment. From this figure, one can see that the spacing of the positioning resolution of the sensor will change as one moves further from the sensor's line of action. Since it is not practical to find all of the motion errors for every offset distance, the angle errors in the motion must be measured to calculate the position error away from the measurement line. This is one of the main justifications for allocating the error measured in the work space to its source, using the kinematic model.

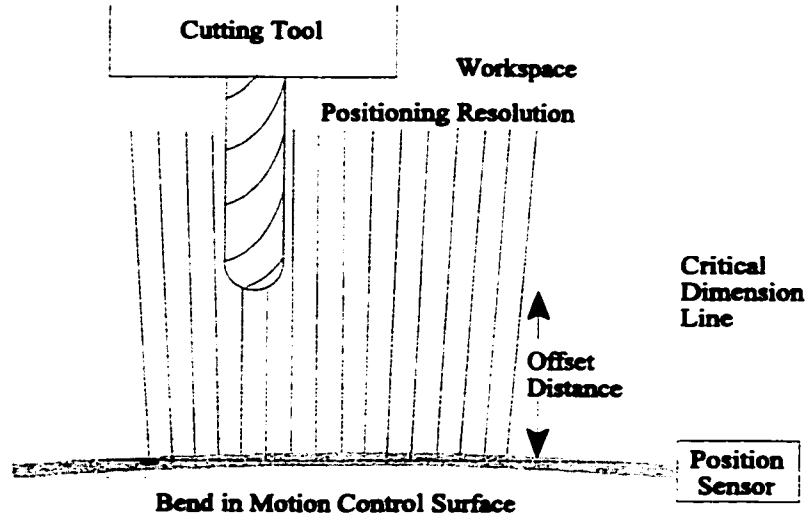

Figure 3.6 Abbe Error Principle

Sine errors are also present in rotary joints. They can arise from errors in angular rotation or from tilt angles in perpendicular directions. With sine errors in a rotary joint, the error in the work space will vary with the distance to the centre of rotation. Also, if the centre of rotation is not properly defined, then error will result due to rotation through an incorrect distance. This aspect is shown in Figure 3.7. Due to the importance of the rotation distance, table mounted rotary axes are more susceptible to sine errors. This is due to the larger distance from the centre of rotation to the cutting zone found on rotary table setups than on machines with rotations built into the spindle area. The spindle rotations are typically much closer to the workpiece, and thus, have a shorter moment arm for the amplification of sine errors.

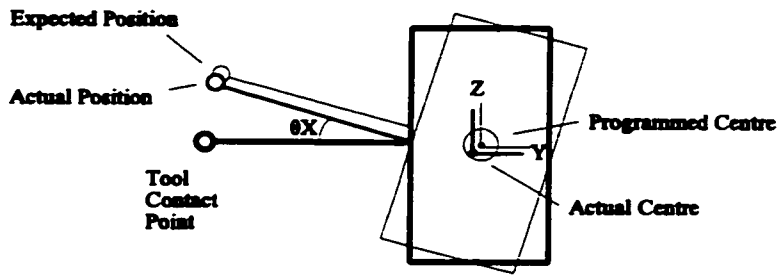

Figure 3.7 Error in Centre of Rotation Distance

Cosine errors, in a measurement system on a machine, would result if the measurement system were not parallel to the axis of motion. Another place cosine errors can occur is in setting up the laser interferometer to measure motion. The importance of aligning the laser parallel to the direction of motion is shown in Figure 3.8. Cosine errors are typically smaller in magnitude, but are also easier to avoid than sine errors, through good setup practices.

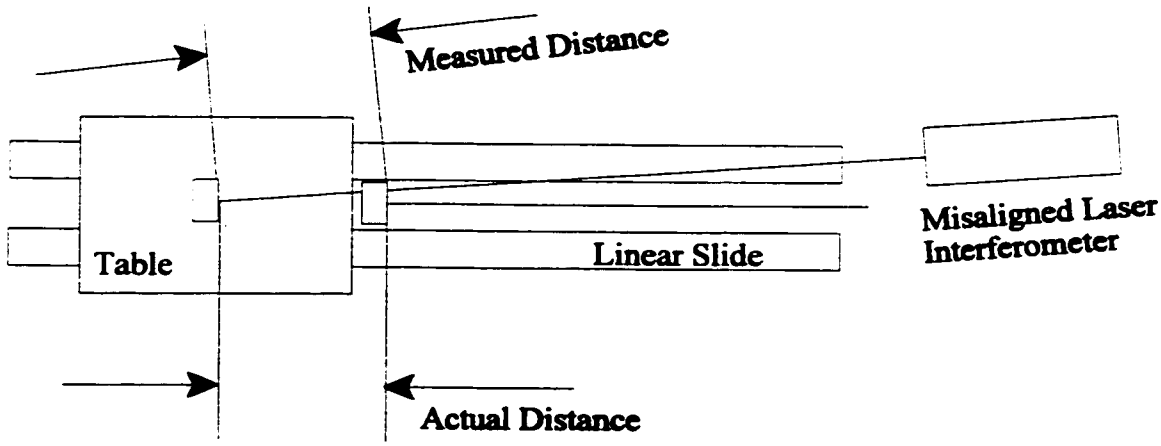

Figure 3.8 Cosine Errors in Laser Interferometer Measurements

3.5 Thermal Errors

Thermal errors are a special case of geometric errors and are considered separately because of their large impact on machining accuracy. For many years, errors of this nature were simply attributed to the random behaviour of a machine. However, over time, operators began to associate room temperature fluctuation and later, actual machine temperature variation to the accuracy of part production. As part tolerances have become increasingly critical, more in-depth thermal error knowledge is required to maintain the stable references necessary to machine increasingly complicated parts.

As the machine operates, its castings, slides, and motion controlling components will all heat up. Critical motion controlling components include: slide surfaces, ballscrews, couplers, gears, and bearings. If the machine was exposed to direct sunlight, the exposed surface would warm up. This would generate a thermal gradient in the structure and cause the machine to bend. Figure 3.9 shows the progression of a major thermal effect as the machine tool is operated. For clarity, just the movement of the spindle is shown.

The largest heat source on this machine was the spindle motor and bearings due to their size, power and rotational speed. The heat from the spindle motor produced a significant thermal gradient in the spindle support arm. The heat from the spindle bearing was largely removed through the use of the chilling unit. Deformation due to temperature change of the spindle shaft was minimized by providing the support of the spindle bearing near the end cap, thus minimizing the unsupported length. This was done primarily for stiffness but resulted in a thermally stable design as well. Over time the motors, ballscrews,

and gears heated up. The longest time constant for a deformation that was observed was the for the Z column. It is large in size and has relatively small heat sources acting on it. The base of the machine was not found to vary significantly during testing.

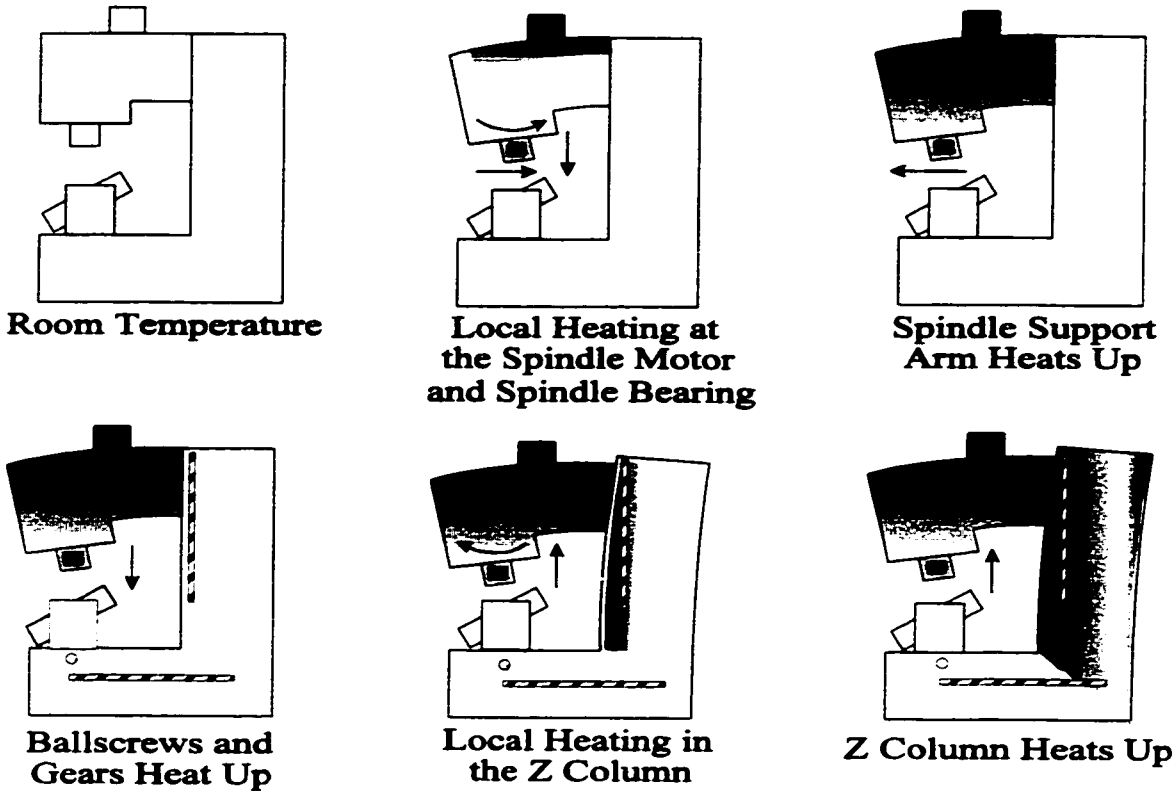

Figure 3.9 Examples of Thermal Errors

If a structural component undergoes a uniform temperature change, then the dimension along its critical length L will change by ΔL as described in Equation 3.1, where the temperature change is measured from the reference temperature of 20°C and α_c is the material's coefficient of thermal expansion. A typical value for α_c is $12.1\times10^{-6}/°C$, and thus,

a 1 °C temperature change in a 1 m section will result in a displacement error of 12.1μm. Given that temperature changes of 5 °C to 10 °C are not unrealistic in a typical machine shop environment, thermal errors can be significant.

$$\Delta L = \alpha_c \, \Delta T \, L \tag{3.1}$$

If this relationship is used to describe a ballscrew, then the distance L would be a function of both the axis position and the temperature distribution in the ballscrew. The temperature distribution would be a function of the heat generated by the ballscrew nut and the heat transferred to a section of the ballscrew shaft. The heat transferred to any one region on the shaft would vary depending on how much time the nut spends at one location. The error across the X axis ballscrew would be as shown in Equation 3.2. Here the distance X+ℓ defines the distance from the nut to the mounting point, where X is equal to the X axis position and ℓ is equal to the non-travelled portion of the ballscrew, which connects the motor to the ballscrew.

$$\Delta L = \alpha_c \int_0^{X+\ell} \Delta t(x) \, dx \tag{3.2}$$

If the structure is mounted across a large vertical distance, then it will be subjected to a temperature gradient in the room as warm air rises and cool air falls. An approximation of the change in dimension would be described by Equation 3.3, where ΔT_T and ΔT_B are the temperature changes at the top and bottom of the structure respectively.

$$\Delta L = \alpha_c \frac{\left(\Delta T_B + \Delta T_T\right)}{2} L \tag{3.3}$$

Another important relationship describes the bending of a component due to a thermal gradient across the structure. The relevant formulas for a cantilever beam are shown in Equations 3.4 and 3.5. In these equations, ΔT is a measure of the temperature gradient across the height H of the component, Δd is the resulting deflection, and $\Delta\theta$ is the resulting angle error at the tip. Using a typical value for α_c of $12.1\times10^{-6}/°C$ and a 1 °C temperature gradient acting across a distance of 0.5 m, over a length of 1 m, the resulting error is 0.0014° and 12.1μm. If the angle error of 0.0014° is allowed to act over a distance of 1 m, then an additional positional error would result of 12.1μm. The angle error at the distance of 1 m would be unchanged.

$$\Delta\theta = \frac{\alpha_c \Delta T L}{H} \times \frac{180°}{\pi} \tag{3.4}$$

$$\Delta d = \frac{\alpha_c \Delta T L^2}{2 H} \tag{3.5}$$

3.6 Summary

This chapter discussed the major errors of interest in a five-axis machine. Information was given as to how the error terms interact and affect one another. Simple physical relationships describing the error of the basic structures which make up the machine were also presented. The next chapter deals with building a kinematic model to relate the errors in the individual links and joints described in this chapter to the volumetric error in the work space of the machine.

CHAPTER 4

KINEMATIC MODEL

4.1 Introduction

This chapter outlines the development of the kinematic model for a five-axis machine tool. First, the transformation equations associated with ideal links and joints are considered. Second, the method for including individual error terms, such as those described in the previous chapter, is discussed. Following that, the procedure used to formulate the kinematic model of the entire machine tool is presented. Next, the application of the kinematic model for solving the allocation of errors from the work space to the individual components is shown along with the method used in calculating the compensation values. The results of the simulation of the compensation strategy are also shown.

4.2 Model Development

A Homogeneous Transformation Matrix (HTM) model of a five-axis machine is used to represent the geometric, kinematic and thermal errors in the machine. The advantage of the HTM method in general is that it is based on matrices which are capable of translational as well as rotational transformations. However, the HTM method assumes rigid bodies, and therefore, the errors associated with the deformation of a link must be accounted for with errors at the joints. Given the small deformations expected, this is considered a reasonable approximation. The individual matrices of the HTM model are based on shape and joint transformations in place of Denavit and Hartenberg (1955) transformations. The shape and joint method provides a better physical relationship between the parameters used to describe the error in the elements of each transformation matrix and the machine's kinematics than the Denavit and Hartenberg approach.

Typically, five-axis machine tools are made up of a series of links with either moving slides (prismatic joints) or rotating joints (revolute joints). When assembled, these components comprise a closed chain between the tool contact point and the work piece. Before considering the influence of error on this closed chain, a systematic development of an idealized machine is conducted using HTMs. Then, the inclusion of error terms in the formulation of the transformation matrices for links and joints is considered.

Equation 4.1 shows the 4x4 matrix which is needed to represent the relative position of a rigid body in three-dimensional space. The 3×3 sub-matrix's O elements represent the orientation components, with each column contributing a direction cosine to the matrix, and

the 3×1 sub-matrix's P elements represent the positional components. The digit in the lower right corner of the T matrix provides the matrix with a scaling factor. Its value has been set to one for convenience. The first three columns in the last row are used to provide the matrix with perspective; these values have been set to zero as perspective is not used in this application.

$$ {}^{R}T_{0} = \left[\begin{array}{cccc} O_{ix} & O_{iy} & O_{iz} & P_{x} \\ O_{jx} & O_{jy} & O_{jz} & P_{y} \\ O_{kx} & O_{ky} & O_{kz} & P_{z} \\ \hline 0 & 0 & 0 & 1 \end{array}\right] \tag{4.1} $$

The necessary coordinate transformation of the rigid body $\{X_0Y_0Z_0\}$ with respect to the reference coordinate system $\{X_RY_RZ_R\}$ is shown in Equation 4.2.

$$ \begin{bmatrix} X_R \\ Y_R \\ Z_R \\ 1 \end{bmatrix} = {}^{R}T_{0} \begin{bmatrix} X_0 \\ Y_0 \\ Z_0 \\ 1 \end{bmatrix} \tag{4.2} $$

For ideal translational motions in the X, Y, or Z directions, the corresponding HTM that transforms the coordinate of a point in the $\{X_1Y_1Z_1\}$ coordinate frame into the $\{XYZ\}$ coordinate frame is given by Equation 4.3 for each translational motion respectively.

$$ {}^{XYZ}T_{X_1Y_1Z_1} = \begin{bmatrix} 1 & 0 & 0 & X \\ 0 & 1 & 0 & 0 \\ 0 & 0 & 1 & 0 \\ 0 & 0 & 0 & 1 \end{bmatrix} \quad OR \quad \begin{bmatrix} 1 & 0 & 0 & 0 \\ 0 & 1 & 0 & Y \\ 0 & 0 & 1 & 0 \\ 0 & 0 & 0 & 1 \end{bmatrix} \quad OR \quad \begin{bmatrix} 1 & 0 & 0 & 0 \\ 0 & 1 & 0 & 0 \\ 0 & 0 & 1 & Z \\ 0 & 0 & 0 & 1 \end{bmatrix} \tag{4.3} $$

Similarly, corresponding HTMs exist for ideal rotational motions. Equation 4.4 outlines the resulting HTM if the $\{X_1Y_1Z_1\}$ system is rotated by an angle θ about the X axis, Y axis, or the Z axis respectively.

$$ \begin{bmatrix} 1 & 0 & 0 & 0 \\ 0 & \cos(\theta_X) & -\sin(\theta_X) & 0 \\ 0 & \sin(\theta_X) & \cos(\theta_X) & 0 \\ 0 & 0 & 0 & 1 \end{bmatrix} $$

OR

$$ {}^{XYZ}T_{X_1Y_1Z_1} = \begin{bmatrix} \cos(\theta_Y) & 0 & \sin(\theta_Y) & 0 \\ 0 & 1 & 0 & 0 \\ -\sin(\theta_Y) & 0 & \cos(\theta_Y) & 0 \\ 0 & 0 & 0 & 1 \end{bmatrix} \tag{4.4} $$

OR

$$ \begin{bmatrix} \cos(\theta_Z) & -\sin(\theta_Z) & 0 & 0 \\ \sin(\theta_Z) & \cos(\theta_Z) & 0 & 0 \\ 0 & 0 & 1 & 0 \\ 0 & 0 & 0 & 1 \end{bmatrix} $$

It is important to watch the order of operations when describing a compound rotary joint, as the order in which the rotations are applied to a solid body affect the final orientation of the body in space. This is not the case with pure translational motion as translations can be applied in any order and the final vector will still end at the same point.

An entire machine tool structure can be decomposed into a series of HTMs, starting at the tool tip and progressing around the machine. In this way, a machine with N rigid bodies can be connected in series, where the position of the tool tip (which is connected to the N^{th} axis), expressed in terms of the reference coordinate system, is a sequential product of all of the associated HTMs. This sequential product of matrices is shown in Equation 4.5.

$$ {}^{R}T_{0} = \prod_{m=1}^{N} {}^{m-1}T_{m} = {}^{0}T_{1}\ {}^{1}T_{2}\ {}^{2}T_{3} \ldots \qquad (4.5) $$

When defining a solid link, as shown in Figure 4.1, the ideal HTM corresponding to the dimensions a, b, and c would be as shown in Equation 4.6.

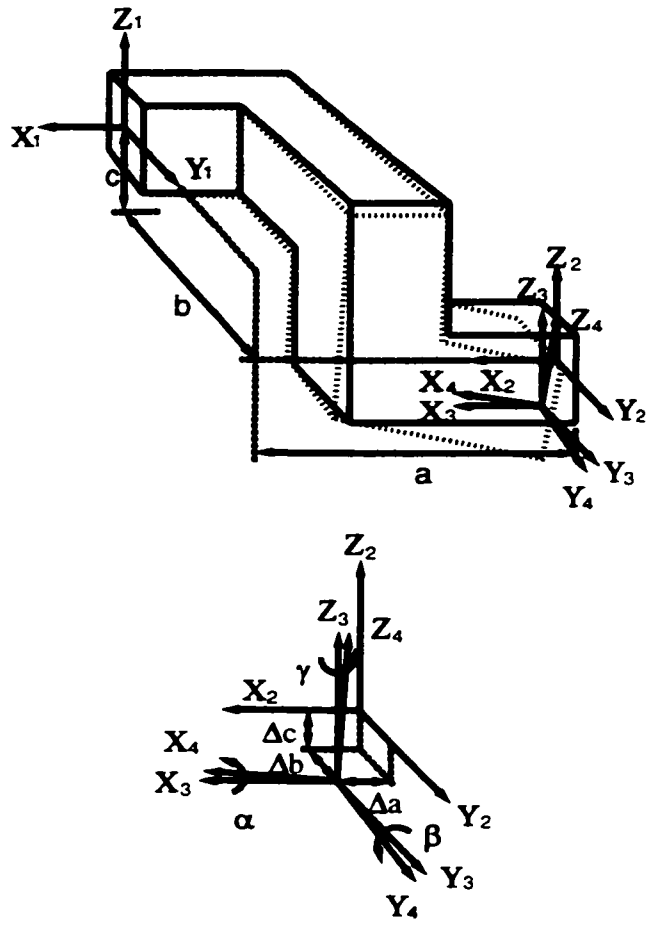

Figure 4.1 Solid Link with Error

$$ {}^{R}T_{0} = \begin{bmatrix} 1 & 0 & 0 & a \\ 0 & 1 & 0 & b \\ 0 & 0 & 1 & c \\ 0 & 0 & 0 & 1 \end{bmatrix} \tag{4.6} $$

The HTM associated with the three translational errors $\{\Delta a(t)\ \Delta b(t)\ \Delta c(t)\}$ and the three rotational errors $\{\alpha(t)\ \beta(t)\ \gamma(t)\}$ can be formulated by multiplying the related matrices containing the error terms. This is done in a similar manner to forming the closed form shaping function of the machine, except that in this case the transformations correspond to terms situated within the same link or joint. This formulation is shown in Equation 4.7.

$$ {}^{0}E_{0} = E_{\theta_x} E_{\theta_y} E_{\theta_z} E_{\Delta a} E_{\Delta b} E_{\Delta c} \tag{4.7} $$

When higher order error terms are dropped from the matrix multiplication, the resulting HTM for the error concentrated at a joint 0 is shown in Equation 4.8. If the error terms are large, then the assumptions associated with dropping the higher order terms are no longer valid and the order of matrix multiplication must be done carefully to match the physics of the problem. The error terms are expressed as functions of time to allow for their variation over time. In this manner, the quasi-static error associated with thermal deformations can be accounted for.

$$ {}^{0}E_{0} = \begin{bmatrix} 1 & -\gamma(t) & \beta(t) & \Delta a(t) \\ \gamma(t) & 1 & -\alpha(t) & \Delta b(t) \\ -\beta(t) & \alpha(t) & 1 & \Delta c(t) \\ 0 & 0 & 0 & 1 \end{bmatrix} \tag{4.8} $$

When the error terms associated with a link, as shown in Figure 4.1, are included in the HTM of the link, a matrix multiplication must be done with the HTM defining the

dimensions of the structure. For a general link in three dimensional space with error terms, the corresponding HTM would be as follows:

$$ {}^{R}T_{0err} = {}^{R}T_{0}\ {}^{0}E_{0} = \begin{bmatrix} 1 & -\gamma(t) & \beta(t) & a+\Delta a(t) \\ \gamma(t) & 1 & -\alpha(t) & b+\Delta b(t) \\ -\beta(t) & \alpha(t) & 1 & c+\Delta c(t) \\ 0 & 0 & 0 & 1 \end{bmatrix} \tag{4.9} $$

HTMs assign the rotational errors within a component to the ends of the link. On large machines, this can result in an error arising due to the angle error being accounted for at the wrong location on the machine. If this assignment leads to a large source of error, then it would be necessary to break the link up into two or more smaller links. The point at which the two transformation matrices meet on the structure should be at the location of the heat source which is causing the angle error.

For the case of linear motion in the X direction, as shown in Figure 4.2, the errors are a function of time and position. This allows for the representation of quasi-static thermal errors, as well as geometric and kinematic errors due to wear on sliding surfaces or inaccuracy in the motion controlling components.

A positional error for motion in the X direction would be $\Delta X(x,t)$ and corresponding straightness errors in the X axis would be represented by the integration of the two angles perpendicular to X, namely $\gamma(x,t)$ and $\beta(x,t)$ over the distance dx. To be more compatible with the way in which these straightness values are measured using the laser interferometer,

these integral terms are referred to as $\Delta y(x,t)$ and $\Delta z(x,t)$ further on. The HTM associated with this motion and the related errors is shown in Equation 4.10.

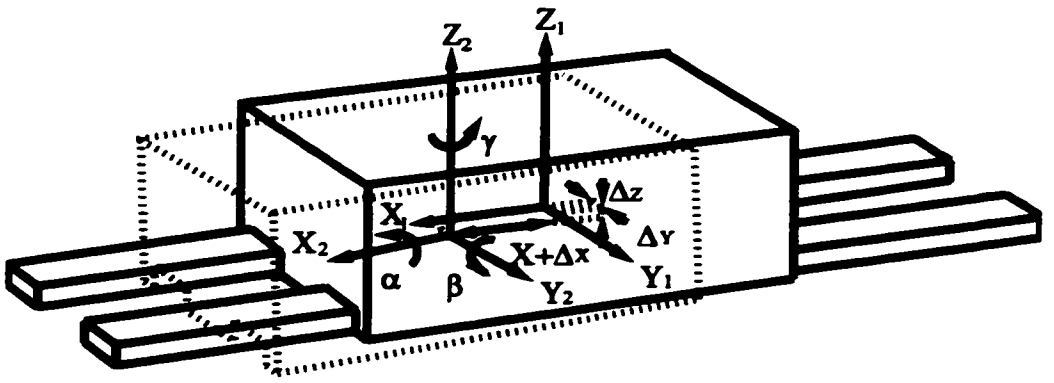

Figure 4.2 X Axis Motion

$$T = \begin{bmatrix} 1 & -\gamma(x,t) & \beta(x,t) & X+\Delta x(x,t) \\ \gamma(x,t) & 1 & -\alpha(x,t) & \int_0^x \gamma(x,t)dx \\ -\beta(x,t) & \alpha(x,t) & 1 & -\int_0^x \beta(x,t)dx \\ 0 & 0 & 0 & 1 \end{bmatrix} \tag{4.10}$$

The HTM model of a rotational axis is developed in much the same way as that of a translational axis. The rotational model takes into account the fact that an axis never rotates purely about one axis, and that rotation can generate positional errors due to a shift in the centre of rotation. All of these errors are taken to be functions of the rotational angle

θ_Y, as shown in Figure 4.3. The corresponding HTM developed for this axis is shown in Equation 4.11. For clarity, C refers to Cosine and S refers to Sine. In the generation of Equation 4.11, small angle approximations were made such that $C\beta = 1.0$ and $S\beta = 0.0$, and second order error terms were neglected. For example, $\alpha \times \beta$ and higher order terms are set equal to zero as the error is expected to be small. Similar matrices could be obtained for rotations about the X and Y axes.

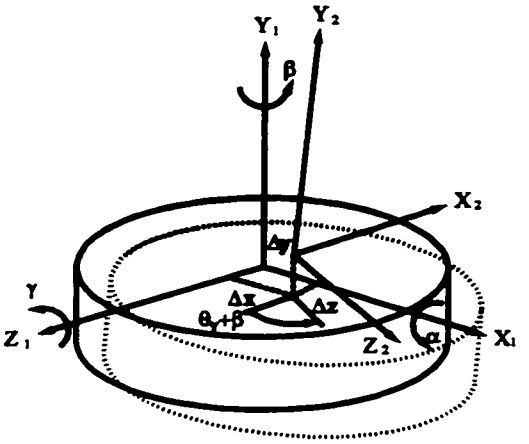

Figure 4.3 θ_Y Axis Motion

$$
{}^{R}\Theta_{0err} = \begin{bmatrix}
C\left(\begin{matrix}\theta_y(t)+\\ \beta(\theta_y,t)\end{matrix}\right) & -\gamma(\theta_y,t)\ C\left(\begin{matrix}\theta_y(t)+\\ \beta(\theta_y,t)\end{matrix}\right) & S\left(\begin{matrix}\theta_y(t)+\\ \beta(\theta_y,t)\end{matrix}\right) & \Delta x(\theta_y,t) \\
\gamma(\theta_y,t)\ + & & & \\
\alpha(\theta_y,t)\ S\left(\begin{matrix}\theta_y(t)+\\ \beta(\theta_y,t)\end{matrix}\right) & 1 & -\alpha(\theta_z,t)\ C\left(\begin{matrix}\theta_y(t)+\\ \beta(\theta_y,t)\end{matrix}\right) & \Delta y(\theta_y,t) \\
 & \alpha(\theta_y,t)\ + & & \\
-S\left(\begin{matrix}\theta_y(t)+\\ \beta(\theta_y,t)\end{matrix}\right) & \gamma(\theta_y,t)\ S\left(\begin{matrix}\theta_y(t)+\\ \beta(\theta_y,t)\end{matrix}\right) & C\left(\begin{matrix}\theta_y(t)+\\ \beta(\theta_y,t)\end{matrix}\right) & \Delta z(\theta_y,t) \\
0 & 0 & 0 & 1
\end{bmatrix}
\tag{4.11}
$$

Typically, five-axis machines have three translational (T) and two rotational (θ) axes. These axes can be arranged in different ways depending on the user's requirements. The machine tool used in this study has a tilt or rotary table mounted on the bed of a traditional three-axis machine. This configuration is outlined in Figure 4.4. Other common configurations of five-axis machines have the two rotary axes mounted at the spindle, or have the two rotary axes separated, with one on the table and the other at the spindle.

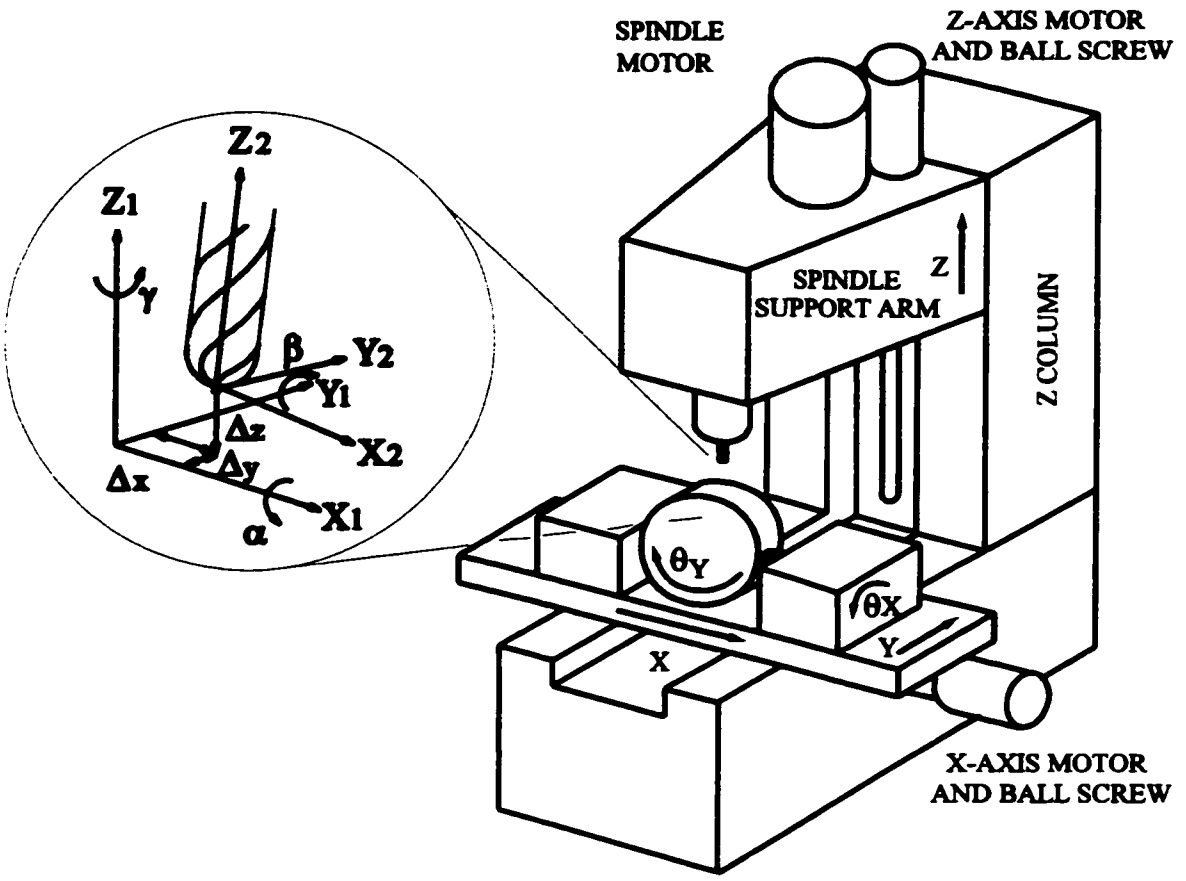

Figure 4.4 Five-Axis Machine Tool with Error

The wire frame model in Figure 4.5 shows the assignment of transformation matrices to the machine tool. A closed form mathematical representation of the machine can be established using the sequential product of matrices as outlined previously in Equation 4.5. In this case, the sequence starts at the work piece and proceeds around the machine to the tool tip which is mounted in the spindle. The corresponding HTM for the machine, based on the wire frame, is outlined in Equation 4.12.

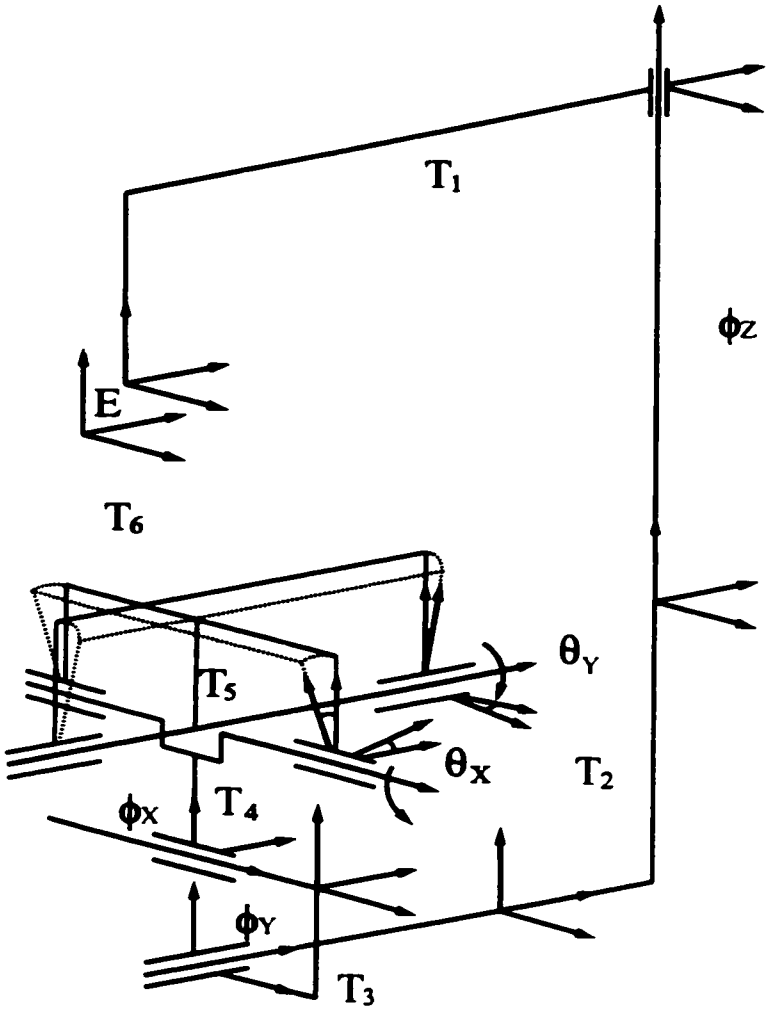

Figure 4.5 Wire Frame Model of Machine Tool

$$\left[\begin{array}{c|c} R_s & \overline{P}_s \\ \hline O^T & 1 \end{array}\right] = [E][T_1][\Phi_Z][T_2][\Phi_Y][T_3][\Phi_X][T_4][\Theta_X][T_5][\Theta_Y][T_6]\left[\begin{array}{c|c} R_w & \overline{P}_w \\ \hline O^T & 1 \end{array}\right] \tag{4.12}$$

The links and joints of the machine were chosen as the natural dividing points for the generation of the HTM matrices. Equations 4.13 - 4.18 describe the individual matrices that make up the links and joints of the machine tool. The matrix E represents the error measured in the work space which forces the spindle coordinate system to match the work piece coordinate system.

$$T_i = \begin{bmatrix} 1 & -\gamma_i(t) & \beta_i(t) & a_i+\Delta a_i(t) \\ \gamma_i(t) & 1 & -\alpha_i(t) & b_i+\Delta b_i(t) \\ -\beta_i(t) & \alpha_i(t) & 1 & c_i+\Delta c_i(t) \\ 0 & 0 & 0 & 1 \end{bmatrix} \quad i = 1, 2, 3, 4, 5 \text{ and } 6 \tag{4.13}$$

$$\Phi_X = \begin{bmatrix} 1 & -\gamma(x,t) & \beta(x,t) & X + \Delta x(x,t) \\ \gamma(x,t) & 1 & -\alpha(x,t) & \int_0^x \gamma(x,t)\, dx \\ -\beta(x,t) & \alpha(x,t) & 1 & -\int_0^x \beta(x,t)\, dx \\ 0 & 0 & 0 & 1 \end{bmatrix} \tag{4.14}$$

$$\Phi_Y = \begin{bmatrix} 1 & -\gamma(y,t) & \beta(y,t) & -\int_0^y \gamma(y,t)\, dy \\ \gamma(y,t) & 1 & -\alpha(y,t) & Y + \Delta y(y,t) \\ -\beta(y,t) & \alpha(y,t) & 1 & \int_0^y \alpha(y,t)\, dy \\ 0 & 0 & 0 & 1 \end{bmatrix} \tag{4.15}$$

$$\Phi_Z = \begin{bmatrix} 1 & -\gamma(z,t) & \beta(z,t) & \int_0^z \beta(z,t)\ dz \\ \gamma(z,t) & 1 & -\alpha(z,t) & -\int_0^z \alpha(z,t)\ dz \\ -\beta(z,t) & \alpha(z,t) & 1 & Z + \Delta z(z,t) \\ 0 & 0 & 0 & 1 \end{bmatrix} \tag{4.16}$$

$$\Theta_X = \begin{bmatrix} 1 & -\gamma(\theta_x,t) & \beta(\theta_x,t) & \Delta x(\theta_x,t) \\ \beta(\theta_x,t)\ S\left(\begin{matrix}\theta_x(t)+\\ \alpha(\theta_x,t)\end{matrix}\right) + \gamma(\theta_x,t)\ C\left(\begin{matrix}\theta_x(t)+\\ \alpha(\theta_x,t)\end{matrix}\right) & C\left(\begin{matrix}\theta_x(t)+\\ \alpha(\theta_x,t)\end{matrix}\right) & -S\left(\begin{matrix}\theta_x(t)+\\ \alpha(\theta_x,t)\end{matrix}\right) & \Delta y(\theta_x,t) \\ -\beta(\theta_x,t)\ C\left(\begin{matrix}\theta_x(t)+\\ \alpha(\theta_x,t)\end{matrix}\right) + \gamma(\theta_x,t)\ S\left(\begin{matrix}\theta_x(t)+\\ \alpha(\theta_x,t)\end{matrix}\right) & S\left(\begin{matrix}\theta_x(t)+\\ \alpha(\theta_x,t)\end{matrix}\right) & C\left(\begin{matrix}\theta_x(t)+\\ \alpha(\theta_x,t)\end{matrix}\right) & \Delta z(\theta_x,t) \\ 0 & 0 & 0 & 1 \end{bmatrix} \tag{4.17}$$

$$\Theta_Y = \begin{bmatrix} C\left(\begin{matrix}\theta_y(t)+\\ \beta(\theta_y,t)\end{matrix}\right) & -\gamma(\theta_y,t)\ C\left(\begin{matrix}\theta_y(t)+\\ \beta(\theta_y,t)\end{matrix}\right) & S\left(\begin{matrix}\theta_y(t)+\\ \beta(\theta_y,t)\end{matrix}\right) & \Delta x(\theta_y,t) \\ \gamma(\theta_y,t) + \alpha(\theta_y,t)\ S\left(\begin{matrix}\theta_y(t)+\\ \beta(\theta_y,t)\end{matrix}\right) & 1 & -\alpha(\theta_y,t)\ C\left(\begin{matrix}\theta_y(t)+\\ \beta(\theta_y,t)\end{matrix}\right) & \Delta y(\theta_y,t) \\ -S\left(\begin{matrix}\theta_y(t)+\\ \beta(\theta_y,t)\end{matrix}\right) & \alpha(\theta_y,t) + \gamma(\theta_y,t)\ S\left(\begin{matrix}\theta_y(t)+\\ \beta(\theta_y,t)\end{matrix}\right) & C\left(\begin{matrix}\theta_y(t)+\\ \beta(\theta_y,t)\end{matrix}\right) & \Delta z(\theta_y,t) \\ 0 & 0 & 0 & 1 \end{bmatrix} \tag{4.18}$$

The ideal transformation matrix with no error terms is shown in Equation 4.19. It was calculated by setting all of the error terms $\{\alpha,\beta,\gamma,\Delta a,\Delta b,\Delta c,\Delta x,\Delta y,\Delta z\}$ in the individual transformation matrices to zero. Both the ideal and the real transformation matrices were solved using Maple, a symbolic mathematical computer package. The ideal and real transformation matrices were used in initial computer simulations to study the proposed compensation strategy.

$$T_{Ideal} = \begin{bmatrix} C\theta_y & 0 & S\theta_y & \begin{matrix} a_{T_6}C\theta_y + c_{T_6}S\theta_y + \\ a_{T_5} + a_{T_4} + a_{T_3} + a_{T_2} + a_{T_1} + X \end{matrix} \\ S\theta_x S\theta_y & C\theta_x & -S\theta_x C\theta_y & \begin{matrix} a_{T_6}S\theta_x S\theta_y + b_{T_6}C\theta_x \\ -c_{T_6}S\theta_x C\theta_y + b_{T_5}C\theta_x - c_{T_5}S\theta_x + \\ b_{T_4} + b_{T_3} + b_{T_2} + b_{T_1} + Y \end{matrix} \\ -C\theta_x S\theta_y & S\theta_x & C\theta_x C\theta_y & \begin{matrix} -a_{T_6}C\theta_x S\theta_y + b_{T_6}S\theta_x + \\ c_{T_6}C\theta_x C\theta_y + b_{T_5}S\theta_x + c_{T_5}C\theta_x + \\ c_{T_4} + c_{T_3} + c_{T_2} + c_{T_1} + Z \end{matrix} \\ 0 & 0 & 0 & 1 \end{bmatrix} \quad (4.19)$$

Notice how the 3×3 orientation sub-matrix of Equation 4.19 is independent of the translational motion in X, Y, or Z, while the 3×1 position sub-matrix is dependent on both translation and rotation.

The real transformation matrix, including the error terms, is considerably more complex. It was impractical to solve this matrix multiplication problem symbolically, due to the large number of terms in each element. Therefore, it was necessary to ignore the

higher order error terms after every multiplication of the matrices in Equation 4.12. Even with this simplification, the real transformation matrix is still too large to be included here. This complexity in the real transformation matrix arises from the interaction of the error terms in the body of the machine in establishing the volumetric error in the work space. Due to the complexity of the final transformation matrix, which contained all of the error terms, it was not realistic to get a closed form solution for the compensation values which canceled the error in the work space. Therefore, a different approach to solving for the compensation values was used. It is outlined further in the section on compensation value calculation.

When studying the accuracy of the machine, many error terms have very small contributions which can be ignored. An example is a small angle error term which only acts through a small distance. For the model used in this work, the full transformation matrix was considered so as to be general enough to deal with the variety of configurations and error sources that are possible on a machine tool.

4.3 Error Allocation

The inverse kinematic model was used to allocate the error measured in the work space, that is the matrix E, to the region on the machine where the error was generated. If the error was generated due to the spindle motor, then the error should be allocated to matrix T_1. The formula describing this relationship is shown in Equation 4.19. Similar relationships between the error in the work space and individual components were generated

for each major component on the machine. This process of allocation was done to better understand the relationship between the error terms in the structural components and the temperature distribution in the machine. Previously, researchers related the data from a limited number of error points in the work space to different temperatures measured on the machine. This would force their identification technique to learn the kinematics, as well as the error relationships.

$$T_1 = [E]^{-1}[T_6]^{-1}[\Theta_Y]^{-1}[T_5]^{-1}[\Theta_X]^{-1}[T_4]^{-1}[\Phi_X]^{-1}[T_3]^{-1}[\Phi_Y]^{-1}[T_2]^{-1}[\Phi_Z]^{-1} \qquad (4.20)$$

The relationships which define the error terms making up the matrices in Equation 4.20, must be established one at a time based on separate tests. This was necessary so that the error measured in the work space could be allocated to the one region with the active heat source. In this way, the full error relationship was constructed. This method increased the number of tests required to gather all of the error data. Originally, all of the error terms in the individual matrices are set to zero. Then, the error in the work space measured during one test is added, and the error terms for the area in question are solved and added to the model before the results of the next test are included.

The order in which the individual error matrices were solved and added to the complete model was important because of the interrelation of the machine components. This order was carefully considered so as to relate the error generated in the work space to only one specific region on the machine. If too many heat sources were run at one time, it

would have been difficult to relate the error in the work space to the specific condition on the machine that generated the error.

The spindle support structure was modelled first because it contained the dominant heat sources, namely the spindle motor and bearings. The next closest structure in the chain was the Z axis which was mounted on the Z column. This heat source was then activated by moving the Z axis back and forth with a high feedrate. Since the model already contained the relationship between the spindle support structure and the error in the work space, any additional error measured could be related to the Z axis. The next interaction considered was the error due to the Y axis motion.

The Y axis motion influenced two areas on the machine. One was related to the Y axis sliding surfaces, ballscrew, and motor, while the other was the heating of the Z column by the Y axis motor. The Z column was warmed by the heat travelling up from the Y axis motor, which was mounted in the bottom of the Z column. Since the relationship for the temperature distribution in the Z column was already included in the model, the residual error could be attributed to the contribution from the Y axis slides and ballscrews. As each error relationship was developed, it was added to the model and any unmodelled error was attributed to the new heat source that was activated during the next test.

If the error is not allocated to the specific region on the machine where it is generated, then one runs the risk that a good correlation to the error shown by a thermocouple might only be temporary, since a change in the environment might affect this relationship. This would occur if a thermocouple were mounted on a component which happened to have the same time constant as the error in the work space. This would be less likely to occur if the

error were related to the specific region where it was generated, and only the thermocouples that were located close to the source of the error were used. In this way, there is a higher level of certainty that models are based more on the underlying physical relationship of the machine, instead of on coincidental, and thus, unreliable relationships.

The process of inverting the transforms required to solve Equation 4.20 is greatly simplified when the matrices are in the form of HTMs as shown previously in Equation 4.1. With this form, one can take advantage of the inherent structure of the matrix. The formulation of the matrix inversion is outlined in Equations 4.21 and 4.22. Any unmodelled error that remained after off-line modelling would have to be built into a separate model using on-line data taken while production was running.

$$ {}^{R}T_{0} = \left[\begin{array}{c|c} O & P \\ \hline 0 & 1 \end{array}\right] \tag{4.21} $$

$$ {}^{R}T_{0}^{-1} = \left[\begin{array}{c|c} O^{T} & -O^{T}P \\ \hline 0 & 1 \end{array}\right] \tag{4.22} $$

Error values were measured on-line using a procedure of process intermittent probing and gauging. This is described further in the experimental methods section of this thesis. The model created for the on-line errors was kept separate from the off-line model because of the nature of the data. The data that could be collected during production could not be allocated to individual components by the same method as that used to allocate errors

measured off-line. This was due to the difficulty in separating the individual heat sources which were already dictated by the programmed machining path. Thus, separate models relating the error in the work space to individual sensor terms had to be created. However, the experience gained in allocating the error terms in the off-line model could be applied to the on-line model by relating the same inputs to the error components measured in the work space. For example, if thermocouples mounted on the Z column showed the highest degree of correlation to the Z error in the off-line model, then they would be ideal candidates for forming the on-line model.

4.4 Compensation Value Calculation

Compensation was conducted in a similar way to the allocation of the error terms. In this case, however, the transformation equations were solved to find the axis motions which cancelled the error in the work space. This was done by adding special compensation terms compX, compY, compZ, compθ_Y and compθ_X to the relevant elements in the matrices associated with the degrees of freedom in Equations 4.14 - 4.18. Sample transformation matrices, including the compensation terms, are show in Equations 4.23 and 4.24, for the X axis translation and the θ_Y axis rotation respectively.

$$\Phi_X = \begin{bmatrix} 1 & -\gamma(x,t) & \beta(x,t) & X+\Delta x(x,t)+compX \\ \gamma(x,t) & 1 & -\alpha(x,t) & \int_0^x \gamma(x,t)dx \\ -\beta(x,t) & \alpha(x,t) & 1 & -\int_0^x \beta(x,t)dx \\ 0 & 0 & 0 & 1 \end{bmatrix} \tag{4.23}$$

$$\Theta_Y = \begin{bmatrix} C\begin{pmatrix}\theta_y(t)+\\ \beta(\theta_y,t)+\\ comp\theta_y\end{pmatrix} & -\gamma(\theta_y,t)\ C\begin{pmatrix}\theta_y(t)+\\ \beta(\theta_y,t)+\\ comp\theta_y\end{pmatrix} & S\begin{pmatrix}\theta_y(t)+\\ \beta(\theta_y,t)+\\ comp\theta_y\end{pmatrix} & \Delta x(\theta_y,t) \\ \alpha(\theta_y,t)\ S\begin{pmatrix}\gamma(\theta_y,t)+\\ \theta_y(t)+\\ \beta(\theta_y,t)+\\ comp\theta_y\end{pmatrix} & 1 & -\alpha(\theta_z,t)\ C\begin{pmatrix}\theta_y(t)+\\ \beta(\theta_y,t)+\\ comp\theta_y\end{pmatrix} & \Delta y(\theta_y,t) \\ -S\begin{pmatrix}\theta_y(t)+\\ \beta(\theta_y,t)+\\ comp\theta_y\end{pmatrix} & \gamma(\theta_y,t)\ S\begin{pmatrix}\alpha(\theta_y,t)+\\ \theta_y(t)+\\ \beta(\theta_y,t)+\\ comp\theta_y\end{pmatrix} & C\begin{pmatrix}\theta_y(t)+\\ \beta(\theta_y,t)+\\ comp\theta_y\end{pmatrix} & \Delta z(\theta_y,t) \\ 0 & 0 & 0 & 1 \end{bmatrix} \tag{4.24}$$

The compensation terms for each degree of freedom are updated as new thermocouple data becomes available. An example of the transformation equations used to solve for the angle matrix Θ_X and the translational matrix Φ_Z are shown in Equations 4.25 and 4.26 respectively. The angle compensation terms are solved first and applied to the

equations before solving for the translation compensation terms. This is done to include the angle component in the position compensation value calculation. These compensation values are directly applied to the next motion command for each of the respective axes' motions. The method of applying the compensation values is discussed in the implementation section of this thesis.

$$\Theta_X = [T_4]^{-1}[\Phi_X]^{-1}[T_3]^{-1}[\Phi_Y]^{-1}[T_2]^{-1}[\Phi_Z]^{-1}[T_1]^{-1}[T_6]^{-1}[\Theta_Y]^{-1}[T_5]^{-1} \quad (4.25)$$

$$\Phi_Z = [T_1]^{-1}[T_6]^{-1}[\Theta_Y]^{-1}[T_5]^{-1}[\Theta_X]^{-1}[T_4]^{-1}[\Phi_X]^{-1}[T_3]^{-1}[\Phi_Y]^{-1}[T_2]^{-1} \quad (4.26)$$

4.5 Simulation Results

A simulation study, using the kinematic model of the machine in place of the actual machine, was done to test the performance of the compensation strategy. This was done to learn more about the interaction between the individual error terms for machine components and the volumetric error in the work space. Since the experiments required to identify the empirical model had not yet been done, relationships for the error terms (α, β, γ, Δx, Δy, Δz, Δa, Δb, Δc) in each matrix were modelled using linear and exponential terms. Link errors were defined as changing exponentially with time, while joint errors were defined as varying linearly with position and exponentially with time. The linear functions modelled the kinematic errors in the joints, while the exponential functions modelled the thermal errors. Terms were also included for backlash in the axes and the positioning resolution of the machine. The coefficients used to establish the model were based on the results report by Venugopal (1985) for a horizontal three-axis milling machine. Since the machines were structurally different, similarly sized components were given coefficients to match the errors reported on the horizontal machine. The coefficients were assigned values based on their relative size and closeness to major heat sources as compared to the machine configuration reported by Venugopal. The coefficients making up the model are included in Appendix A.

From the simulation results, the interaction of error terms at each link and joint can be seen to generate nonlinear error relationships in the work space. See Figure 4.6 for details on the error in the work space resulting from a simple case of machine error.

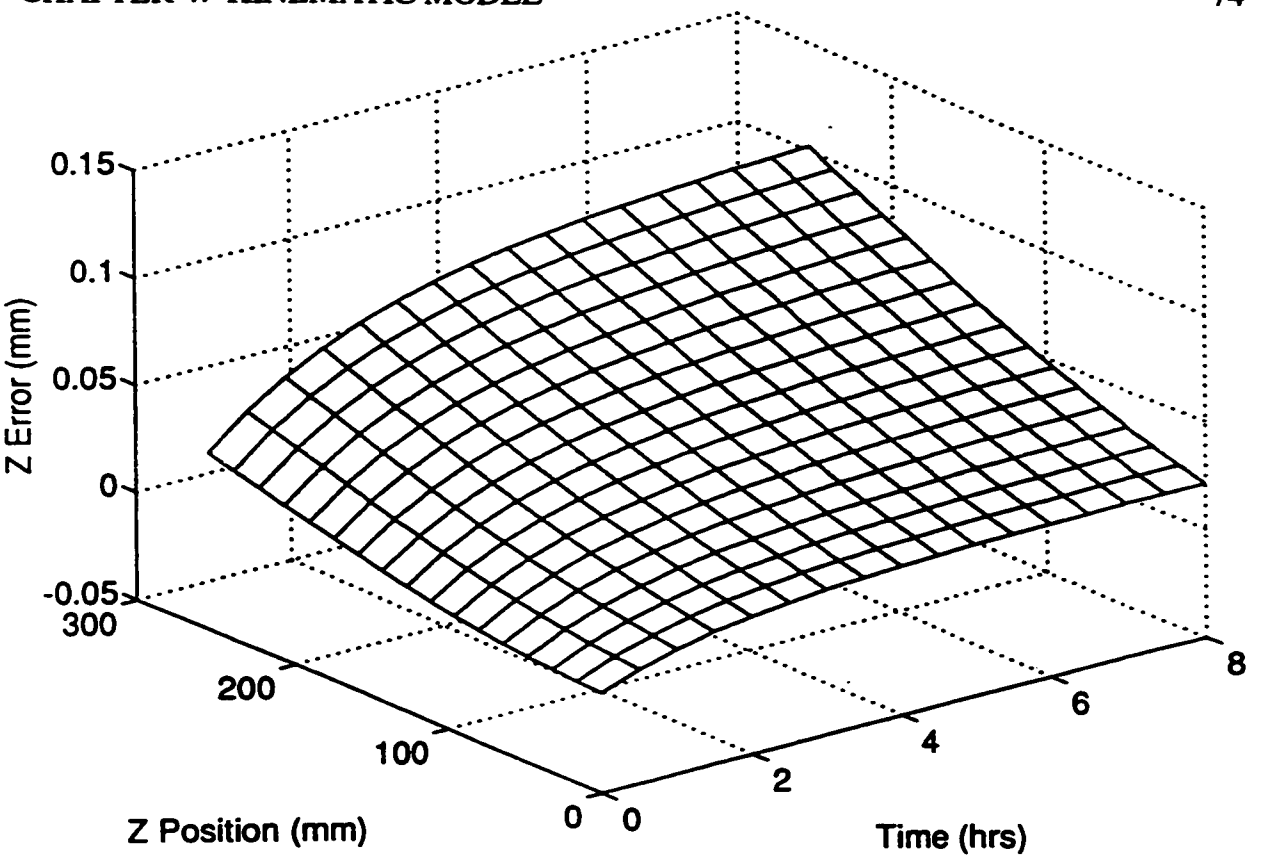

Figure 4.6 Simulation of Error in the Work Space

Figures 4.7 and 4.8 show the results of the compensation strategy on the simulated error terms. The programmed motion was a sinusoid for all of the axes, hence the oscillations in the data. The uncompensated error in the figure was due to the positioning resolution of the machine.

These results showed that if the error terms could be fully modelled, then the compensation strategy would be able to reduce the error in the work space to the level of the resolution of the machine tool, provided that the machine was set up in its optimum orientation. The simulation of the kinematic model also showed that to compensate fully for a θ_X angle error, motions in Z, Y, and θ_X axis were all required for this configuration of

machine. From this, it can be seen that the kinematic model captured the coupling of the translational joints with the rotational joints.

Setting up the machine and work piece in their optimal orientation was necessary to account for the fact that there were only five axes available to compensate for six degrees of freedom. The sixth error term in the work space, which was aligned with the roll angle error for the Z axis would typically not be relevant as this angle error would be in the direction of the rotating spindle and would not transfer itself onto the part. However, if this angle error acted through a distance, it would result in a translation error which must be compensated for by appropriate translations in the plane. For this reason, the roll error for the Z axis motion was still measured and included in the empirical model.

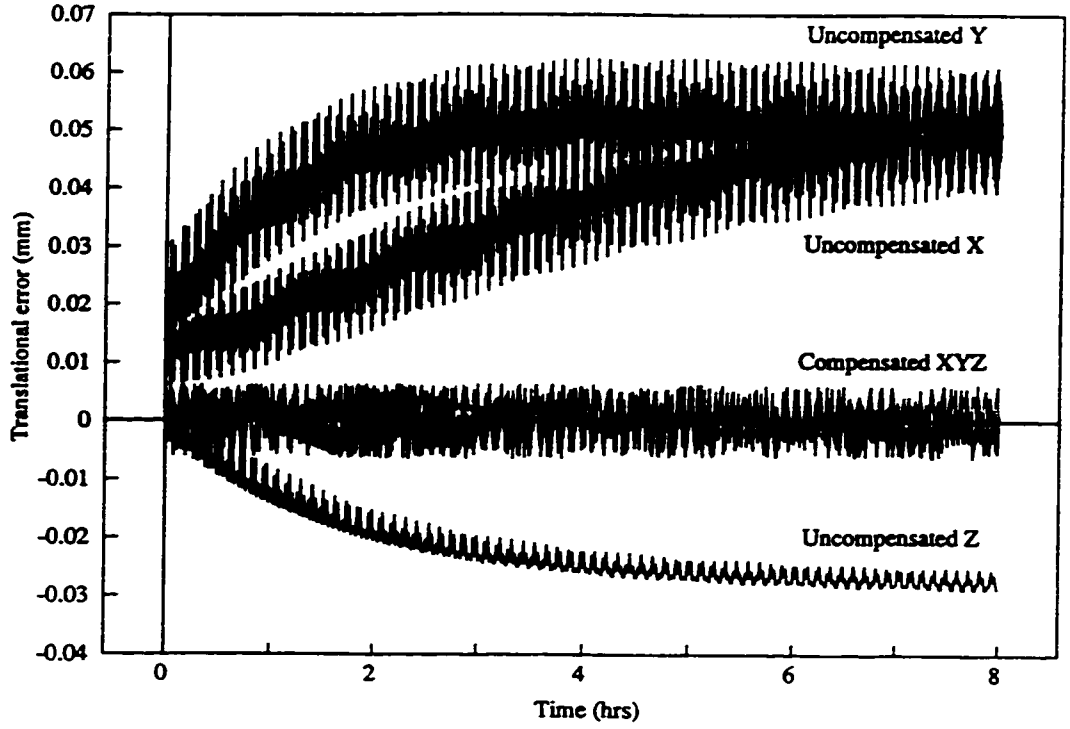

Figure 4.7 Translational Errors With and Without Compensation

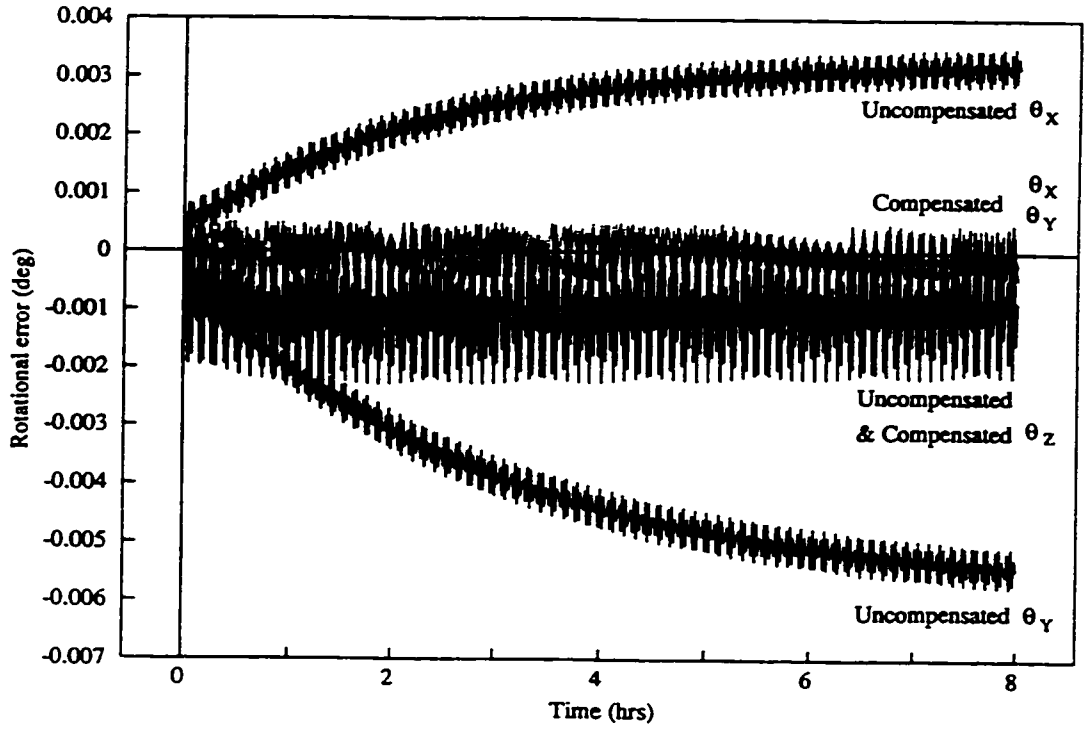

Figure 4.8 Rotation Errors With and Without Compensation

If the axes of the machine are not aligned favourably, for example, if A rotates to align B with the spindle, then the ability of the machine to compensate for errors in the θ_Y direction would be lost. Furthermore, the B axis would be effectively redundant for most operations, in that interpolating X and Y motion would have the same effect as rotating the B axis. Therefore, it was important to align the axes of the rotary table in such a way that the A axis of the rotary table was capable of compensating for the dominant angle error. Also, the part must be mounted in the work space so that an alignment of the B axis with the spindle would not occur when precise machining would be required. Therefore, how the part was fixtured in the work space would play an important role in determining the flexibility of five-axis machining and also the amount of compensation possible.

The accuracy of the machine in different directions and in different orientations can be used to the operator's advantage. This could be done by orientating the part, so that the critical dimension was cut in the machine's most stable direction. Most machines will have a stable direction due to the symmetry of the machine's structure and heat sources. For the machine used in this work, the angle error in the θ_Y direction was small compared to the θ_X direction, and the position error in the X direction was much smaller than the Z direction. Thus, the machine would naturally produce a more accurate surface if the critical plane was angled to be more aligned with the Y-Z plane instead of the X-Y plane of the machine.

4.6 Summary

This chapter discussed the development of the kinematic model for a five-axis machine. The kinematic model includes error terms which capture the geometric, kinematic, and thermal errors described in the machine tool error chapter. The kinematic model was used to allocate the error measured in the work space to the individual components on the machine. It was also used to find the compensation values used in the compensation strategy. The simulation studies showed that the theoretical limit of the compensation strategy would be the resolution of the machine which was 0.0025 mm and 0.001°. This chapter also discussed the issues associated with the configuration of the machine and the placement of the work piece for compensating for the six degrees of freedom using five axes of motion. The next chapter discusses how the error terms were measured in the work space.

CHAPTER 5

EXPERIMENTAL METHODS

5.1 Introduction

This chapter outlines the experimental considerations taken into account when collecting the data to build the empirical models of the machine tool. The design of the thermocouples and methods used for their calibration are discussed. The methods used to measure the errors in the work space are also outlined along with the calibration procedures used. Details are also provided on the equipment setup used during the various tests.

5.2 Experiment Design

Special care was taken when designing the experiments to ensure that the test cases covered realistic operating conditions. Unfortunately, due to the requirements of the laser interferometer, no metal cutting could be done while measuring with the laser. However, the conditions used for identifying the system would be similar to those expected during production. This is because the main application for this compensation strategy is on accurate light finishing cuts in which the cutting forces would be small. Figure 5.1 shows an example of the machine conditions under which the error in the Z axis motion was studied.

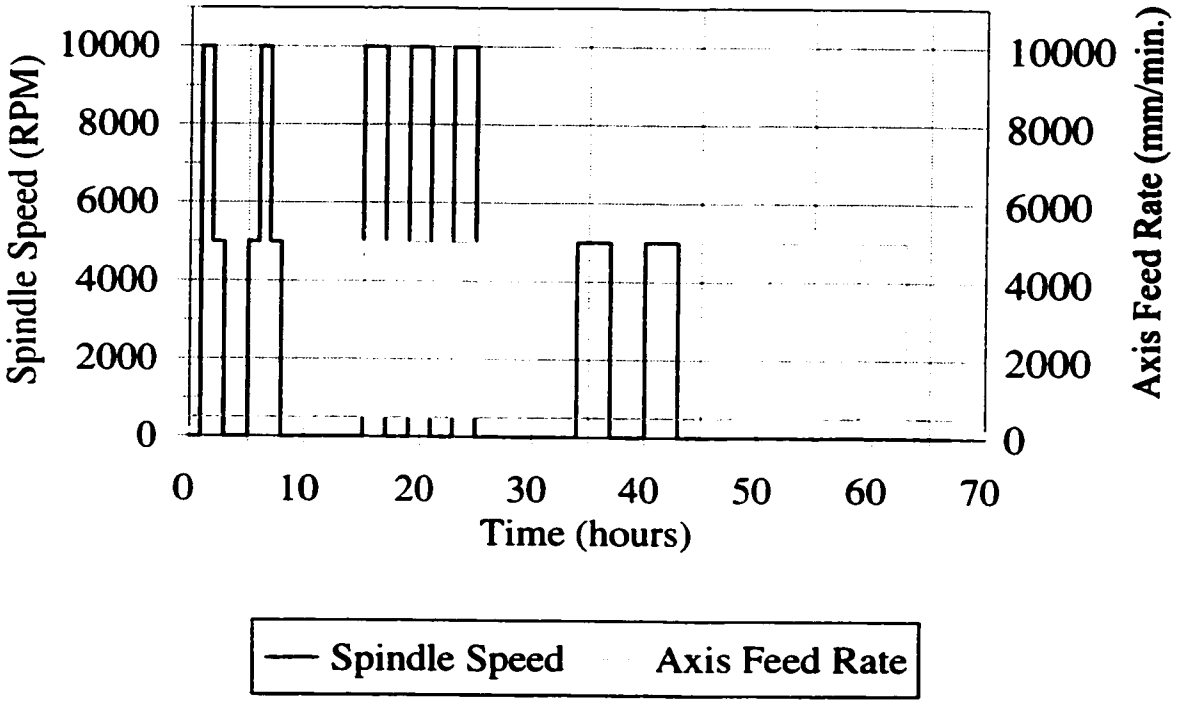

Figure 5.1 Sample Machine Testing Conditions

This test was used to study the effect of thermal gradients present in the structures near the active heat sources. The spindle speed and the axis feed rate were commanded separately to study their contribution independently, and then together to learn about their interaction.

In general, while the machine was operating, the overall temperature in the structure would rise. If the surrounding environment was not climate controlled, it would also be influenced. This tended to make the output from each thermocouple somewhat correlated. Effort was made to separate the temperature rise at each individual thermocouple as much as possible, given the operating constraints of the machine. This was done by carefully controlling the order in which heat sources were added to the test. Certain heat sources could not be separated. For example, the heat from the electronics panel was always present when the machine was on. However, as this would normally be the case, it was not expected to cause serious problems in implementation.

5.3 Temperature Measurement

The thermocouple design used in this research was based on recommendations made by Attia and Kops (1993). They found that the best results for surface temperature measurements on machine tools were made using type E thermocouple wire. Type E wire is a junction of Chromel and Constantan and has low thermal conductivity; therefore, it conducts a small amount of heat away from the junction. Furthermore, type E wire is known

to have a high output level, thereby, making the temperature measurements less susceptible to noise than other wires. Attia and Kops also recommended embedding the thermocouple in a copper disk with a radius greater than twenty times the diameter of the thermocouple wire. A sketch of the thermocouple design is shown in Figure 5.2. Using a high thermal conductivity glue, the thermocouple was glued inside the copper disk and then glued onto the structure of the machine tool. In this way, a high level of thermal conduction between the structure of interest and the thermocouple junction was achieved. Thus, the heat conducting across the thermocouple and machine interface would dominate over the amount convecting across the side exposed to room temperature. Stainless steel shielding on the wire was used to protect it from physical damage, as well as from electrical noise. Furthermore, the thermocouple wires were run as far as possible from known electrical noise sources, like the servo motors and resolvers. During preliminary testing, the output of the thermocouples was not found to vary significantly whether the machine's major electrical noise sources were on or off.

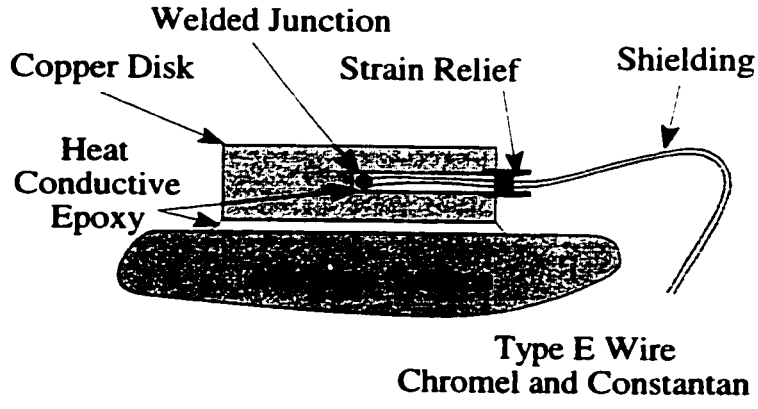

Figure 5.2 Thermocouple Design

The data acquisition card used to collect the temperature values was a DAS-TC, made by Data Translation. This card has the capability to handle the cold junction compensation for the type E thermocouple wire used in this experiment. Experimental testing on a stirred ice bath showed a repeatability of $\pm 0.1\,^{\circ}C$ for the temperature measurements. A procedure for calibrating the thermocouples was also established to take into account any variation between thermocouples due to cable length and the thermocouple weld junction. This information would allow individual thermocouples to be replaced in the future should a thermocouple fail in-service. The thermocouple calibration setup and results are discussed in Appendix B.

The temperature distribution in and around the machine tool was measured using 50 thermocouples. In general, the thermocouples served two distinct functions. The first function was to provide information on heat transferring to and from the system by the heat sources and cooling systems mounted on the machine and through the interaction with the environment. These sensors were mounted near major heat sources like the spindle motor, spindle bearings, spindle drive system, axis motors, axis couplings, ballscrews, bearings, gears, coolant, way lube, and electronics panels. The cooling system was monitored by placing a thermocouple near the spindle bearing, where the chilled fluid flowed. The room temperature was monitored with one thermocouple placed near the top of the machine and the other near the floor. The second function of the thermocouples was to measure the temperature distribution within a structure. This was done by placing a number of thermocouples directly on the surface near the eight corner regions of a structure. Sampling these areas allowed for the estimation of the average temperature and the gradient across a

structural component. Figure 5.3 shows the general location of the thermocouples on the machine and Table 5.1 describes the locations in more detail.

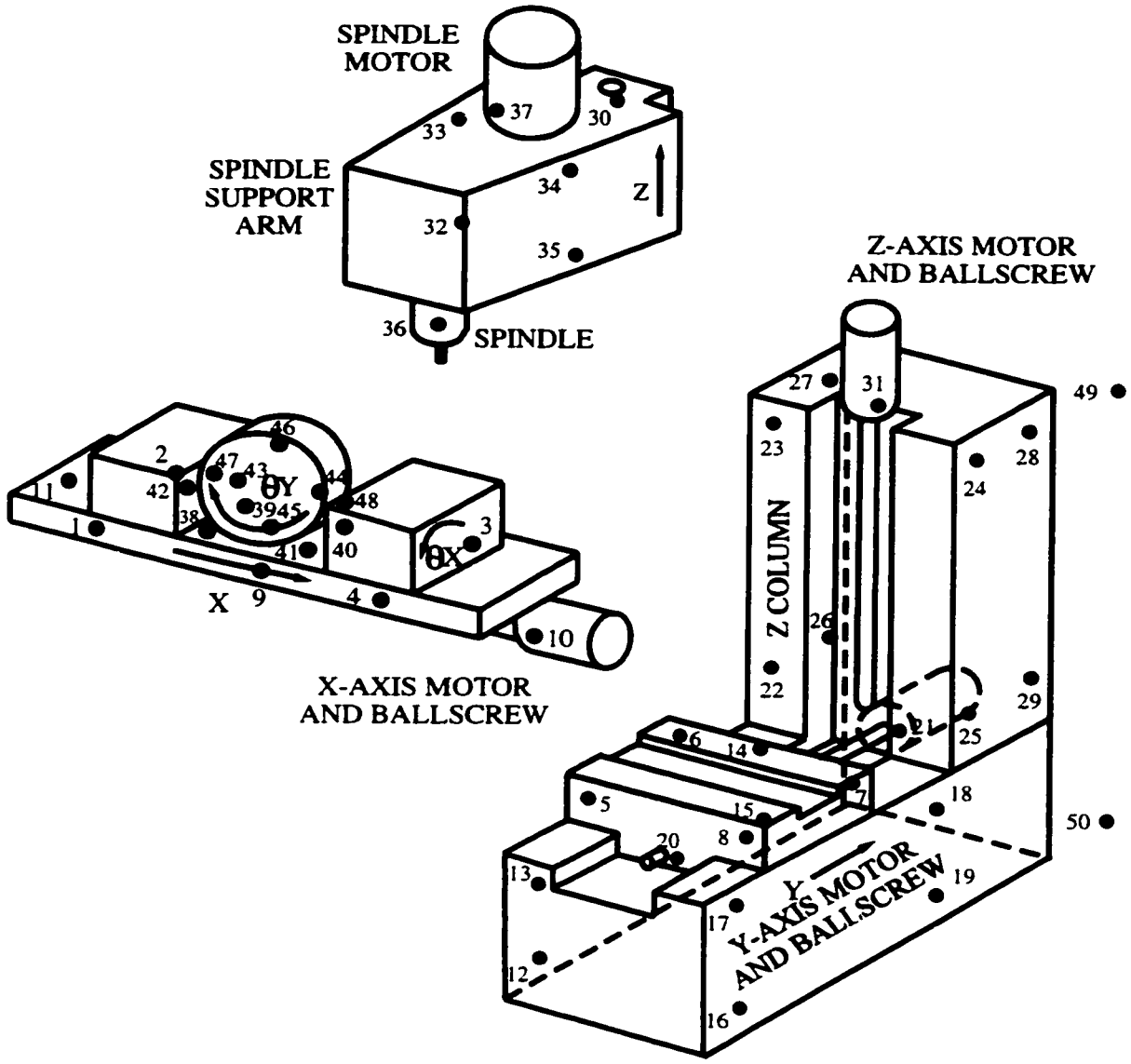

Figure 5.3 Placement of Thermocouples

#T	Location	#T	Location
1	X axis front left corner	26	Lower left back of Z column
2	X axis back left corner	27	Upper left back of Z column
3	X axis back right corner	28	Upper right back of Z column
4	X axis front right corner	29	Lower right back of Z column
5	X-Y carriage front left corner	30	Z axis ballscrew
6	X-Y carriage back left corner	31	Z axis motor
7	X-Y carriage back right corner	32	Lower left spindle support arm
8	X-Y carriage front right corner	33	Upper left spindle support arm
9	X axis ballscrew nut	34	Upper right spindle support arm
10	X axis motor	35	Lower right spindle support arm
11	X axis ballscrew end bearing	36	Main spindle bearing and chilling line
12	Lower left front corner of base	37	Main spindle motor
13	Upper left front corner of base	38	Front left corner of rotary base
14	Upper left back corner of base	39	Back left corner of rotary base
15	Lower left back corner of base	40	Back right corner of rotary base
16	Lower right front corner of base	41	Front right corner of rotary base
17	Upper right front corner of base	42	A Axis motor and gear train
18	Upper right back corner of base	43	Left side of B axis table
19	Lower right back corner of base	44	Right side of B axis table
20	Y axis ballscrew nut	45	Lower side of B axis table
21	Y axis motor	46	Top side of B axis table
22	Lower left front of Z column	47	Left B axis bearing
23	Upper left front of Z column	48	B axis motor and gear train
24	Upper right front of Z column	49	Room temperature at top of machine
25	Lower right front of Z column	50	Room temperature at floor

Table 5.1 Thermocouple Placement

Sample thermocouple outputs for one of the test cases is included in Figure 5.4. The temperature's response to a heat source can be seen as a first order lag function in time. At 12, 30, and 47 hours, the sampling stopped for a short period of time; hence, the sudden steps in temperature at these times. When the spindle was cycled on and off, the temperature near the spindle motor mount was found to vary by close to 20°C. In addition, the figure illustrates how the thermocouples near a heat source, such as the ballscrew, experience large changes, while those far from a heat source, such as the thermocouple on the Z column, experience smaller variations due to the heat generated by the spindle motor. Also, one can see how the temperature changes in the machine follow the room temperature unless a large heat source is active in the direct vicinity around the thermocouple.

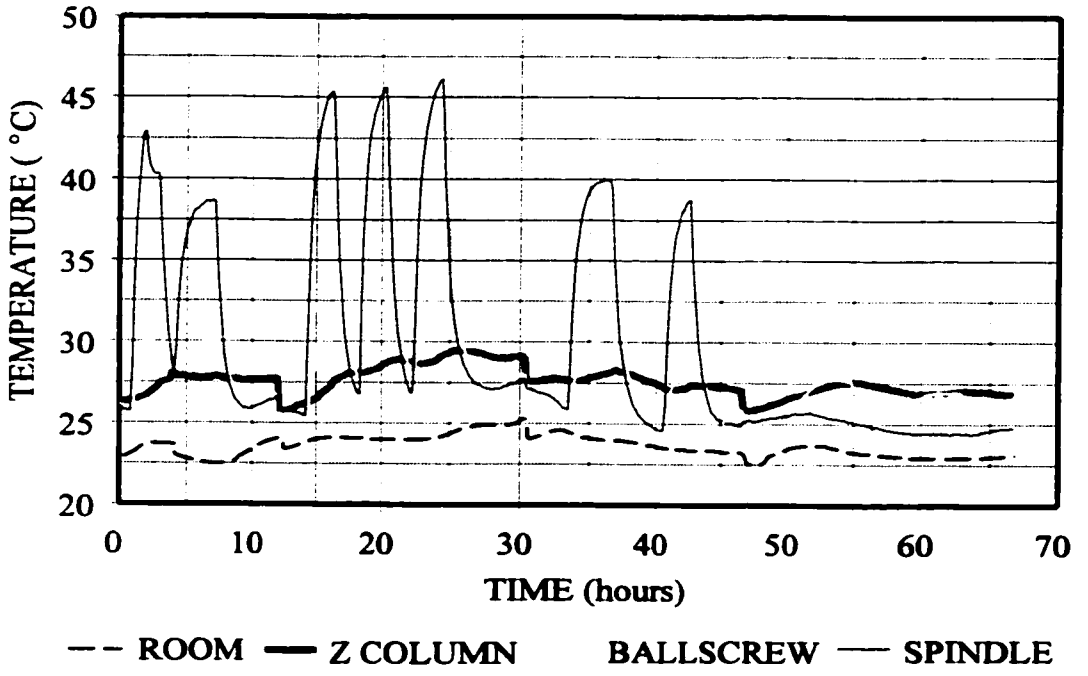

Figure 5.4 Sample Thermocouple Measurements

5.4 Thermocouple Placement

The thermocouple placement strategy involved placing an excess number of them on the machine and reducing their number by studying the correlation between their outputs. Reducing the number of thermocouples was important for improving the robustness of the empirical model and was a necessity for eliminating highly correlated thermocouples for establishing the coefficients of the linear regression model.

Table 5.2 shows the results of a correlation analysis on thermocouples sampled during rapid X axis motion. The measurements were taken in the evening when the room temperature was dropping; hence, the negative correlation between the room temperature thermocouples and those mounted on the machine. In some situations, they could be positively correlated, like when the heat generated by the machine dominated the room and caused a room temperature rise. Room temperature thermocouples provided relevant information as room temperature was a major heat source or heat sink capable of influencing the machine's temperature distribution. Although the ceiling and floor thermocouples were highly correlated, it was important to keep them both, as the relationship could vary depending on whether the air was circulating in the room or if the room temperature was experiencing a change.

Thermocouples T_1-T_4 are mounted on the work piece table and thermocouples T_5-T_8 are mounted on the X-Y carriage. Thermocouples in this area captured the variation in the table and X-Y carriage temperature, due to friction in the sliding surfaces and heat generated in the ballscrew nut. Thermocouples T_1-T_8 were found to correlate very well to one another

	Ceiling	Floor	T_1	T_2	T_3	T_4	T_5	T_6	T_7	T_8	T_9	T_{10}	T_{11}	T_{13}	T_{19}	T_{24}	T_{26}	T_{34}
Ceiling	1	0.98	-0.41	-0.47	-0.52	-0.55	-0.54	-0.58	-0.57	-0.57	-0.48	-0.46	-0.47	-0.16	-0.43	-0.68	-0.70	-0.55
Floor	0.98	1	-0.36	-0.43	-0.47	-0.49	-0.51	-0.53	-0.52	-0.52	-0.47	-0.46	-0.48	-0.12	-0.40	-0.63	-0.66	-0.49
T_1	-0.41	-0.36	1	0.95	0.91	0.90	0.90	0.88	0.88	0.87	0.65	0.57	0.60	0.55	0.53	0.67	0.67	0.55
T_2	-0.47	-0.43	0.95	1	0.96	0.94	0.95	0.94	0.93	0.93	0.76	0.68	0.70	0.48	0.51	0.73	0.73	0.63
T_3	-0.52	-0.47	0.91	0.96	1	0.99	0.97	0.97	0.98	0.98	0.80	0.73	0.75	0.44	0.51	0.81	0.81	0.70
T_4	-0.55	-0.49	0.90	0.94	0.99	1	0.96	0.97	0.99	0.99	0.76	0.69	0.71	0.49	0.56	0.82	0.83	0.69
T_5	-0.54	-0.51	0.90	0.95	0.97	0.96	1	0.98	0.95	0.96	0.83	0.75	0.78	0.45	0.53	0.79	0.79	0.68
T_6	-0.58	-0.53	0.88	0.94	0.97	0.97	0.98	1	0.97	0.97	0.84	0.76	0.79	0.44	0.55	0.83	0.83	0.72
T_7	-0.57	-0.52	0.88	0.93	0.98	0.99	0.95	0.97	1	1.00	0.79	0.73	0.74	0.46	0.55	0.84	0.84	0.71
T_8	-0.57	-0.52	0.87	0.93	0.98	0.99	0.96	0.97	1.00	1	0.81	0.76	0.77	0.43	0.52	0.83	0.83	0.70
T_9	-0.48	-0.47	0.65	0.76	0.80	0.76	0.83	0.84	0.79	0.81	1	0.98	0.98	0.00	0.21	0.69	0.67	0.66
T_{10}	-0.46	-0.46	0.57	0.68	0.73	0.69	0.75	0.76	0.73	0.76	0.98	1	0.99	-0.12	0.09	0.61	0.59	0.58
T_{11}	-0.47	-0.48	0.60	0.70	0.75	0.71	0.78	0.79	0.74	0.77	0.98	0.99	1	-0.05	0.17	0.64	0.63	0.61
T_{13}	-0.16	-0.12	0.55	0.48	0.44	0.49	0.45	0.44	0.46	0.43	0.00	-0.12	-0.05	1	0.73	0.35	0.38	0.21
T_{19}	-0.43	-0.40	0.53	0.51	0.51	0.56	0.53	0.55	0.55	0.52	0.21	0.09	0.17	0.73	1	0.65	0.67	0.50
T_{24}	-0.68	-0.63	0.67	0.73	0.81	0.82	0.79	0.83	0.84	0.83	0.69	0.61	0.64	0.35	0.65	1	0.99	0.92
T_{26}	-0.70	-0.66	0.67	0.73	0.81	0.83	0.79	0.83	0.84	0.83	0.67	0.59	0.63	0.38	0.67	0.99	1	0.89
T_{34}	-0.55	-0.49	0.55	0.63	0.70	0.69	0.68	0.72	0.71	0.70	0.66	0.58	0.61	0.21	0.50	0.92	0.89	1

Table 5.2 Correlation Analysis for Selected Thermocouples

in that they all rose and fell together. Further investigation revealed no significant gradients in this section of the machine. This was because of the thin section of the table and the small heat sources present in the structure. Therefore, thermocouples T_1-T_6 and T_8 were dropped from the analysis. T_7 was selected from this group of correlated thermocouples based on a strategy of evenly distributing the thermocouples throughout the machine. T_7 was part way between the X axis motor and some of the more distant thermocouples on other features.

The main source of error in the X axis direction was due to the elongation of the ballscrew from the heat generated by the rolling friction of the ball bearings under load. Since it was not possible to mount a thermocouple on the ballscrew shaft, it was necessary to predict its temperature by measuring the temperature in the ballscrew nut and driving motor. A thermocouple was placed on both since their heat sources could be independent if the motor was holding a location. Thus, thermocouples T_9 on the ballscrew nut and T_{10} on the motor were saved. T_{11}, which was the thermocouple measuring the temperature of the ballscrew mounting bearing, was not used as it was highly correlated with the temperatures from T_9 and T_{10}, providing little new information.

Thermocouples that were distant from the main heat sources were not highly correlated to thermocouples near the heat source. This was captured in the correlation values relating T_9 or T_{10} to T_{13} and T_{19}. Temperature variation in one section of the machine did not have significant impact on structures far removed from the heat source. Thermocouples T_{24}, T_{26}, and T_{34} were on the Z column and were influenced by the heat generated in the electronics panel mounted on the back of the machine. They showed some degree of correlation with the thermocouples associated with the X axis heat sources because both

areas of the machine heated up. The time constants, however, were different because the masses involved were significantly different.

When building the model, it was very important to keep the physical aspect of the problem in mind. It would be dangerous to try to build a regression model using data that appeared to correlate well to the error, but was in fact coincidental, and therefore, only temporary. This could occur, for example, if the room temperature were rising and a structure with a similar thermal time constant were changing temperature with the error. The stepwise regression technique would identify this as a significant contributor, but if the room temperature were to fall or a nearby heat source were to dominate, then the learned relationship would not hold and significant errors in the prediction would result. This could occur because of the difficulties associated with controlling and separating out the heat sources.

After the analysis on the thermocouple data, the number of thermocouples, as summarized earlier in Figure 5.3, were reduced from 50 inputs to 18. The remaining thermocouples were distributed as follows. The temperature in and around the work piece table and the X and Y axes' structures, were represented by one thermocouple, T_7, which was mounted on the X-Y carriage. The temperature distribution in the ballscrew shafts were represented by three thermocouples T_9, T_{20}, and T_{30} with one mounted on each of the three ballscrew nuts. Each of the five axis motors had a thermocouple with numbers T_{10}, T_{21}, T_{31}, T_{42}, and T_{45} installed on the mounting plate connecting the motor to the machine. In the case of the two rotary axes, these thermocouples also collected the information from the gear train, as they were connected to the wall of the structure where the oil bath flowed for the

rotary gears. The temperature near the spindle motor was captured by T_{37}; it also captured the variation in the spindle temperature. The temperature distribution in the base of the machine was captured using two thermocouples located at the furthest extremes, they were thermocouple numbers T_{13} and T_{19}. Thermocouples T_{24} and T_{26} were used to capture the variation in the Z column of the machine. The temperature distribution in the spindle support arm was captured using thermocouples T_{32} and T_{34}. The room temperature was sampled using two thermocouples T_{49} and T_{50} suspended in the air near the top and bottom of the machine.

5.5 Off-Line Work Space Error Measurement

The error values were measured in the work space using a laser interferometer. Optics were available for measuring errors in position, straightness, and angle in two of the three rotations. The third rotational error was the roll of a moving axis, which could not be measured using a laser interferometer as the movement of the axis caused the beam to be broken. This would necessitate resetting the laser, and thus, losing the initial reference value from the start of the experiment. The means of measuring the error for each of the axes is summarized in Table 5.3. Individual measurement points were sampled ten times with the laser and an average was taken. Sufficient time was left after the motion to ensure that the axis came to a complete stop. Also, each location was sampled by approaching it from both directions. This was done to capture the backlash in the axis. The machine tool had a simple

backlash compensation strategy built into its controller. It was based on backlash values measured at three points along each of its translational axes and one for each of its rotational axes. The parameters which controlled this compensation on the machine were zeroed so that all of the compensation was done in the main compensation strategy.

Axis	Error Terms						
	ΔX	ΔY	ΔZ	θ_X	θ_Y	θ_Z	Squareness
X	Laser	Laser	Laser	Prox / Ref.	Laser	Laser	Reference
Y	Laser	Laser	Laser	Laser	Prox / Ref.	Laser	Reference
Z	Laser	Laser	Laser	Laser	Laser	Prox / Ref.	Reference
A	Prox / Ref.	Prox / Ref.	Prox / Ref.	Laser	Prox / Ref.	Prox / Ref.	Reference
B	Prox / Ref.	Prox / Ref.	Prox / Ref.	Prox / Ref.	Laser	Prox / Ref.	Reference

Table 5.3 Error Measurement Methods

The measurements made by a laser interferometer system were based on the wavelength of light. The Hewlett Packard laser interferometer did not require calibration as the light source was stable; however, the system did require compensation. Compensation was necessary to allow for variations in the wavelength of light in air due to changes in temperature, humidity, and atmospheric pressure. Appropriate compensation values were

set in the laser measurement equipment to account for variation in these weather conditions during every test. The material compensation feature of the laser interferometer was not used in the measurements. This feature would apply a simple two dimensional error estimate of thermal errors in the machine tool structure to the measurements. This would not capture the more complicated three dimensional issues that are of interest in this work.

The typical configuration of the laser system around the machine tool is shown in Figure 5.5, while Figure 5.6 shows how the laser was setup for measuring the Z position error. With this setup, one is capable of measuring position errors to within an accuracy of $\pm$ 0.025 μm, straightness accuracy to within $\pm$ 0.5 μm and angle errors to within $\pm$ 0.1 arc second. The mounting bracket as shown in Figure 5.6 was placed over the spindle and was used to mount the return mirror for the various error measurements. It allowed the laser optics and proximity sensors to be mounted near the spindle while still allowing the spindle to rotate. This position was one step removed from the tool mounting point; however, it was as close to the tool tip as could be realistically achieved while still allowing the spindle to rotate. The error in measurement expected from this component was small, given the bracket's dimensions.

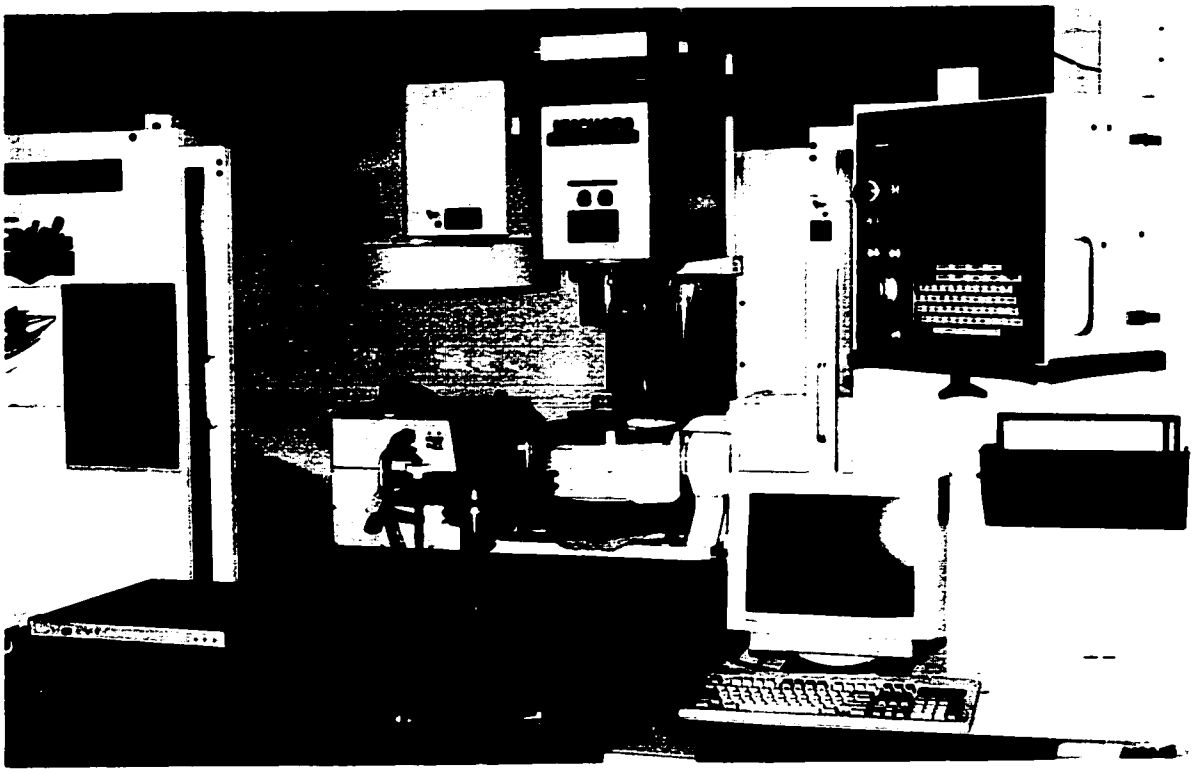

Figure 5.5 Laser Setup by Machine Tool

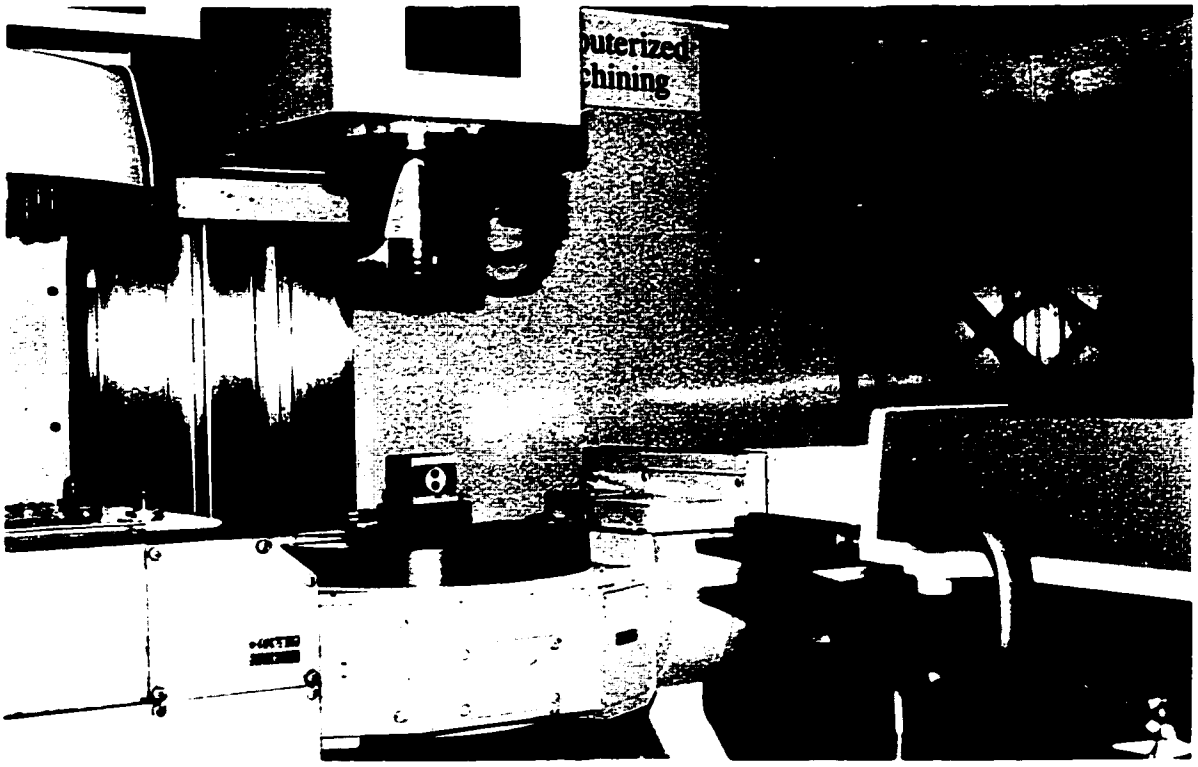

Figure 5.6 Laser Setup for Z Position Error

Figures 5.7 - 5.9 show the laser interferometry components and the path the laser beam took for the various measurement setups used.

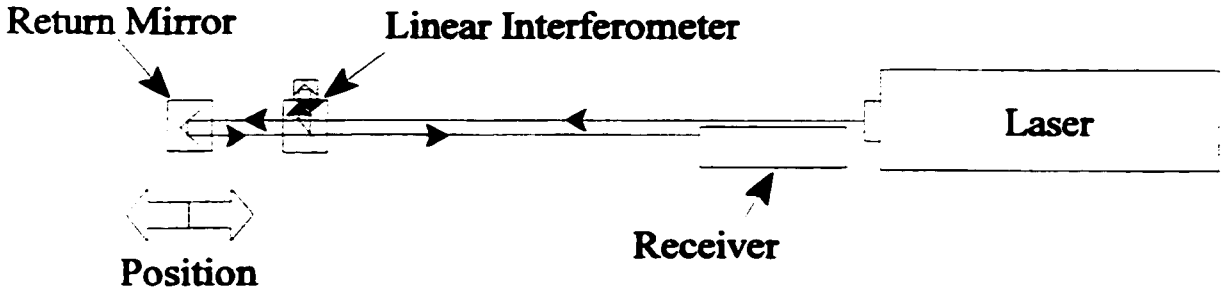

Figure 5.7 Laser Setup for Position Errors

The laser interferometer measured the change in position of the return mirror with respect to the linear interferometer. The return mirror moved with the axis while the linear interferometer was fixed to the machine rigidly.

Straightness measurements are made by comparing the change in length of two different paths between the straightness interferometer and the straightness reflector. The beam path length will change as the straightness reflector translates from side to side. The straightness measurements were adjusted by removing the linear trend across the length. This was necessary to account for the way in which the laser interferometer optics worked when making the measurements.

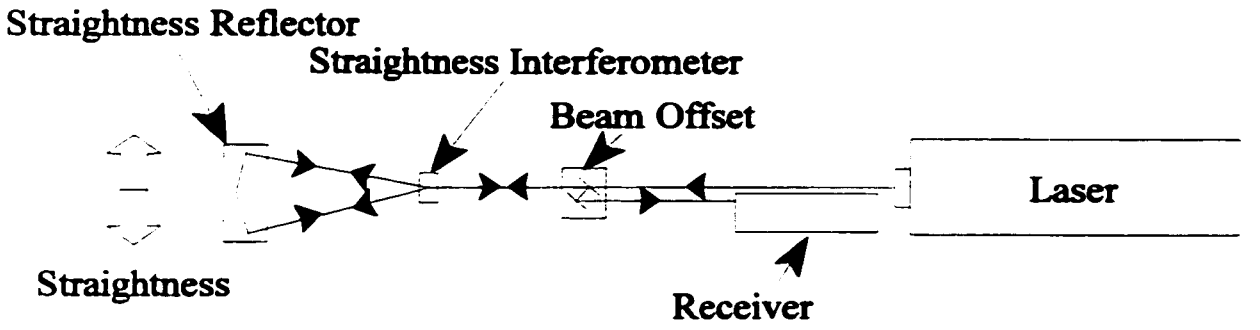

Figure 5.8 Laser Setup for Straightness Errors

The measurement principle of this setup required that the straightness reflector was mounted on the table in place of the work piece and the straightness interferometer was mounted at the tool tip position.

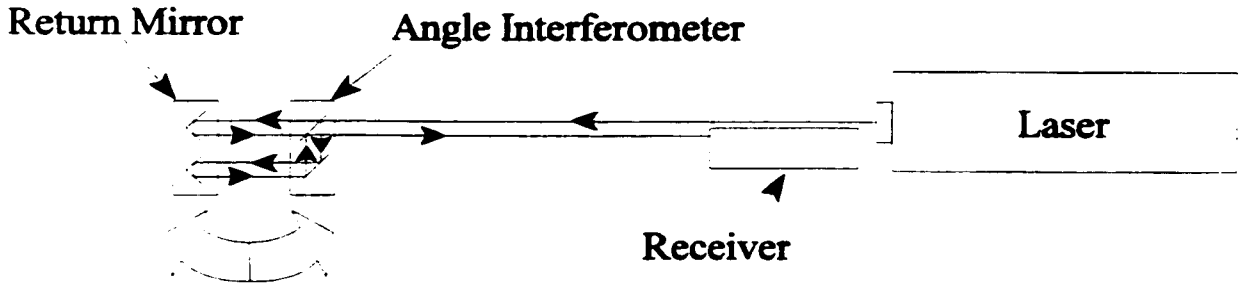

Figure 5.9 Laser Setup for Angle Errors

When measuring angles, the laser interferometer actually measures the change in length between the two mirrors in the return mirror block. Since the distance separating the mirrors is known, then the angle between the return mirror and the angle interferometer can

be calculated. Unfortunately, the laser interferometer was only capable of measuring a small range of angle errors (± 10°) before the optical path was broken. This limited angle range was expanded with the use of a counter rotating table to measure the full 360° of rotation on the rotary table. When the angle advanced to the positive limit of +10°, the counter rotating table would be rotated back -20° to set the laser optics to -10°. Then, the counter rotating table would be fixed in place using a locking pin, and the table could continue rotating to +10° before requiring a counter rotation of -20° again. By measuring the angle before and after moving the rotary table to the next measurement position, any error in the counter rotating table could be subtracted out of the data. The setup of the counter rotating table is shown in Figure 5.10. To facilitate testing, the full 360° range of rotation was only periodically measured, while the main motion that generated the heat was programmed to move within the ± 10° range for extended periods of time.

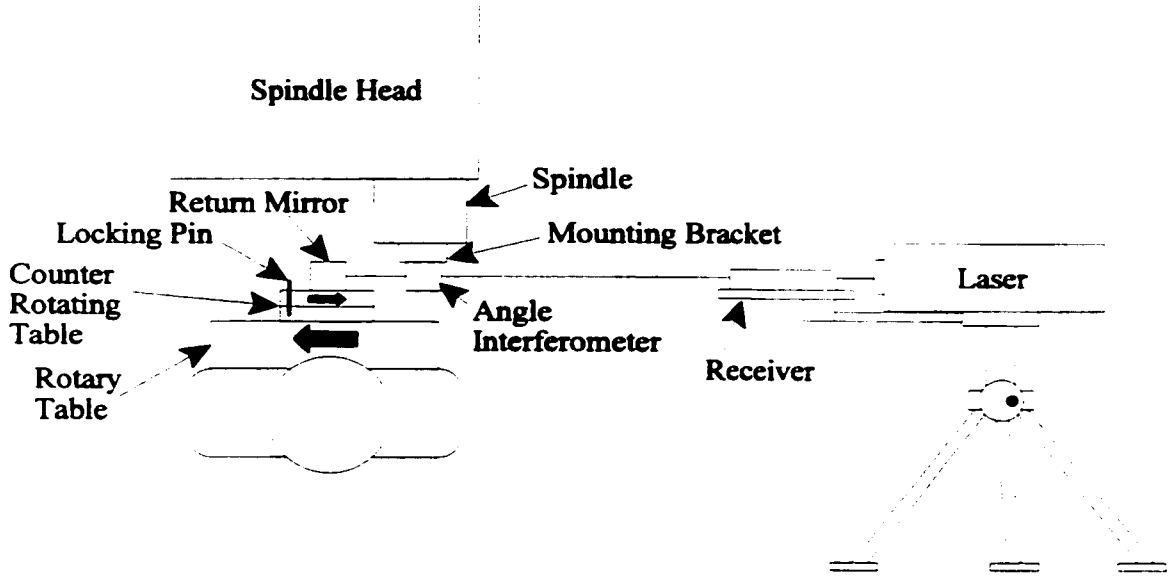

Figure 5.10 Counter Rotating Table to Measure Full 360°

Roll error was measured using a reference surface and a set of proximity probes. For a linear axis, the reference surface consisted of two straight reference lines running parallel to the direction of motion. This setup is illustrated in Figure 5.11. For a rotational axis, the reference surfaces consisted of arcs or cylinders, as shown in Figures 5.12 and 5.13. The centre of the arcs and cylinders coincided with the centre of the axes' rotations. For the case of the arcs, two of these surfaces were placed a known distance apart to provide rotational information in the directions in which the laser could not measure. The proximity sensors were calibrated to relate their voltage output to distance and also to characterize the non-perfect reference surfaces used. The results of the calibration procedure for the proximity sensor setups are included in Appendix C.

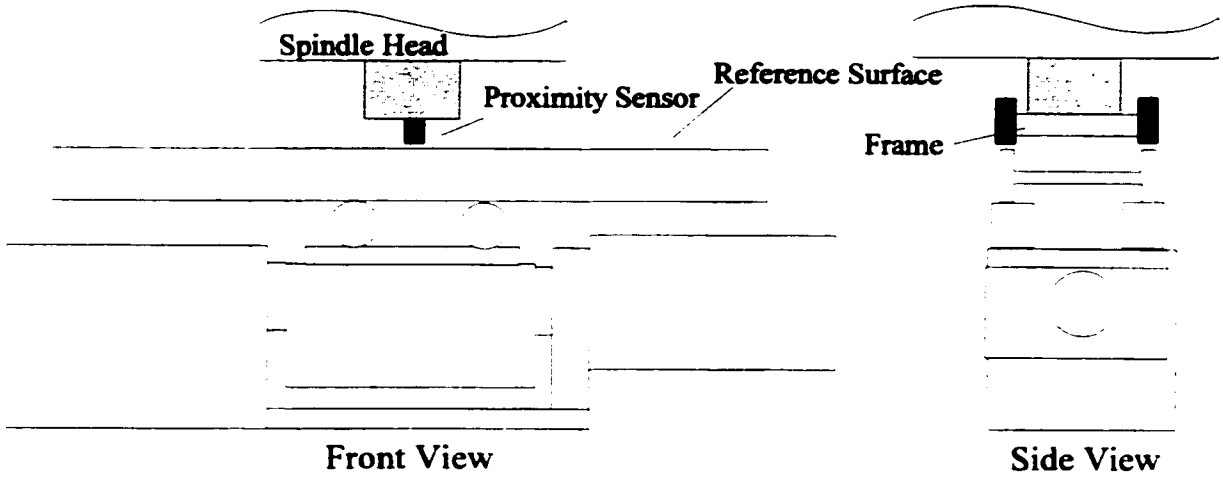

Figure 5.11 Reference Surfaces for Roll Errors in a Linear Axis

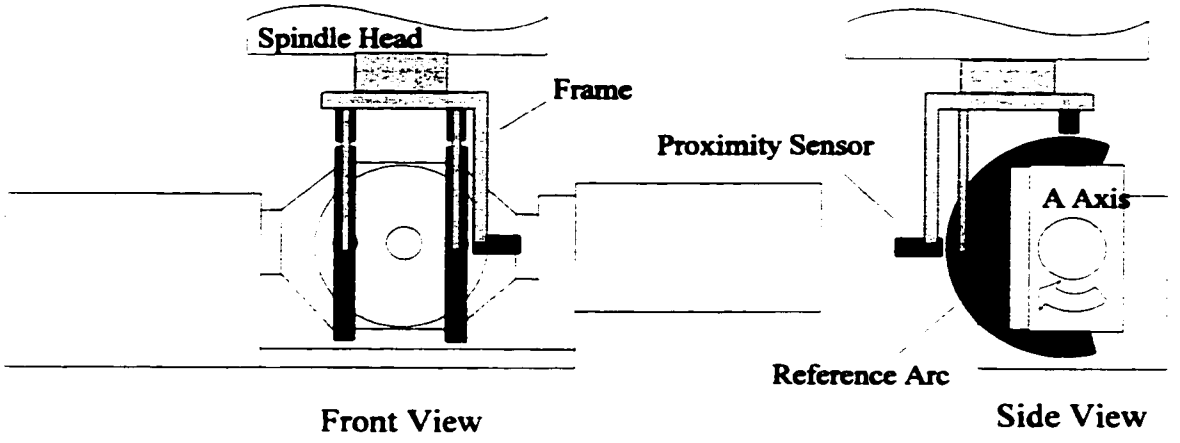

Figure 5.12 Reference Surfaces for Rotary Axis Errors (A Axis)

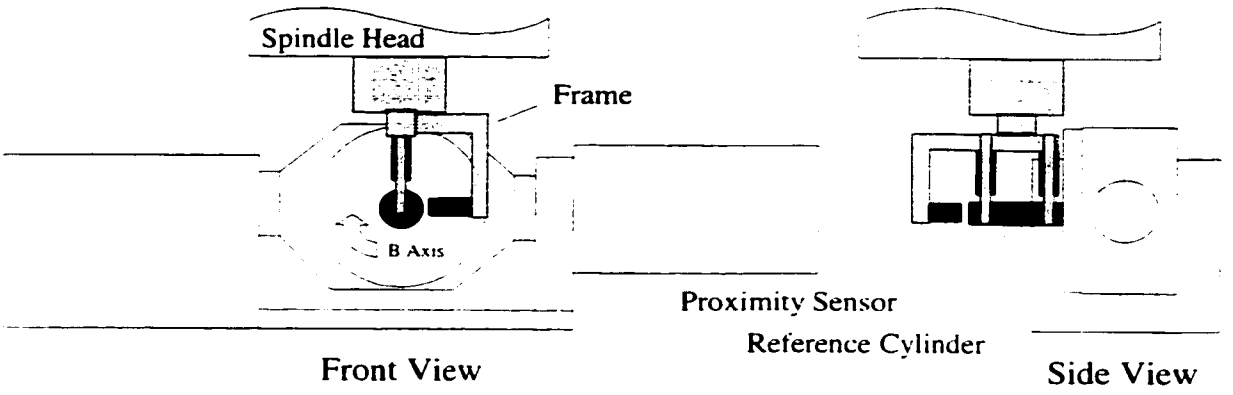

Figure 5.13 Reference Surfaces for Rotary Axis Errors (B Axis)

Error in the perpendicularity between two linear axes and alignment of rotary axes could contribute significantly to the final error in the work space. Such errors were acquired manually by measuring a known reference square with a dial indicator before each angle test. This measurement provided a starting value for the alignment error between two axes and was included in the angle error values for their respective axes. This manual procedure was necessary since the optics required for measuring perpendicularity with the laser were not available at the time of testing.

Equally important to aligning a rotary axis, was determining the location of the centres of rotation. This was found by measuring a reference surface and rotating it three times and then solving for the centre of the arc produced by the three points. These values were used by the post processor to calculate the required offset motion for each angle of rotation. This was necessary to take the linear position change into account when commanding a purely rotational motion. These values were used in the compensation strategy when the kinematics were calculated and when the motion code for a specific part was generated.

The Z position error for the motion of the Z axis is shown in Figure 5.14 and the α angle error for Z motion is shown in Figure 5.15. The α angle is the angle error about the X axis direction for motion in the Z direction. The remaining error graphs for oscillating motion are included in Appendix D. From the slope of the error line with respect to position in Figure 5.14, one can see that the ballscrew pitch varies as the machine warms up over time. Thus the machine tool builder could select their ballscrew pitch based on their expected operating temperature, which due to the friction involved would be typically higher

than 20°C. This would be done to make the machine most accurate at the average operating temperature. This implies that the positioning would be undersized at start up, and oversized if the machine should exceed the average operating temperature chosen by the machine builder. The reversal errors, due to backlash, are not shown in Figures 5.14 and 5.15 since the data points would be obscured by one another, and thus, hard to read. However, the reversal error would create a new plotted surface just below the surface shown and would change over time as the machine warmed up. In a rotary joint, for example, the gears would increase in size, which would reduce the backlash between the individual teeth, and thus, reduce the reversal error.

The superposition of various thermal effects can also be seen in the position error over time. This would occur because different structural components have different thermal time constants depending on their size, coefficient of conduction, and proximity to major heat sources.

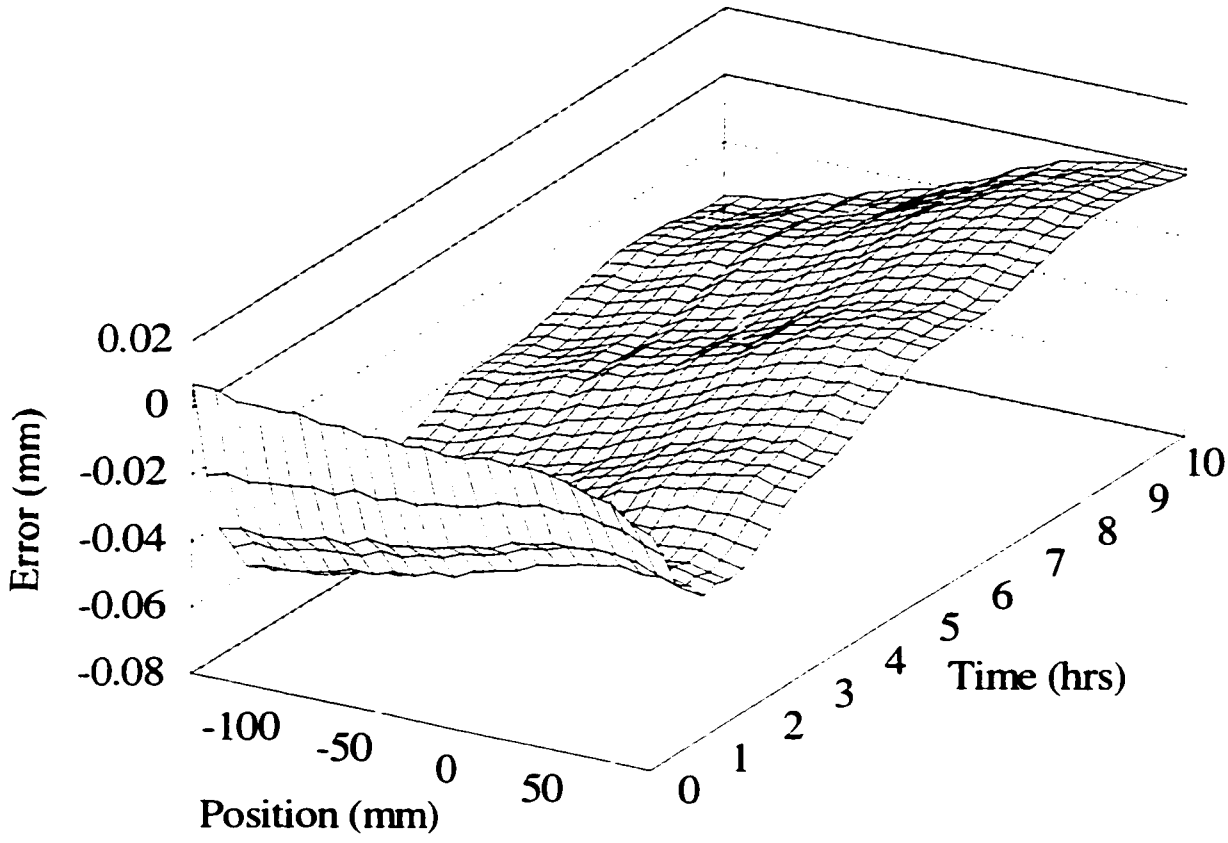

Figure 5.14 Z Position Error for Z Motion

The large initial change in Z position was mainly due to bending in the spindle support arm. This same bending induced an α angle error as well, as shown in Figure 5.15. This error changed rapidly due to the fact that a temperature gradient could occur in the main spindle support section in a short period of time. This was because the spindle motor created a large amount of heat in a confined region of the machine. Once this transient was stable, the angle error did not change, and the position error only changed slowly in response to growth in the Z column, which had a much longer time constant.

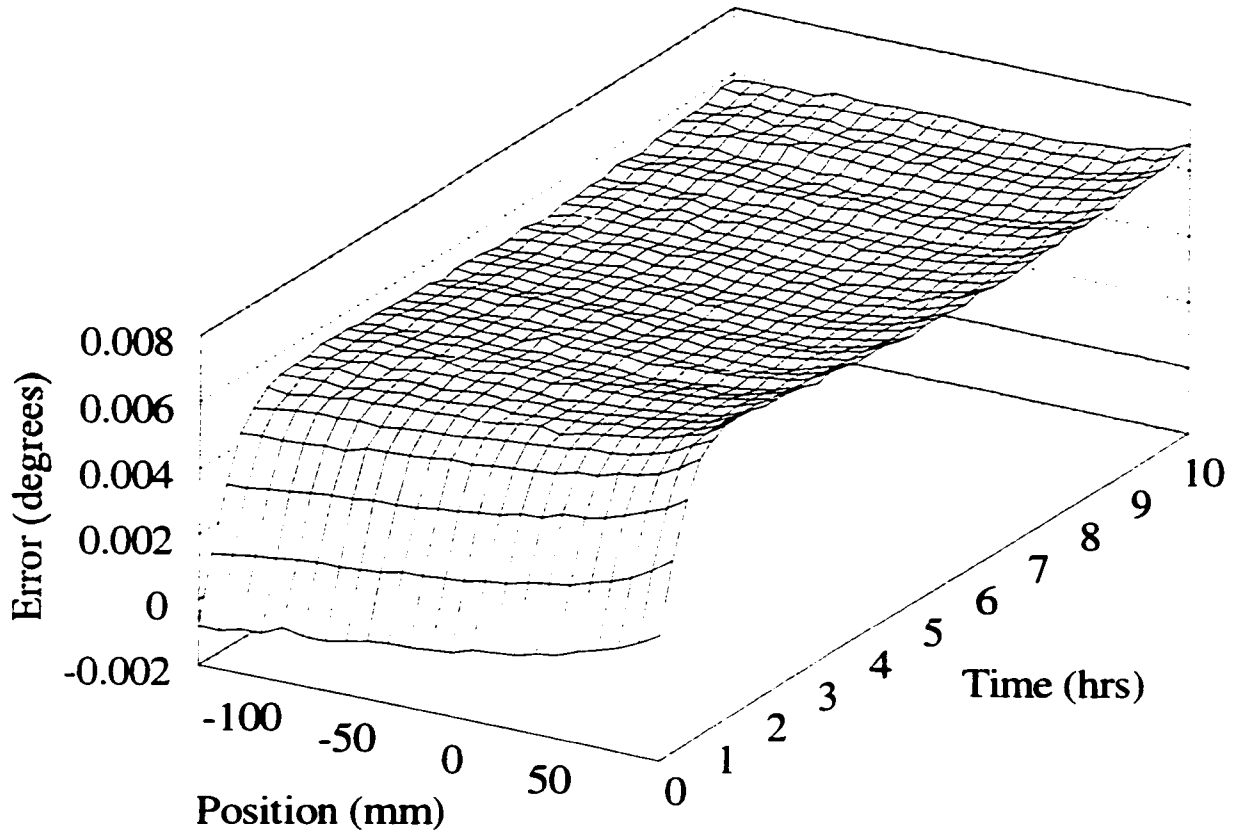

Figure 5.15 θ_x Angle Error for Z Motion

Figure 5.16 shows some of the critical temperature measurements that relate to the errors shown previously in Figure 5.14 and 5.15. The importance of the gradient in the spindle support arm is highlighted in this figure as it was the only variable in the machine with a fast enough time constant to explain the rapid change in error in the first hour of testing. Grouping of the inputs in this way provided physically relevant information to the model so that the identification strategy did not need to learn this relationship based on the presented data.

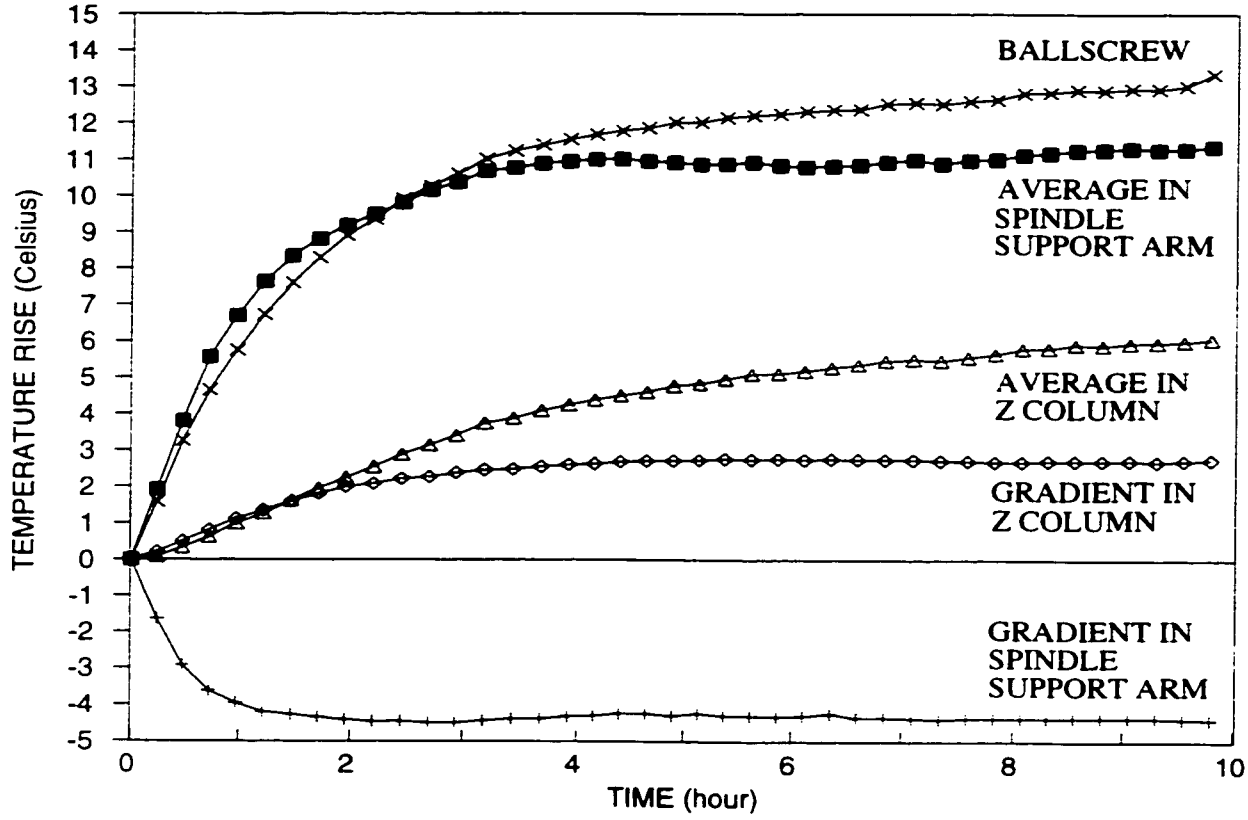

Figure 5.16 Critical Temperature Measurements For Z Errors

5.6 On-Line Work Space Error Measurement

A calibrated touch trigger probe was used to intermittently measure the error in the work space between sections of machining motion code. A touch trigger probe is a very robust means of measuring positions in the work space. The probe, shown in Figure 5.17, is a precise switch which triggers an electronic contact for set amounts of deflection. For the measurements made in this work, the probe was mounted in the spindle and moved around

the work space under the control of the machine. When the probe stylus touched an object, the probe would send a command to the machine tool, through an infra-red light signal, to capture the instantaneous values for each axis and store them in memory. Then the command to stop moving all axes would be issued to avoid a collision between the probe and the part.

A probe has some inherent inaccuracies which can be greatly reduced by calibration. The main inaccuracy is due to three point lobing errors; these arise from the mechanical operation of the three internal electrical contacts in the probe. A lobing error would manifest itself as an out of roundness when sampling points on a circle. By probing a known circular surface, the probing error can be estimated as a function of approach angle and used to compensate for the lobing errors. It was also important to adjust the probe so that it spun true with the centre line of the spindle, and thus, maintained the same coordinate system as the spindle.

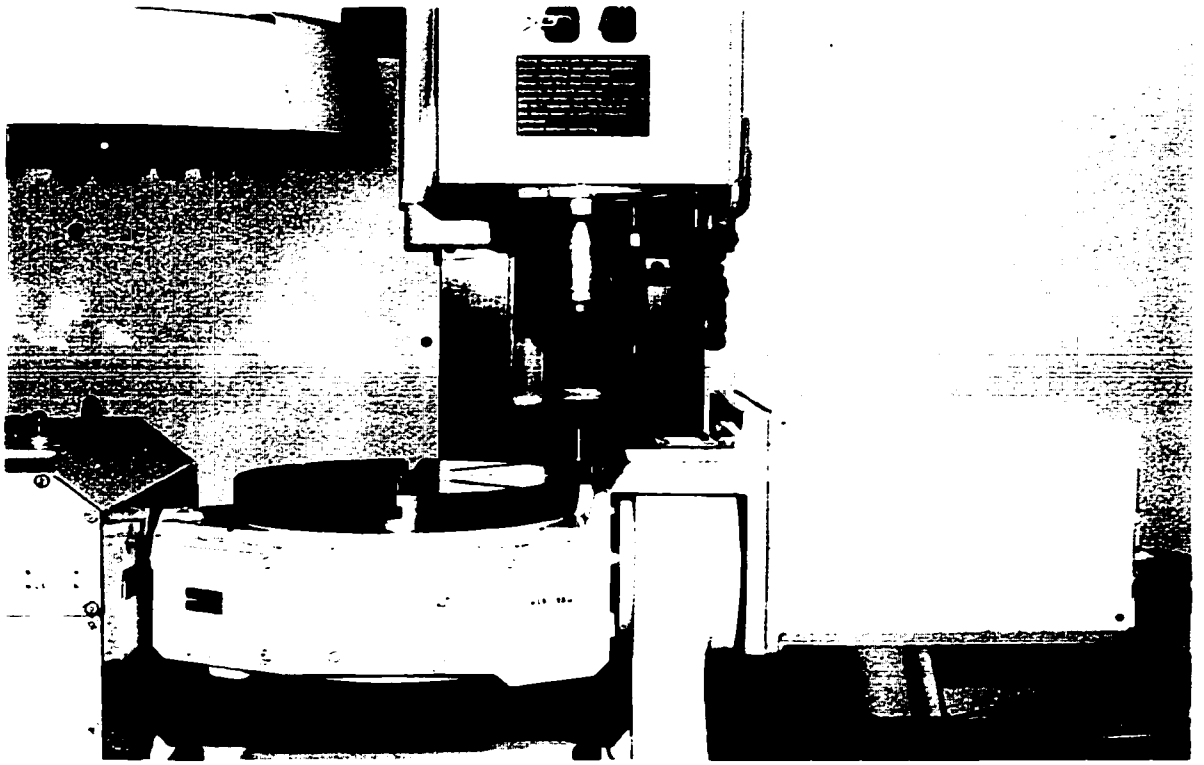

Figure 5.17 Touch Trigger Probe

The error in the work space was measured intermittently during the machining operation. This was done by studying the centre positions of three precision spheres mounted at the extreme of the work space. Each sphere was probed five times, and from these values, its centre point could be accurately determined. The variation in the centre point was an on-line measure of the error at these locations over time.

Two spheres spaced a known distance were used to calculate the angle errors in the table surface. However, since the probe was a single point device, angle errors in the spindle could not be measured using the touch probe. To measure these angles, a setup that used four proximity sensors was mounted at the extreme of the work space. These sensors were

spaced a known distance apart so that they could measure the orientation of the reference bar mounted in the spindle. Figure 5.18 provides a sketch of the setup used.

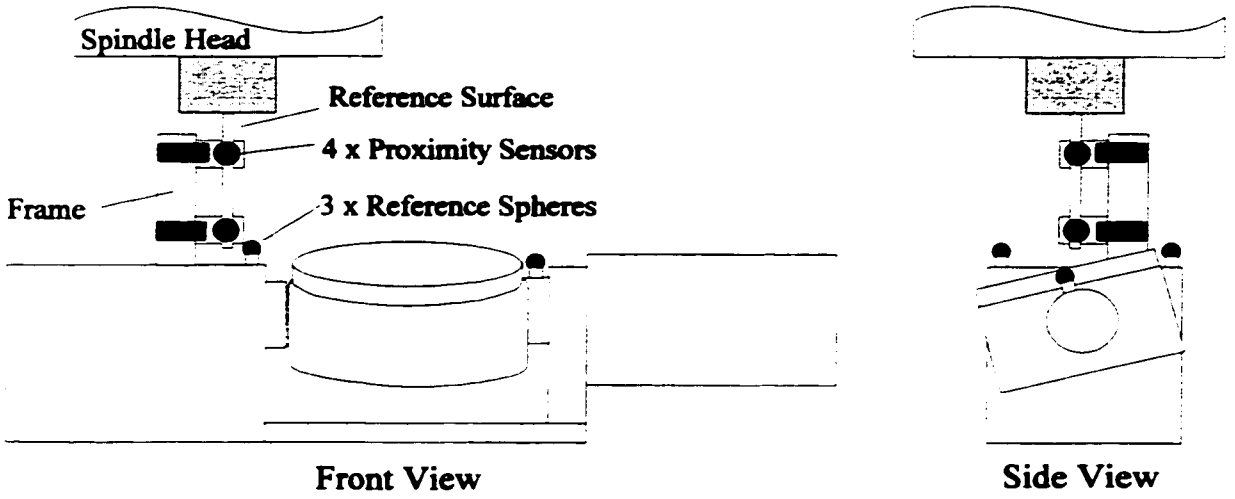

Figure 5.18 On-Line Measurement of Spindle Angles

Although the sampling operation was fast, it still took about 40 seconds away from the machining operation, with most of this time consumed by the tool changes required. On a typical machine, a tool change takes about seven seconds and each point measured takes about one second. To be considered a stable reference, the spheres and the proximity sensor array must be carefully protected in the work space. This would be a serious limitation on the process, given the harshness of the machining environment. Figures 5.19 and 5.20 show the on-line measurements made during a typical machining operation.

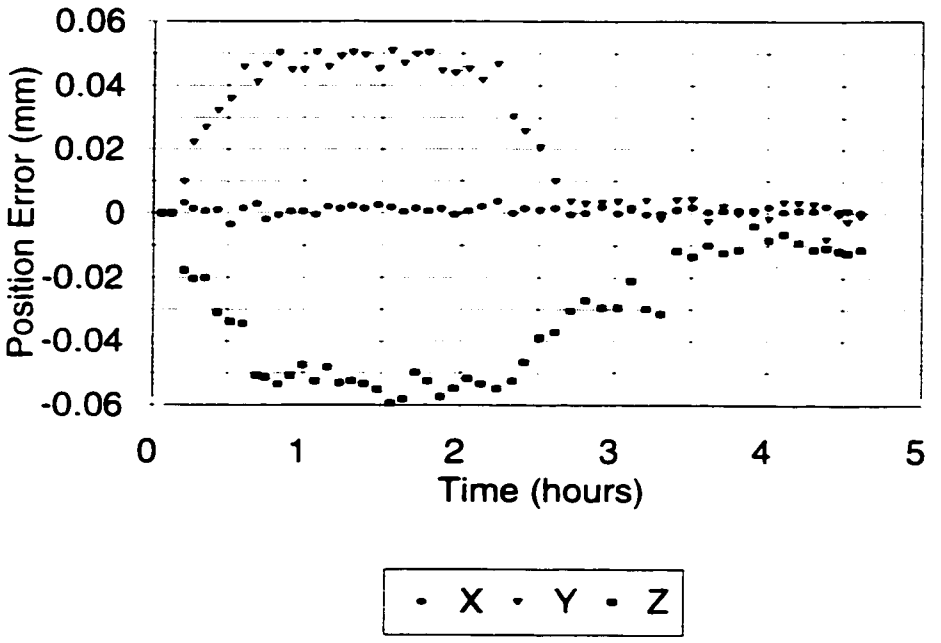

Figure 5.19 Variation in Probed Points While Cutting

With these cutting conditions, the error in position was mostly due to the deformation of the spindle support arm. The axis feed rate possible with the tool used did not reach the feed rates necessary to cause significant thermal errors in the X axis direction.

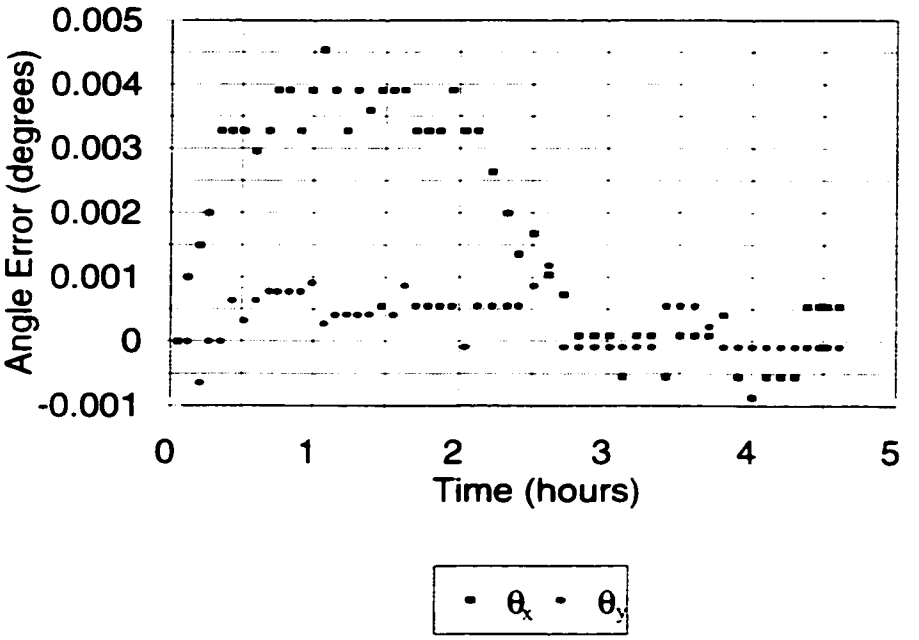

Figure 5.20 Variation in Spindle Angle While Cutting

Also notice that the variation of the error in the θ_Y direction is far less than the variation in the θ_X direction. This is due to the symmetry of the heat sources and structural components about the Y-Z plane of the 'C' column type machine.

5.7 Hardware Setup

A 486. 66MHz Personal Computer (PC) was used as the central source for all of the data collection. The interfaces between the computer and the various other components used in this work are shown in Figure 5.21. The PC used an RS-232 serial communications line to transmit motion code to the machine tool and also to receive the probe information back from the machine. A DAS-TC thermocouple card with cold junction compensation was used to interface with the thermocouples and an IEEE-488 communications line was used to collect data from the laser interferometer processing unit. The proximity sensor values were sampled using a DT2801 Data Translations analog to digital card. The motion code for part production was stored on the PC's hard drive and then processed using the compensation strategy before being sent to the machine tool through the RS-232 serial line.

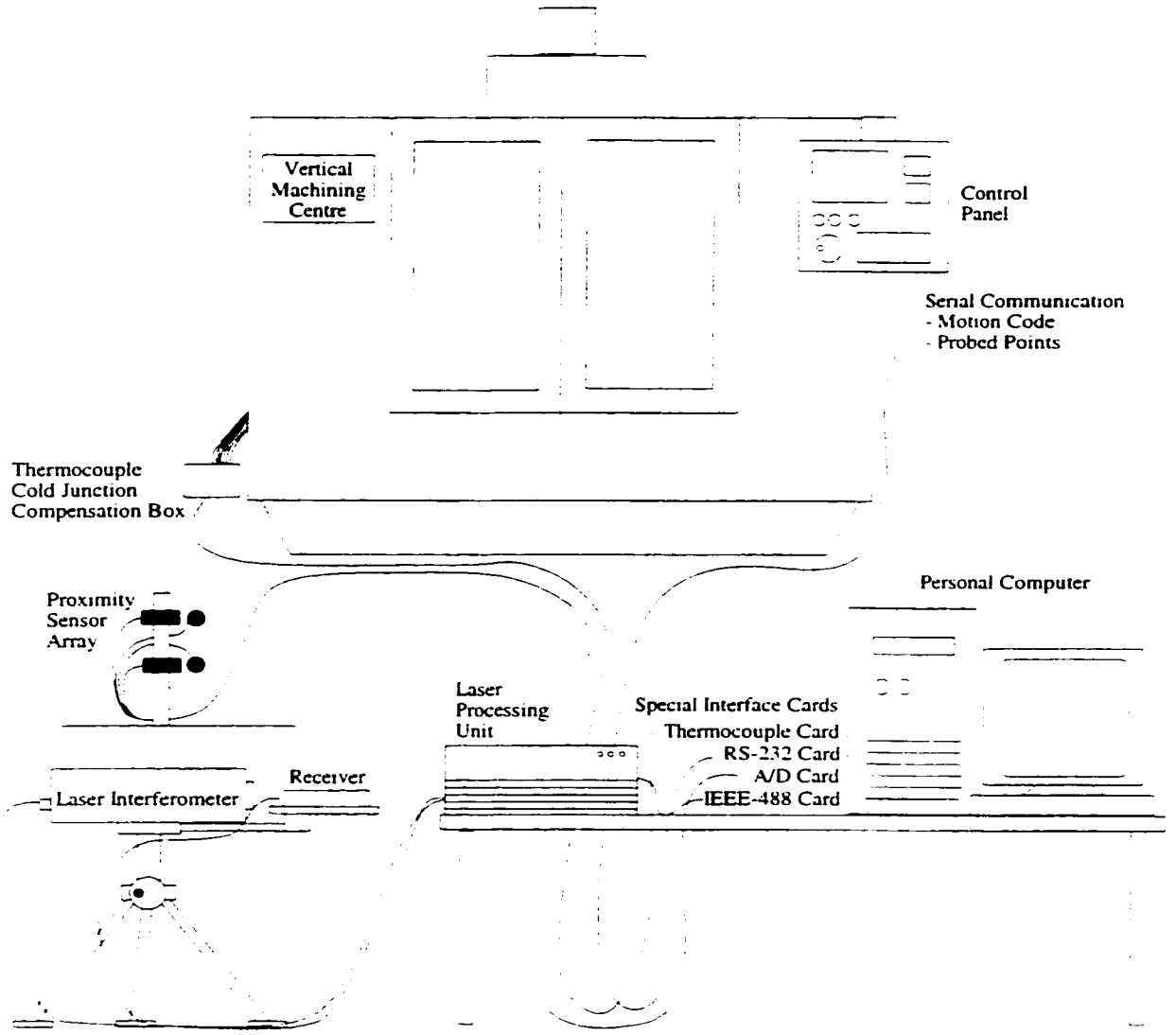

Figure 5.21 Equipment Setup

5.8 Discussion of Machine Errors

The error figures previously shown, and those included in Appendix D, provide insight into the nature of deformation within the machine. Certain errors are inherent in the design of the machine. For example, the fact that the machine is a 'C' column type machine means that there is a lack of symmetry in the design. 'C' column refers to the fact that one side of the machine is open, and therefore, the spindle is cantilevered over the work piece. This proved to have a large impact on the error. The lack of symmetry about the X-Z plane produced larger error in the Y direction than in the X direction. This was most apparent in the Z axis measurements because this test included running a heat source in the spindle support arm. The deflection in the Y direction for Z motion was 0.070 mm while the error in the X direction was only 0.015 mm. In this case, the placement of a large heat source on a non-symmetrical component led to significant deformation.

The spindle motor, which was the largest source of heat, generated significant temperature gradients within the spindle support arm. This temperature difference across the structure induced considerable bending in the spindle support arm. The errors associated with gradients can occur in short time periods and induce significant deflection and angle errors. The angle errors were particularly damaging to the accuracy of the machine in that they vary over the offset distance.

If the gradients in the structure could be eliminated, then the modelling process would be greatly simplified and the compensation strategy's results further improved. The gradients could be greatly reduced by using insulating materials between the heat sources and the

machine's structure. The magnitude of the heat source could be further reduced by directing a fan at the heat source and making more use of cooling fins on the surface on the hot components.

Although the spot light was not used during testing, it was noticed that when the light was directed against the machine, the temperature on the one side of the machine increased by two to three degrees over a long period of time. This is a significant gradient and should be taken into account when designing the lighting system for the machine's work space. If this light source must be used, then the manufacturer should place two on the machine and make them symmetric to minimize the thermal gradients.

Another heat source which could be greatly reduced was the electronic cabinets at the back of the machine. These cabinets use passive cooling through the wall to cool their inner electronics. Significant heat is generated in these cabinets and warms the back of the machine noticeably.

Based on the experience gained when collecting the data and being able to relate it to specific temperature distributions allows one to see the influence of certain design decisions. Although aspects related to design were not the primary focus of this research, they directly impact the success of the compensation strategy. Starting a compensation approach with the best design possible will enhance the potential accuracy of the compensation strategy. The avoidance of thermal gradients and making use of symmetry to balance the design are key design concepts.

The relative accuracy of rotation joints versus linear joints was also noticed. Linear joints are very susceptible to straightness errors and suffer from symmetry problems in

design. Rotary axes are generally far more symmetric in nature and can typically be produced more accurately than linear axes. To produce a rotary axis, one must rotate the part accurately; however, to produce a linear axis, one must move in a straight line accurately. The latter is physically harder to do in practice. Unfortunately, the errors associated with rotary axes, increase linearly as one travels from the centre of rotation. This is due to the coupling of the translation errors with the rotations. However, if the rotation angle can be carefully controlled, then the inherent accuracy and stability of a rotary based machine can be taken advantage of in the design of a machine.

The largest source of error in the rotary axis was the backlash in the gear train. If a direct drive motor was used, then the errors of the gear train would be eliminated and the accuracy of the rotary motion would be greatly improved. Also, an even distribution of heat in the gear train would not cause an increase in the errors, like in the case of heating the ballscrew. Heating would only tighten the gear meshing and serve to reduce the backlash.

5.9 Summary

This chapter presented the equipment and procedures used to measure the temperature distribution in the machine, as well as the errors in the work space. The procedures used to characterize the thermocouples and calibrate the proximity sensors were discussed. Error measurement methods suitable for both off-line and on-line error analysis were considered. The error methods associated with the off-line methods are generally more accurate and better represent the true state of the machine than the methods presently available for on-line measurement. Samples of the measurements were also included with the remaining measurements included in Appendix D.

CHAPTER 6

EMPIRICAL MODEL DEVELOPMENT

6.1 Introduction

In this chapter, the development of the empirical model is discussed. This model relates the individual error terms in each link and joint to the machine's condition and to selected process parameters. Both off-line and on-line empirical models were developed for use in the compensation strategy. For the off-line model, multiple linear regression and neural network methods were considered, while a recursive least squares regression technique was used in the on-line model. The on-line model of the compensation strategy was used to identify errors that were not fully captured by the off-line modelling process.

6.2 System Description

The machine errors that would transfer onto the part during production were those present in the work space. However, the errors in the work space resulted from the errors in the individual links and joints that made up the machine tool. The process of understanding the errors in the work space was greatly simplified by empirically modelling the errors in the individual links and joints, where they were generated. How these individual error terms in the links and joints combined and interacted was dependent on the configuration of the machine. The relationship between the work space and the links and joints was made through the kinematic model. The kinematic equations were based on the configuration of the machine and had error terms such as $\{\alpha, \beta, \gamma, \Delta a, \Delta b, \Delta c, \Delta x, \Delta y, \Delta z\}$ associated with every link and joint as described in Chapter 4.

Since these error terms could not be directly measured during production, modelling of them using measurable quantities was necessary. Due to the difficulty in building precise physical models of the deformation process within the machine tool, empirical modelling of the error terms contained in the kinematic model was necessary. Physical models that use finite element methods or finite difference methods have proven difficult to apply to this problem. However, based on some preliminary testing, and the results reported by others, it has been found that sufficient knowledge of these relationships can be captured by empirical models.

Important variables in establishing the empirical relationships were the temperature distribution in the machine, the environment around the machine, the state of specific heat

sources, and the machine's motion parameters, such as position, orientation, direction, and feed rate. The temperature distribution in the machine was measured by sampling thermocouples mounted on the machine. This was important for quantifying the thermal deformation within the machine. Two thermocouples mounted near the top and bottom of the machine were sampled to provide information on the heat transferred between the machine and the environment. Whether a heat source was warming up or cooling down was found to influence the temperature distribution within the machine. Errors in the machine's motion such as those due to backlash in gears or couplers, positioning errors in the ballscrews, straightness, or angle errors in the axes are all functions of axis motion parameters. These values are readily available through access to the motion code prior to transmitting it to the machine tool.

Knowledge of the underlying relationships involved in the deformation of structural components was valuable for establishing the order of the model, and for reducing the amount of information that must be identified by the empirical model. The previous sections on machine tool errors and kinematic modelling outlined some of the basic relationships present in the machine. The kinematic model of the machine was used to allocate the error to specific components and establish the correct axis adjustments to best compensate for the modelled error in the work space.

6.3 Data and Testing

Two sources of data for establishing the empirical models have been used by researchers. One involved the use of special off-line tests, while the other involved using the errors measured directly during part production, either from the part or from artifacts. The quality of the data was generally higher with off-line testing since the tests could be specifically setup to capture a wide range of operating conditions with better control over the influencing parameters. Due to the demands of production, on-line testing was limited by the amount of time available to make a measurement and by the number of points that could be sampled practically. The generality of the data from on-line testing was a concern as the work pieces produced in the past may not be representative of future production.

One of the main concerns with the implementation of this strategy in industry was the time taken to conduct the off-line tests. In the case of this thesis, the test machine was available for a long period of time, so the initial focus could be placed on collecting the best data possible on the machine's errors. The experience gained from thorough testing in a laboratory setting would focus any future effort and reduce the amount of testing required to implement the strategy on different machines. On-line measurement methods were also considered to capture any relationships missed during off-line measurements or due to changes over long periods of time.

The off-line experiments were designed to separate the effects of the various heat sources as much as realistically possible, given the general operation of the machine. Unfortunately, the heat sources could not always be separated as some are automatically

coupled. For example, the heat generated by the main electronics panel would always be present whenever the machine was turned on. In general, however, only one heat source was added at a time, and the temperature in areas far removed from the heat source was still collected to ensure that the active heat source did not excessively influence distant areas. This process allowed the error components arising due to different factors to be separated out, thus isolating the impact of different inputs from one another. This was important since the machine components were all connected to one another, and in general, would interact for a typical machining process, and thus, be difficult to separate with on-line testing.

For example, it was typical when machining a part to move a number of axes at a time. If this multiple axis motion were done when establishing the off-line model, allocating the error in the work space to specific components on the machine would be difficult. This would be due to the fact that differentiating between a straightness error in one axis and a position error in a perpendicular axis would be hard. Even more significant would be the misinterpretation of a rotational error acting through a distance, as purely a translational error. If this occurred, then the error across the work space would be considered a constant, when in fact it would vary with the critical distance from the centre of rotation.

In an effort to capture data over a wide range of temperatures, tests had to be run for long periods of time. This was done to ensure that the machine reached a high steady state temperature, which would provide the broadest range of training data. Due to the size, thermal conductivity, and boundary conditions of the structural components, some of the time constants for the thermal rise were on the order of three hours or more.

The decision to measure thermocouple outputs was made based on preliminary

testing, general engineering knowledge, and the results reported by others. The basic premise for the placement of the thermocouples was to install an excess number of them, and to remove them based on whether they provided new and useful information to the model. The temperature sensors were distributed to provide physical information, which was expected to be important in the identification of the model. It was expected that the average temperature and the presence of temperature gradients in structures would have a large impact on the thermal errors. This aspect was discussed previously in the machine tool error chapter and in the experimental methods chapter.

The data was inspected after every test to ensure that no outliers or breaks in the error data was present. If the laser beam was broken during a test, the measurements would reset themselves and the reference to the initial position or orientation would be lost. The thermocouple board conducted considerable smoothing of the data, and thus, no additional smoothing was done on the temperature measurements.

A correlation analysis was performed to see which input provided new information and what underlying relationships existed in the thermal profile of the machine. Also, individual thermocouples could be inspected to see if they would contribute significantly to the error estimate. The correlation coefficient between T_1 and T_2 was found using Equation 6.1, where $\sigma^2(T_1)$ and $\sigma^2(T_2)$ are the variances of the time series $\{T_1\}$ and $\{T_2\}$, and the cov(T1,T2) is found using Equation 6.2.

$$R\left(T_1,T_2\right) = \frac{cov\left(T_1, T_2\right)}{\left(\sigma^2\left(T_1\right)\sigma^2\left(T_2\right)\right)} \tag{6.1}$$

$$cov\left(T_1, T_2\right) = \frac{1}{n}\sum_{i=0}^{n} T_{1_i} T_{2_i} \tag{6.2}$$

The screening of the inputs did not rely solely on statistical procedures, but included knowledge of the physics of the problem as discussed in the machine tool error section. For example, a thermocouple may not be significant in one test, but one could imagine a realistic cutting condition where it would be significant and therefore should be kept.

6.4 Candidate Models

A wide range of regression models are available in the literature; of these, a linear regression model was considered because it is simple and robust. A neural network model was also considered because of the favourable results reported in the literature. A neural network is known for its ability to model complex nonlinear systems without constraining the number of inputs to the same degree as a linear regression technique. The main criteria for selecting the model was its ability to provide the most accurate representation, over the widest range of operating conditions, with the smallest data requirements. Selecting a model

capable of including nonlinearities was important given that the problem contains nonlinear relationships between the variables. A multiple linear regression model is capable of including nonlinearities by recasting its parameters, while a neural network model contains exponentials in its formulation. Also, the identification technique should be capable of including known physical relationships to ease the effort in establishing the model.

The final decision as to which technique to use was based on its capability of interpolating within the range of measured values as indicated by the mean square error of the residuals. Unfortunately, there was no guarantee that the testing data was complete. Therefore, the model must also be capable of providing reasonable estimates when extrapolating beyond the off-line testing conditions. Aspects of robustness were tested by introducing new data not used during training. Also, the ability to handle new situations was investigated with realistic cutting tests for the final validation of the model. This introduced cutting forces and torques that were not present during the initial training of the models.

When modelling, there is always a trade-off between flexibility in a model and the parsimony of a model. Flexibility in a model structure offers good capabilities in describing the many different possible conditions to which the system may be exposed. Flexibility can be obtained either by using many parameters or by strategically placing them. Parsimony relates to the number of parameters used to build a model. If too many parameters are used, there would be a risk that two or more of the parameters might be somewhat correlated. This would lead to problems when solving for the coefficients. One must also be aware of over fitting the data. This could cause the parameters to adjust themselves to particular features such as noise, which would not be relevant to the error estimates in general.

6.4.1 Neural Network

Based on the results reported by others in the literature, a neural network modelling approach was considered. A neural network is a parallel distributed processor, which stores experiential data as model coefficients called weights and biases. These weights and biases are established using an iterative approach called training, which seeks to minimize the mean square error of a sample set of data relationships. The reference to neurons comes from the similarities of the network structure to that of the human brain. The neural network architecture is made up of many simple elements operating in parallel. This parallel nature makes it ideally suited to fast parallel processing operations where time is critical. An example of a neural network configuration is shown in Figure 6.1. The basic form of this model is available in the work by Haykin (1994).

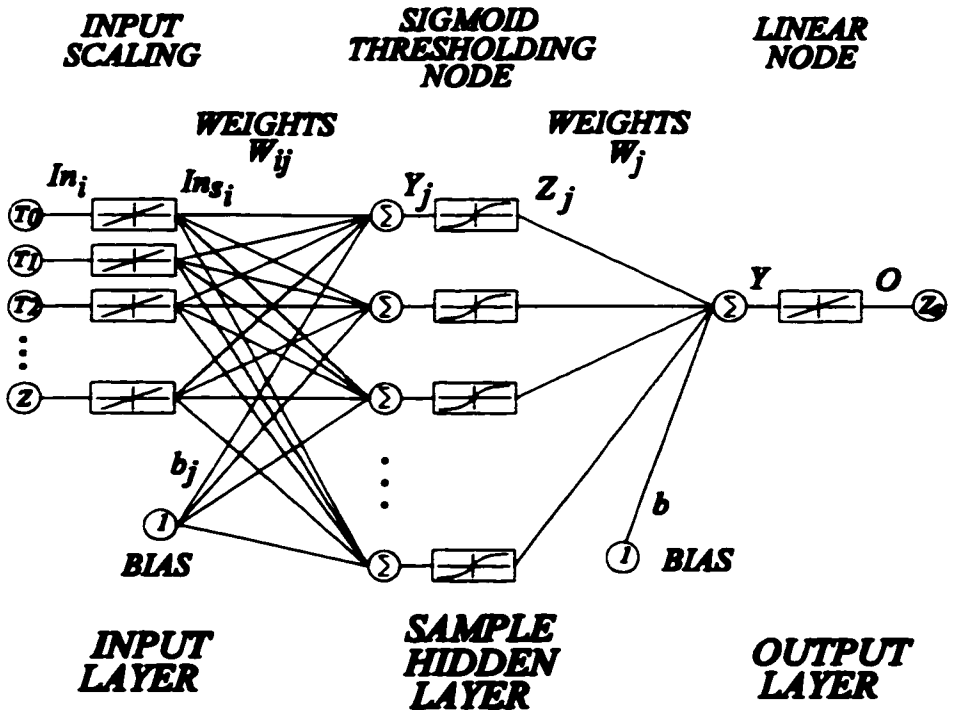

Figure 6.1 Neural Network Configuration

Special features used in the neural network model that improved its modelling capability were scaled inputs and the use of a sigmoidal hidden layer and a linear output layer. The scaling of inputs was required to avoid placing any unnecessary emphasis on specific inputs in the training of the weights. The scaling of the inputs could also include a thresholding function, which would limit the inputs from going beyond the training range. This would avoid the danger of using a neural network for extrapolating beyond the test data. Unfortunately, it would also limit its usefulness beyond this range as well. This is a known shortcoming of neural networks and was of considerable concern given the possibility that

the thermocouples could go beyond the range established when training the model. Different loads on the motors or changes in the surrounding environment could easily drive the thermocouples beyond the training range.

By initially setting the weights and biases to small random numbers and scaling the input values, none of the inputs were initially favoured. Scaling was especially important in this case since some of the inputs, such as spindle speed and axis feed, were orders of magnitude higher than the thermocouple temperature measurements. The thresholding nature of the exponential sigmoidal hidden layer provided the model with its nonlinear aspect. Linear output nodes were used so as not to restrict the final value of the error estimate. The scaling formula is shown in Equation 6.3, the equation of the summing junction is shown in Equation 6.4, and the nature of the nonlinearity is provided in Equation 6.5. The final output is calculated using Equation 6.6.

$$In_s = \frac{1.8\left(In - In_{MIN}\right)}{\left(In_{MAX} - In_{MIN}\right)} - 0.9 \tag{6.3}$$

$$Y_j = \sum_{i=1}^{N}\left(W_{ij}\, In_{Si}\right) + b_j \tag{6.4}$$

$$Z_j = \frac{1 - e^{-Y_j}}{1 + e^{-Y_j}} \tag{6.5}$$

$$O = \sum_{j=1}^{M} \left(W_j Z_j \right) + b \tag{6.6}$$

Organizing the sensor values before passing them to the input layers of the neural network is possible. This could be done to capture known physical relationships, such as those discussed in the machine tool error section. For example, sensors could be grouped to calculate the average in a section, or a gradient could be calculated using the difference between sensors on one side of a component versus the other side. Also, the values from the output layer could be interpreted with the kinematic model so that the interaction of the links and joints of the machine would not need to be captured by the neural network. Unfortunately, the weights within the neural network model are difficult to interpret, and therefore, it is best not to apply any physical significance to them.

The process of training the weights of a neural network did not require the inversion of any matrices. Therefore, it was less sensitive to the requirements of the parsimony principle. However, highly correlated inputs could still cause coefficients to become excessively large during the iterative search for a minimum mean square error. This could lead to stability problems if the correlation was altered slightly over time or if one of the inputs failed in service.

There are various update rules which can be implemented in the iterative process for establishing the weights and biases of a neural network model. The results in this study were based on a Levenberg-Marquardt approximation of Newton's method for finding a minimum. Equation 6.7 outlines how the weight, W, is changed to reduce the sum of the

square error, where J is the Jacobian matrix of derivatives of the error with respect to the weight, I is the identity matrix, and e is the error vector associated with the sample's input-output values.

$$\Delta W = \left(J^T J + \mu I \right)^{-1} J^T e \tag{6.7}$$

The nature of the update rule is controlled by μ and its scalar value changes depending on the rate of the error change from one iteration to the next. Increasing the value of μ has the effect of shifting the update rule from a Gauss-Newton method to an approximation of gradient descent. Gauss-Newton has been found to be faster in regions where the error was changing rapidly. However, when the solution nears a final value, gradient descent was faster at settling in on a final solution.

The training input and output data was randomly sampled from the full set to create batches of data with 500 samples. New batches of data were presented to the learning algorithm until the error target could be consistently reached, even with unused data values.

There are no specific rules regarding setting the number of hidden layer nodes. Therefore, determining the optimal number was very much dependent on the nature of the problem, and therefore, required testing. For this reason, different trials were run with a varying number of hidden layers and neurons per layer, until the desired level of representation was achieved.

6.4.2 Multiple Linear Regression

The other off-line method that was considered was a regression technique where the coefficients were linear but the terms could be recast based on nonlinear functions. The basic form of the model was taken from Ljung (1987) and is shown in Equation 6.8, where y(t) is the dependant variable, $\varphi(t)$ is the independent variable, and v is a record of the equation error. The least squares estimate for the coefficient θ is shown in Equation 6.9, where α_t is used to provide different weights for different observations. In this case, it was set equal to one so that all of the observations were treated equally.

$$y(t) = \theta^T \varphi(t) + v(t) \tag{6.8}$$

$$\hat{\theta}(N) = \left[\sum_{t=1}^{N} \alpha_t \varphi(t) \varphi^T(t)\right]^{-1} \sum_{t=1}^{N} \alpha_t \varphi(t) y(t) \tag{6.9}$$

The off-line algorithm required that all of the input and output data were available before the process of establishing the coefficients was started. Also, the matrix inversion associated with Equation 6.9 required that the φ be uncorrelated. Therefore, special attention was paid when setting up the test conditions to ensure that the input data presented was as uncorrelated as possible, subject to the constraints of the machine's operating conditions. If the independent variables did not show sufficient variation or were highly correlated, then

the matrix in Equation 6.9 would be singular and no inverse could be found.

The nonlinear terms chosen when recasting the regression model could be carefully chosen so that the model would behave well beyond the range of testing. This was especially true if the terms of the regression equation were based on known physical relationships such as the ones discussed in the chapter on machine tool errors. Other nonlinearities which were tried, involved selected temperature changes and machine conditions taken to the second and third order, as well as temperature and machine condition combinations. A stepwise regression technique was used to select the significant variables from a list of potential ones that produced the highest degree of relationship between the independent and dependent variables as described by the R^2 value. It was guided by the notion of building a model by adding and removing variables depending on their effect on the model's descriptive properties. The statistical significance of a coefficient was calculated to see if it was significantly different from zero. This was a means of isolating variables that did not add relevant information content to the model. When the stepwise technique was used, care was taken with input variables that were known to be somewhat correlated. If this was the case with two variables, then the presence of one variable might mask the significance of a second more relevant variable. This made the order of adding and subtracting variables very important when defining the model.

Neural networks were reported in the literature to provide better robustness in case of sensor failure (Chen, 1992). To balance this, a technique to improve the robustness of the linear regression technique was also considered. This technique involved modelling each thermocouple as a function of surrounding thermocouples using a linear regression

relationship. If the measured value did not fall within a set range of the estimate provided by the modelled value, then the operator would be notified, and the estimated value would be used until the thermocouple was repaired or the new condition verified.

6.4.3 On-Line Regression

An on-line regression algorithm was considered for use in the compensation strategy to account for the error remaining after the use of the off-line regression model. The basic form of the regression equation was the same as for the earlier regression model except that the least squares estimate was rewritten in a recursive form. The form of this model was taken from Ljung (1987). The recursive form allowed for the input and output data to be presented individually whenever new values became available from the intermittent error measurement operation. The basic form of the equation is shown in Equation 6.10 with y(t) being the dependant variable, $\varphi(t)$ the independent variable, and v the equation error.

$$y(t) = \theta^T(t)\ \varphi(t) + v(t) \qquad (6.10)$$

The recursive least squares estimate for the coefficient θ is shown in Equation 6.11. For the recursive case, the present estimate of the coefficient θ was based on making a correction to the previous estimate of the coefficient using knowledge of the estimation error based on the past coefficient.

$$\hat{\theta}(t) = \hat{\theta}(t-1) + L(t)\left[\, y(t) - \varphi^T(t)\,\hat{\theta}(t-1)\right] \tag{6.11}$$

The L term in the equation is the factor which determines how the corrections are to be weighted for the present estimate. It is determined using the relationship described in Equation 6.12.

$$L(t) = \frac{P(t-1)\,\varphi(t)}{\lambda(t) + \varphi^T(t)\,P(t-1)\,\varphi(t)} \tag{6.12}$$

The P term, defined in Equation 6.13, is a symmetric matrix which can be described as a covariance matrix of the estimate. To start the recursive approach, the θ vector was set equal to small random numbers and P(0) was set equal to a small constant times the identity matrix. The memory requirements of the recursive algorithm were not excessive because the only information that was carried forward over time was the last P matrix and the coefficient vector θ. A forgetting factor of $\lambda(t)$ was applied to the data so that over time past information would be de-emphasized. The forgetting factor could vary with time depending on the problem. This would allow the on-line method to slowly change to adapt to new machine conditions, such as wear on sliding surfaces, while limiting the updates associated with small random changes.

$$P(t) = \frac{P(t-1) - \dfrac{P(t-1)\ \varphi(t)\ \varphi^T(t)\ P(t-1)}{\lambda(t) + \varphi^T(t)\ P(t-1)\ \varphi(t)}}{\lambda(t)} \tag{5.13}$$

Unfortunately, the quality of the data that can be collected while the process operated was limited. This was because actual error data was only available periodically, as frequent updating of the model was not possible due to the cost of lost production time. Also, data was only available at a limited number of points located at the extreme of the work space. This made it difficult to allocate the limited point data to specific regions on the machine. Therefore, the on-line update information was kept separate from the off-line model. This was also done to allow the operator to see the changes in the errors as they occurred over time. This could be useful information for determining when important maintenance needed to be done on the machine or when the off-line model needed to be updated with new data.

6.5 MODEL VALIDATION

Model validation involved looking at the mean square error of the estimates obtained when new data, not used in training, was tested on the model. For the linear regression model, it was also possible to look at the coefficients and compare them to reasonable

physical values given knowledge of the system. This was not possible with the neural network, since the weights and biases did not have any underlying physical meaning outside of the context of the neural network. The coefficients of the on-line model were also difficult to relate back to physical values since the model predicted the error in the work space, which was removed from the source of the errors, namely joints and links, where physical relationships were known. The most relevant test of the full implementation of the compensation strategy was how it worked during a realistic cutting test. This was done using machining parameters typical of a finishing operation for the mold and die industry.

6.6 Empirical Modelling Results

A neural network model structure was developed in the form previously outlined. Various numbers of layers and nodes per hidden layer were considered. The final one chosen for testing consisted of three hidden layers with thirty, fifteen, and seven nodes per hidden layer respectively. The data was presented to the neural network model in batches of 500 randomly selected data points. Of the 24,120 data points available for the Z position error, 10,000 data points were randomly selected for training before the mean square error value was reduced to be consistently below 0.0025 mm. This value was chosen as it was the resolution of the machine's position sensor. Care was taken to ensure that all of the inputs used during the testing fell within the range of data used when training the structure of the neural network.

Even though the neural network was capable of handling many inputs, it still would benefit from a careful selection of its inputs. For this reason, the results of the thermocouple selection strategy previously discussed were applied. The results of the correlation analysis were verified by studying the relationship between the residual error of the model versus the dropped thermocouple. This relationship is plotted in Figure 6.2 and shows that little new information was provided by this thermocouple. Therefore, the robustness of the model would be improved if this thermocouple were not used in the model with no significant loss in the neural network's modelling ability.

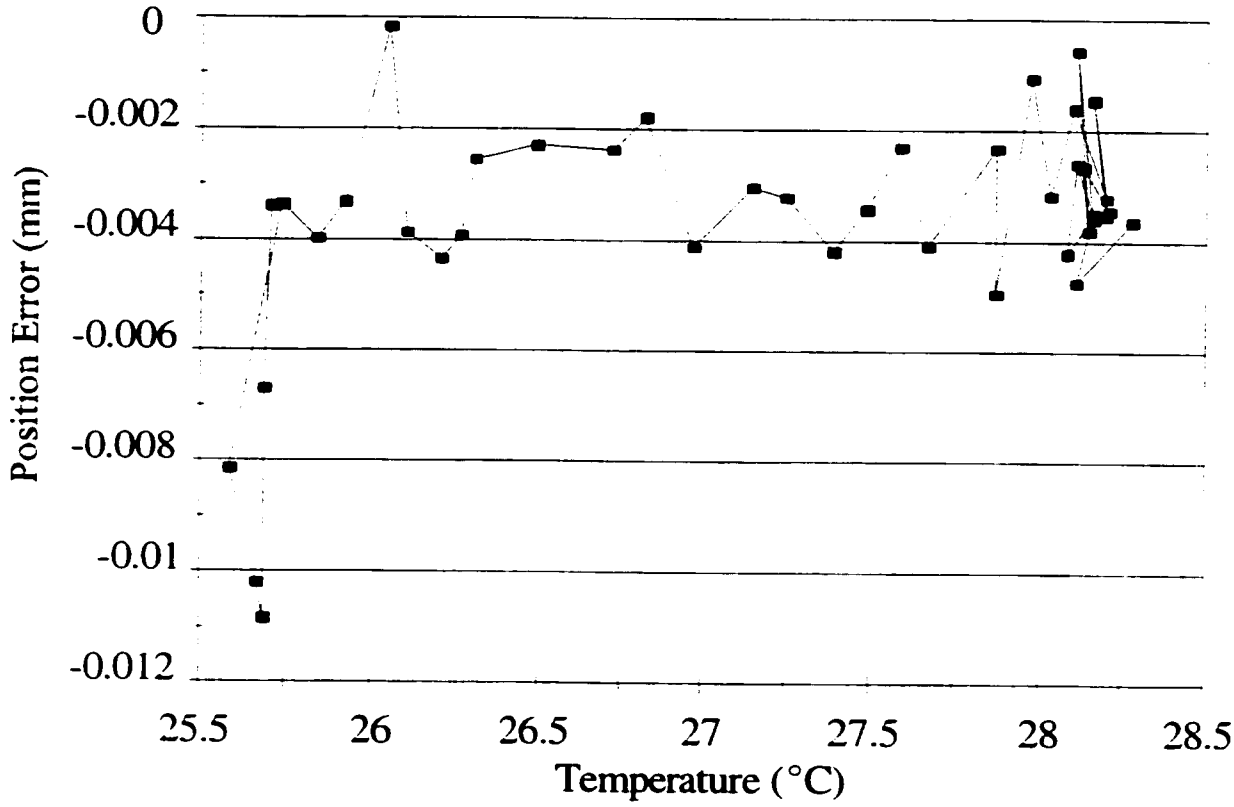

Figure 6.2 Residual Position Error Versus Dropped Thermocouple Output

A neural network's ability to model the positional error in the Z direction and angular error in the θ_X direction in the work space is shown in Figures 6.3 through 6.6

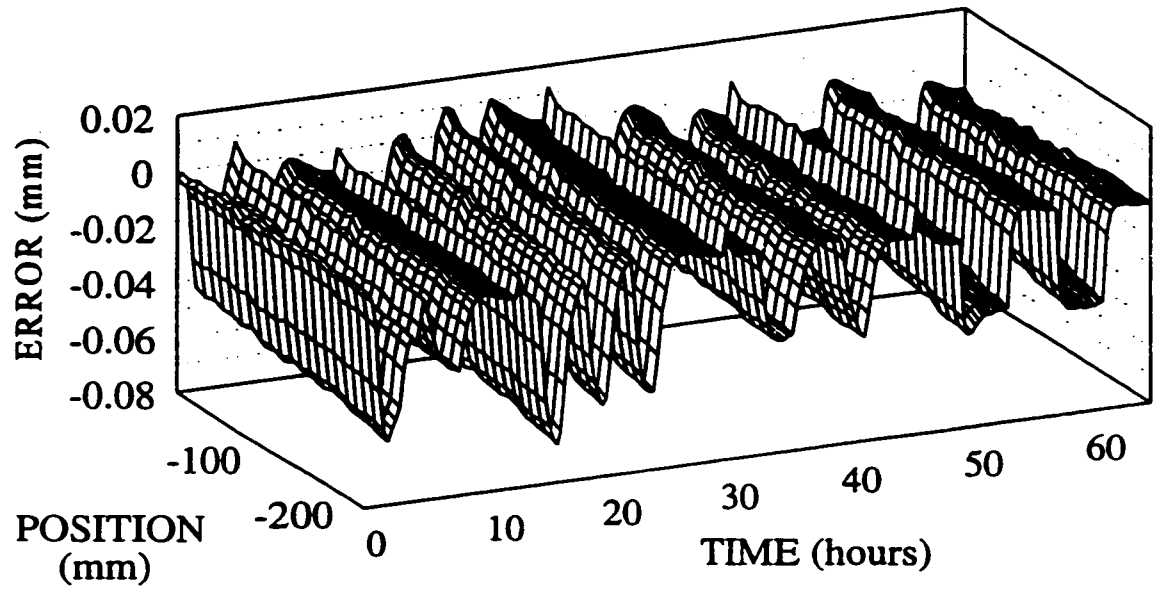

Figure 6.3 Z Position Error

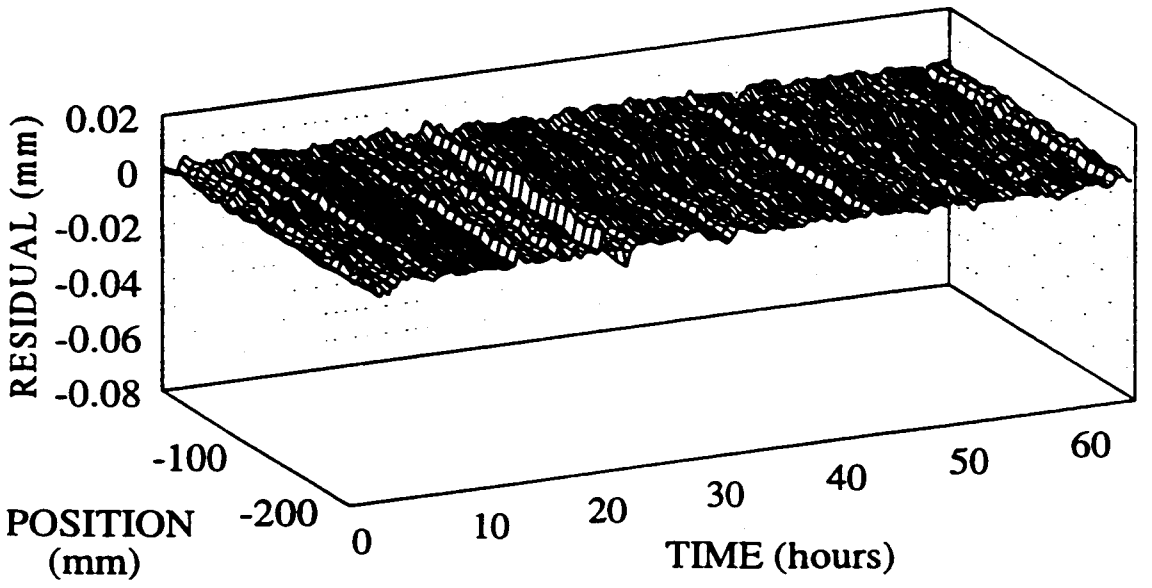

Figure 6.4 Residual Error in Z after Neural Network Modelling

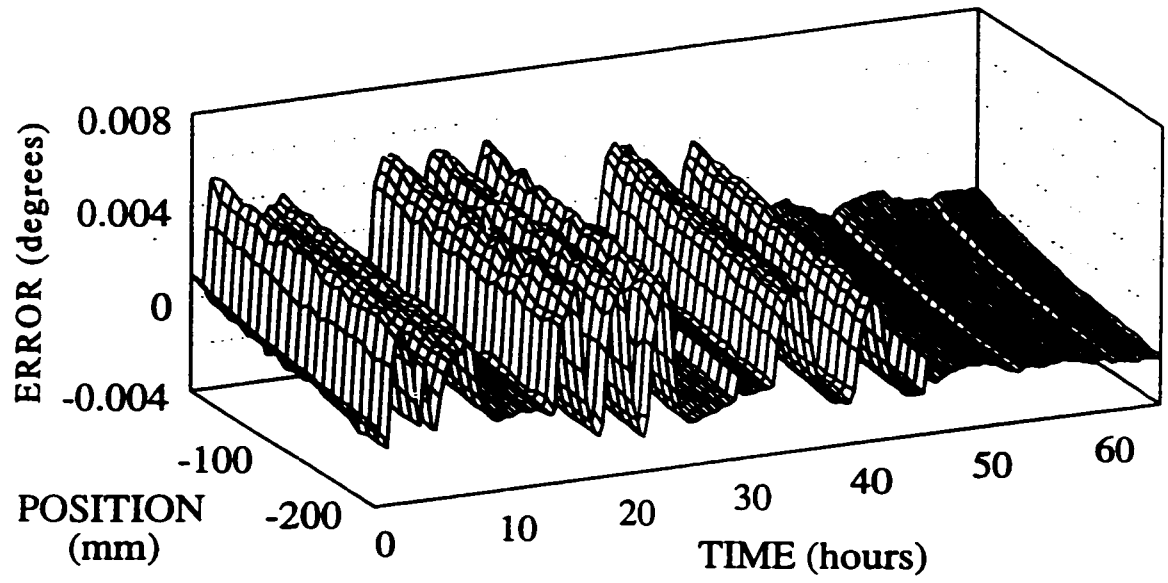

Figure 6.5 α Angle Error for Z Motion

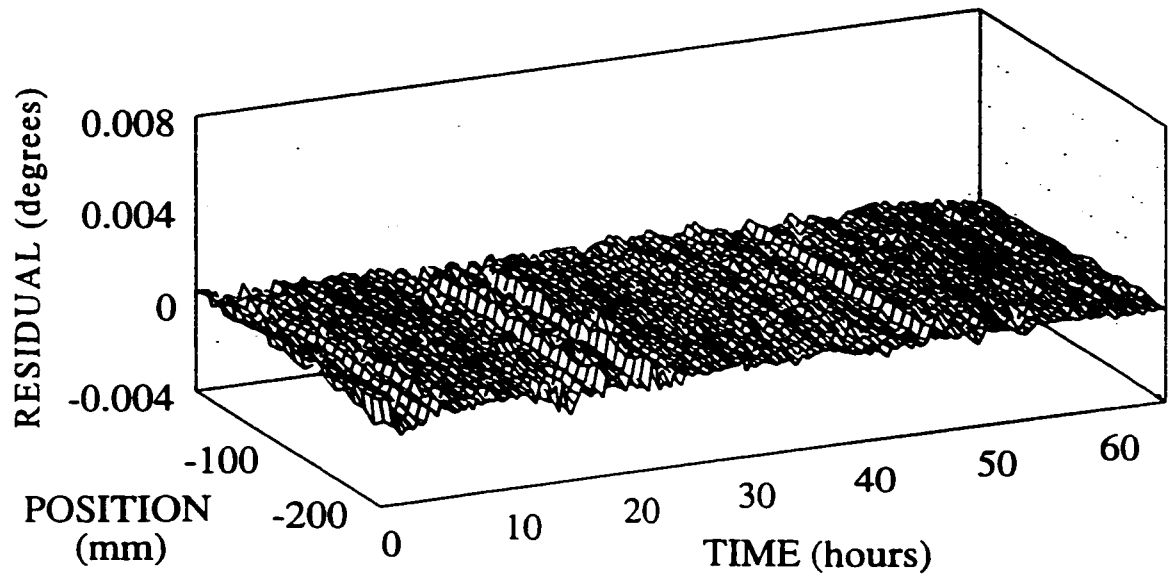

Figure 6.6 Residual Error in α After Neural Network Modelling

The neural network was also tested on new data. The results for the Z position error test are shown in Figures 6.7 and 6.8.

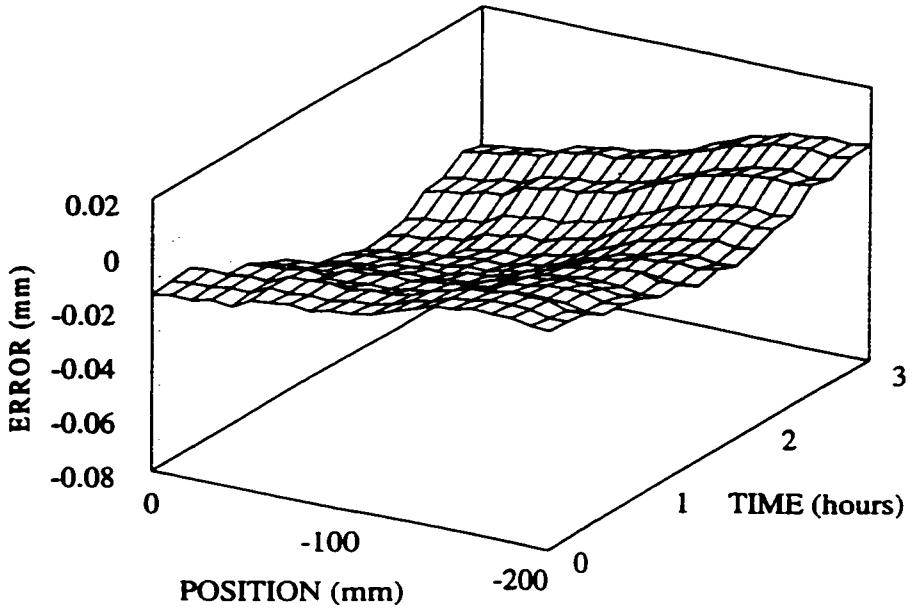

Figure 6.7 New Z Position Error Data

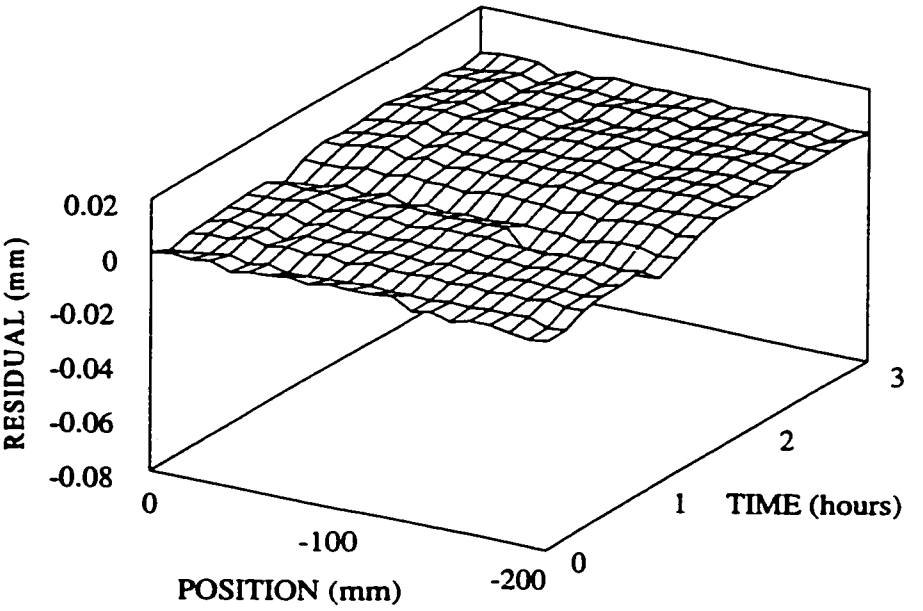

Figure 6.8 Residual Z Position Error After Neural Network Modelling

The multiple linear regression model was built using the inputs selected from the correlation analysis described earlier. A stepwise regression technique was used to establish the coefficients of the model. The results of the multiple linear regression technique are summarized in Tables 6.1 and 6.2.

Axis	Error Measurement	RMSE (mm)	R^2	F
X	Position	0.003252	0.9804	20,720
	Y Straightness	0.000815	0.855	2,118
	Z Straightness	0.0005152	0.9444	6,099
	Roll	0.0003974	0.832	2,426
	Pitch	0.0000843	0.9252	3,916
	Yaw	0.0000062	0.9519	5,912
Y	Position	0.003341	0.9933	53,360
	X Straightness	0.001114	0.6709	1,833
	Z Straightness	0.001676	0.837	1,976
	Roll	0.0005297	0.967	10,510
	Pitch	0.00005128	0.9837	25,060
	Yaw	0.00006691	0.9405	8,519
Z	Position	0.003295	0.9613	29,770
	X Straightness	0.002603	0.8154	2,267
	Y Straightness	0.004172	0.9654	15,410
	Roll	0.0007702	0.9502	12,000
	Pitch	0.0003289	0.9756	51,970
	Yaw	0.0002638	0.6681	850.6

Table 6.1 RMSE of Regression Modelling for Translational Axes

Axis	Error Measurement	RMSE (degrees)	R^2	F
A	Rotation	0.0002748	0.7868	1,808
	θ_Y Error	0.0005398	0.9445	13,110
	θ_Z Error	0.0002552	0.9164	5,912
	X Deflection	0.0000073	0.8642	2,858
	Y Deflection	0.0004098	0.9593	14,130
	Z Deflection	0.0001055	0.8685	5,098
B	Rotation	0.0006223	0.996	14,780
	θ_X Error	0.0002578	0.9664	19,380
	θ_Z Error	0.0002804	0.9442	10,140
	X Deflection	0.0004499	0.9245	6,000
	Y Deflection	0.0000071	0.9123	5,098
	Z Deflection	0.0000514	0.9738	18,230

Table 6.2 RMSE of Regression Modelling for Rotational Axes

Table 6.3 shows that the calculated empirical values agree with the physical values found using the relationships discussed in the machine tool error section of this thesis. The physical values were based on the material's coefficient of expansion under elongation or bending.

Axis	Regression Value	Relationship	Physical Value
X Position (T_9)	0.0115 mm/°C	$\alpha_c \Delta T L$	0.0130 mm/°C
Y Position (T_{20})	0.0065 mm/°C	$\alpha_c \Delta T L$	0.0087 mm/°C
Z Position (T_{30})	0.0114 mm/°C	$\alpha_c \Delta T L$	0.0104 mm/°C
Z Position (T_{34}-T_{32})	0.0103 mm/°C	$\alpha_c \Delta T L^2 / 2H$	0.0121 mm/°C
θ_X Angle (T_{34}-T_{32})	0.00095 degrees/°C	$\alpha_c \Delta T L^2 / H \times 180/\pi$	0.0014 degrees/°C

Table 6.3 Comparison of Regression Coefficients to Physical Values

The neural network's interpolation ability with an RMSE of 0.0026 mm was better than that obtained for the regression results of 0.0032 mm for the same data set. However, during further testing, the problem with extrapolation was revealed. This occurred when one of the thermocouple values went beyond the range of the data initially used for identifying the model. When the room temperature increased by two degrees beyond the testing conditions, it produced a 0.015 mm error in the estimate on the neural network, but only a 0.005 mm error in the regression model. The only way around this problem of extrapolating with the neural network would be to threshold the inputs to ensure that the inputs would never exceed the training value. This problem is likely to occur in general use, as most machine shops are not able to control their room temperature. The regression model's behaviour beyond the training range was better controlled because of the inclusion of physical relationships in the model. Unfortunately, the neural network does not carry known physical relationships in its weights and biases.

The main advantage of the neural network model as reported in the literature survey

was its robustness and insensitivity to individual sensor failure. Since sensor failure can occur during normal use of the system, a means of adding this protection to the linear regression model was considered. It involved modelling a thermocouple with the use of surrounding ones, so that if the thermocouple went outside of a set range defined by the model, then the operator could be notified to check the integrity of the sensor. If a single thermocouple failed either by breaking a lead or becoming dislodged from the surface, the regression model's estimate of the thermocouple could be used until the sensor was repaired. This would result in less error then when using a completely incorrect value, such as room temperature for the case where the thermocouple was dangling in the air, or the error signal which the thermocouple board naturally outputs if the wire leads were broken. Figure 6.9 shows the ability to model a thermocouple using surrounding thermocouples. Monitoring the variation of the thermocouples in this way was more powerful than relying on the thresholding feature in a neural network input node to limit the response of a defective thermocouple. This information could also prove useful to alert the operator if a thermocouple went out of range due to a lack of lubrication or significant wear in a bearing.

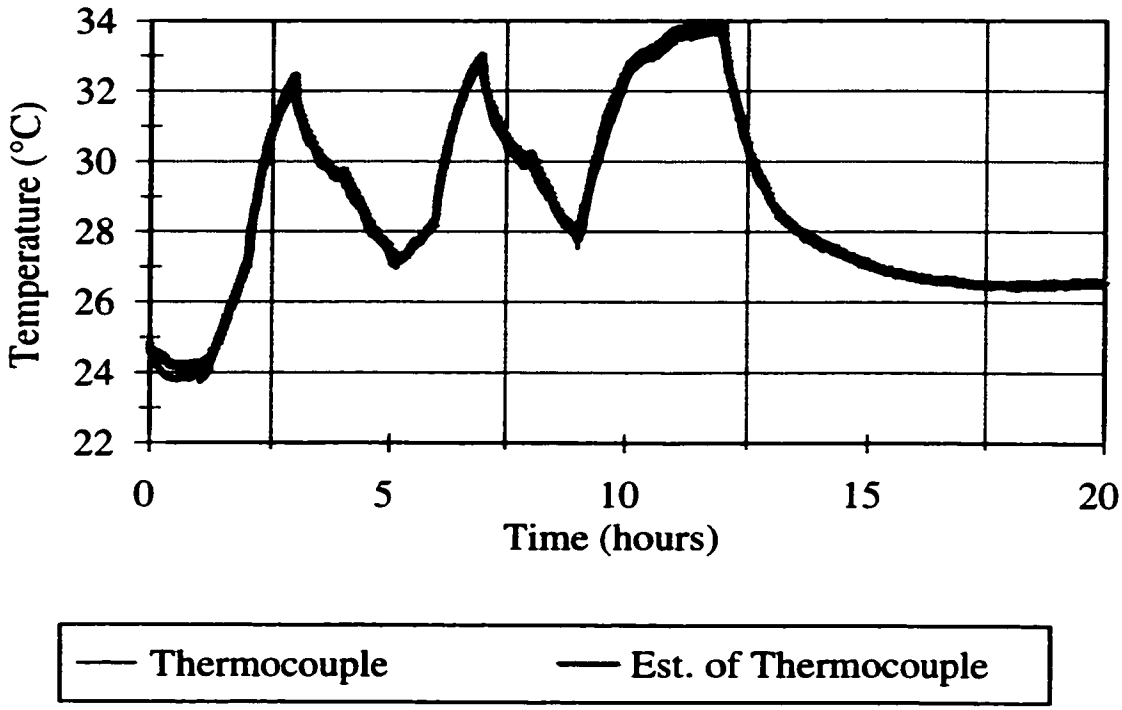

Figure 6.9 Modelling of a Thermocouple Using Surrounding Thermocouples

6.7 Summary

This chapter outlined the empirical models considered for identifying the errors in the links and joints of the machine. Neural network and multiple linear regression techniques were both considered. A recursive form of the regression equation was also considered for use in the on-line modelling of the error relationships. The main concern with the neural network model was its inability to extrapolate beyond the limited testing conditions. However, its main advantage was the fact that it could handle a large number of inputs. The limitation of the multiple linear regression model was its tighter requirements with regards to correlated inputs. Methods for removing highly correlated inputs and techniques for enhancing the robustness of the multiple linear regression technique were considered in an effort to reduce the limitations of the multiple linear regression technique in this application. The modelling capability of each technique was also summarized. The next chapter shows how the empirical models were applied in the compensation strategy.

CHAPTER 7

IMPLEMENTATION

7.1 Introduction

Chapter 7 discusses how the error terms solved using the empirical model and interpreted using the kinematic model are sent to the machine tool's controller in order to update the path. Issues associated with the timing of the calculations and the data transmission to the machine tool are also discussed. The results of the cutting tests are discussed comparing the work piece dimensions without compensation, to those with partial and full compensation.

7.2 Control Strategy

Desired axis positions entered the program as motion commands on the PC. These values were updated by the first model, as shown in Figure 7.1. This model was established using data collected during extensive off-line testing. The model calculated the error in each link and joint for the present conditions of the machine. The model's inputs included temperature sensors, axis positions, velocity, and spindle speed data.

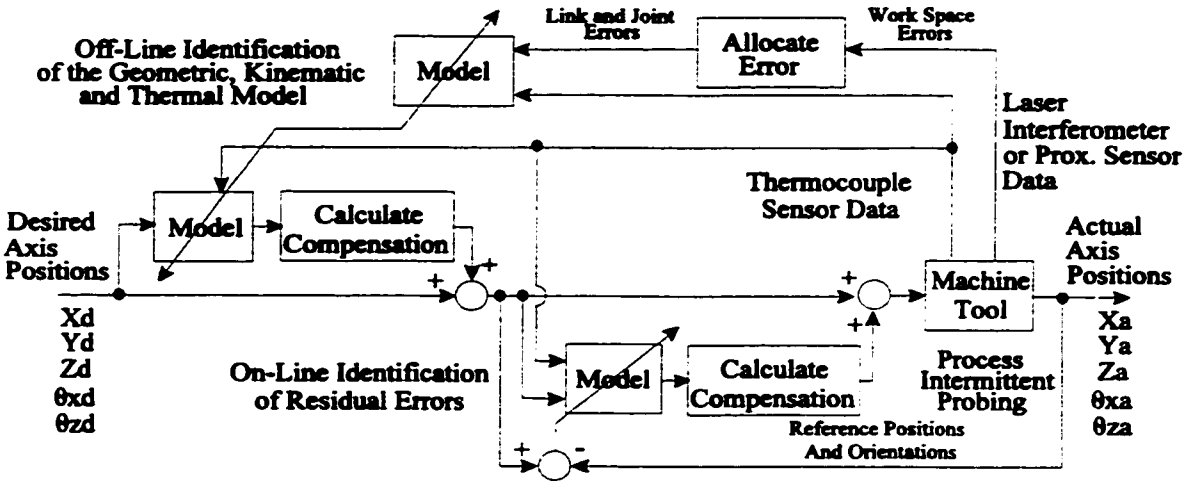

Figure 7.1 Control Strategy

A linear regression model was chosen over the neural network for the off-line modelling, because of its ability to provide reasonable estimates beyond the range of the experimental data. A neural network is known to provide poor estimates when extrapolating beyond the experimental data set. Extrapolation was likely to occur under realistic

machining conditions since the machine would experience higher loads and varying environmental conditions.

Compensation values were then calculated which forced the error terms in the work space to zero, by taking into account the errors in joints and links solved for in the model. The axis positions were then adjusted by the output of the second on-line model, which was based on a recursive least squares algorithm. Periodically, the on-line model was updated with new error data. This error data was based on touch probe measurements made on spheres located at the extreme of the work space and on proximity sensor readings made with respect to a reference bar.

The data acquired from these on-line measurements was not as complete as that available from the off-line procedures. For example, with the touch probe it was not possible to separate out whether the error measured by the probe was a Z position error or an X straightness error in the Z direction. Therefore, the model output must be applied directly to the axis positions where they could be best compensated. The order in which they were applied was important, however, as the position changes associated with compensating angle motions must be taken into account.

The second model was required to account for any unmodelled errors or changes in the performance of the machine over time. Unmodelled error could appear when the machine was operating under conditions for which the model was not trained. An example is if the room temperature were higher than that experienced under the training conditions. Another example of change over time would be wear on critical motion controlling surfaces like ways and gears. Once all of the compensation values were applied, the information was

sent from the PC to the machine for use. In this case, the machine's RS232 serial port was used for communication.

The timing for the communication of machining code from the PC to the machine tool for processing was very important, since the best compensation estimates would be made with up-to-date temperature information. However, if the machine code was not supplied to the machine fast enough, the machine would be starved for code. This would compromise the interpolation strategy used by the machine for contouring. The machine required a look ahead of a number of points to smooth its motion. Also, if the machine did not have any new points, the motion would stop until the next stream of points arrived. This would be highly undesirable as it would leave a chatter mark on the surface of the work piece.

Due to the problems associated with starving the machine tool and given that the time constant for the thermal errors was long, on the order of hours, the code was always buffered and waiting at the PC. The PC would wait for the machine tool's buffer to reach a low point before sending more data. The code should never be allowed to wait more than two minutes before being updated. The buffer in the machine tool was set low so as to keep the compensation values relevant, yet not so low as to limit the look ahead feature of the machine's controller.

Friction and inertia in the machine made it difficult to compensate for small error values. Therefore, the compensation movements were either grouped together with major axis motion or accumulated until they reached a level near the positioning resolution of the machine.

Complicated molds and dies are typically machined based on a series of short line segments. These segments are blended together by the machine tool controller to make a smooth surface. The compensation values are added to each small line segment. If a long tool path segment were programmed, it would have to be broken into a series of smaller segments so that the kinematic error could be taken into account between the original end points.

An open architecture machine would provide a way of seamlessly adding the compensation values to the machine's code. This would allow for offset values to be applied directly to axis values independent of the timing of the motion code being sent to the machine's controller. However, this controller concept was not implemented on the machine tool used in this study so this approach could not be tested.

7.3 Cutting Tests

A surface was designed which would require the motion of all of the axes and be realistic compared to the surfaces created in the mold and die industry. The designed surface is shown in Figure 7.2. The material selected was a P20 mold steel with a hardness of 32Rc. The cutting conditions used were: 10,000 RPM on the spindle, a feed rate of 2000 mm/min translation and 300 degrees/min rotation. The depth of cut was 0.4mm and the step over was 0.5 mm. A two flute ball nose, BZN end mill was used. A BZN tool was selected because of its excellent wear resistance under these conditions. This was important when studying

the variation in the surface dimensions over a long period of cutting time. The tool was inspected for wear before and after every cutting test. No significant wear was found during this period of testing. A single pass of the endmill up the centre of the part was done to provide a reference surface for aligning the part on the machine and later on the CMM. The part was measured on the CMM using a probe radius of 1.5 mm. Fifteen points were sampled across the width of the part and 99 points were sampled along the length of the part. The direction of the 99 points coincided with the dimension of time on the work piece.

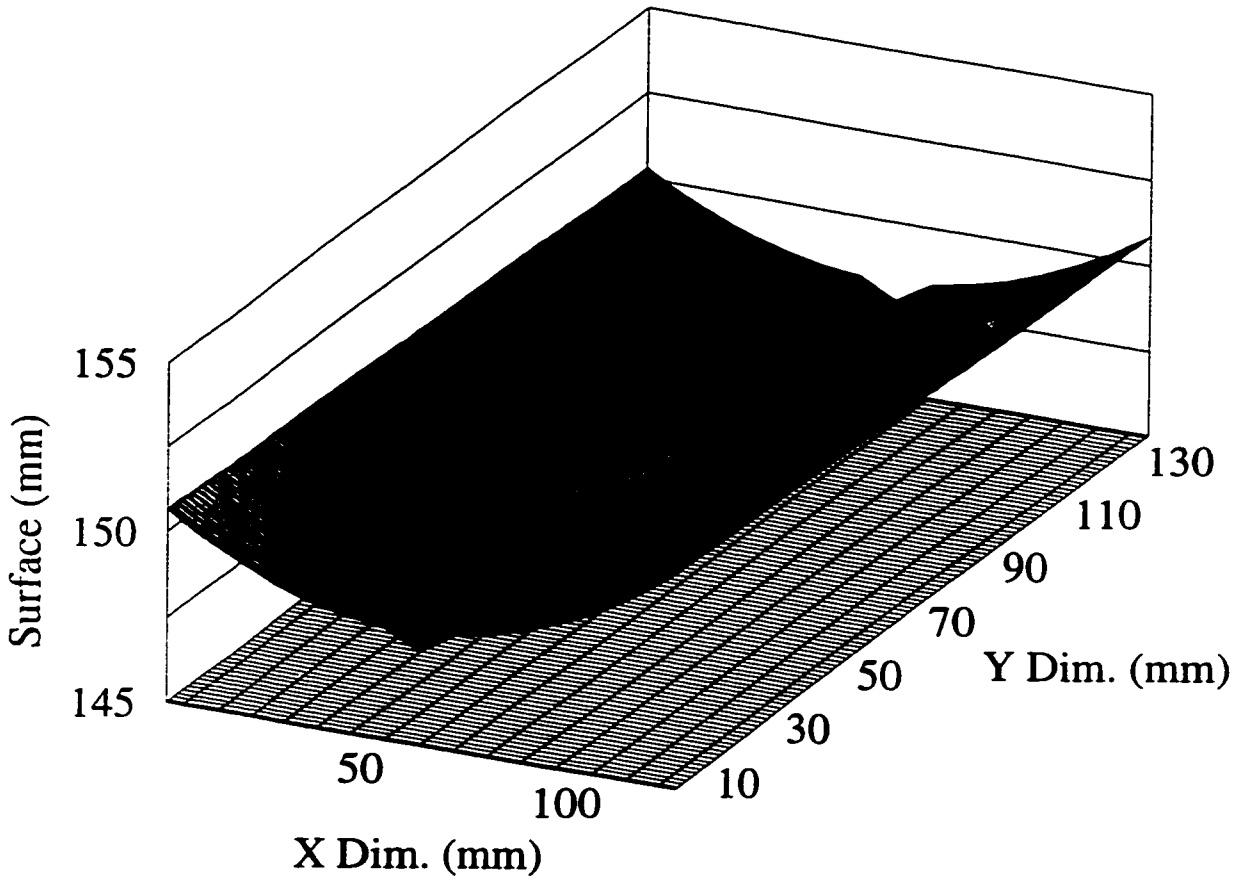

Figure 7.2 Shape of the Machined Surface

The cutting tests revealed the same order of magnitude of errors as the training data revealed and a similar time constant for the error variation. The RMSE of the machined surface without compensation was 0.060 mm and the maximum error was 0.082 mm. Figure 7.3 shows the surface measurements from the CMM for the part without compensation. The line machined down the centre of the part has been removed from all further figures of the surface. This was done to make viewing the surface easier. However, the presence of the line is still noticeable in the surface. This is most likely due to the effect of the tool leaving and entering the cut.

When compensation was applied to the code, the RMSE was reduced to 0.005 mm and the maximum error was reduced to 0.015 mm. The surface machined with the off-line compensation strategy is shown in Figure 7.4. This is comparable to the results of the training data when the surface roughness of the process is taken into account.

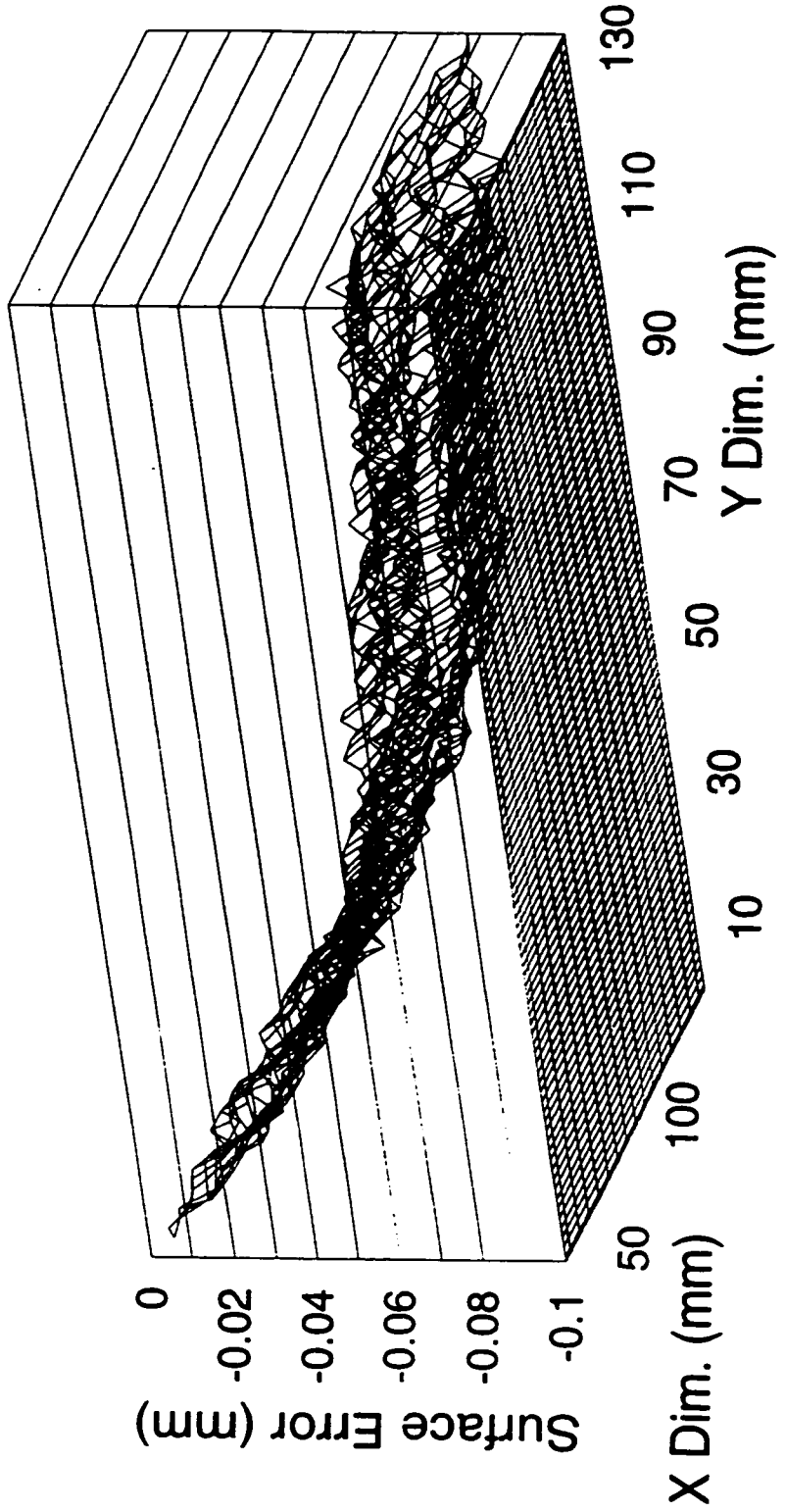

Figure 7.3 Errors in Machined Surface Before Compensation

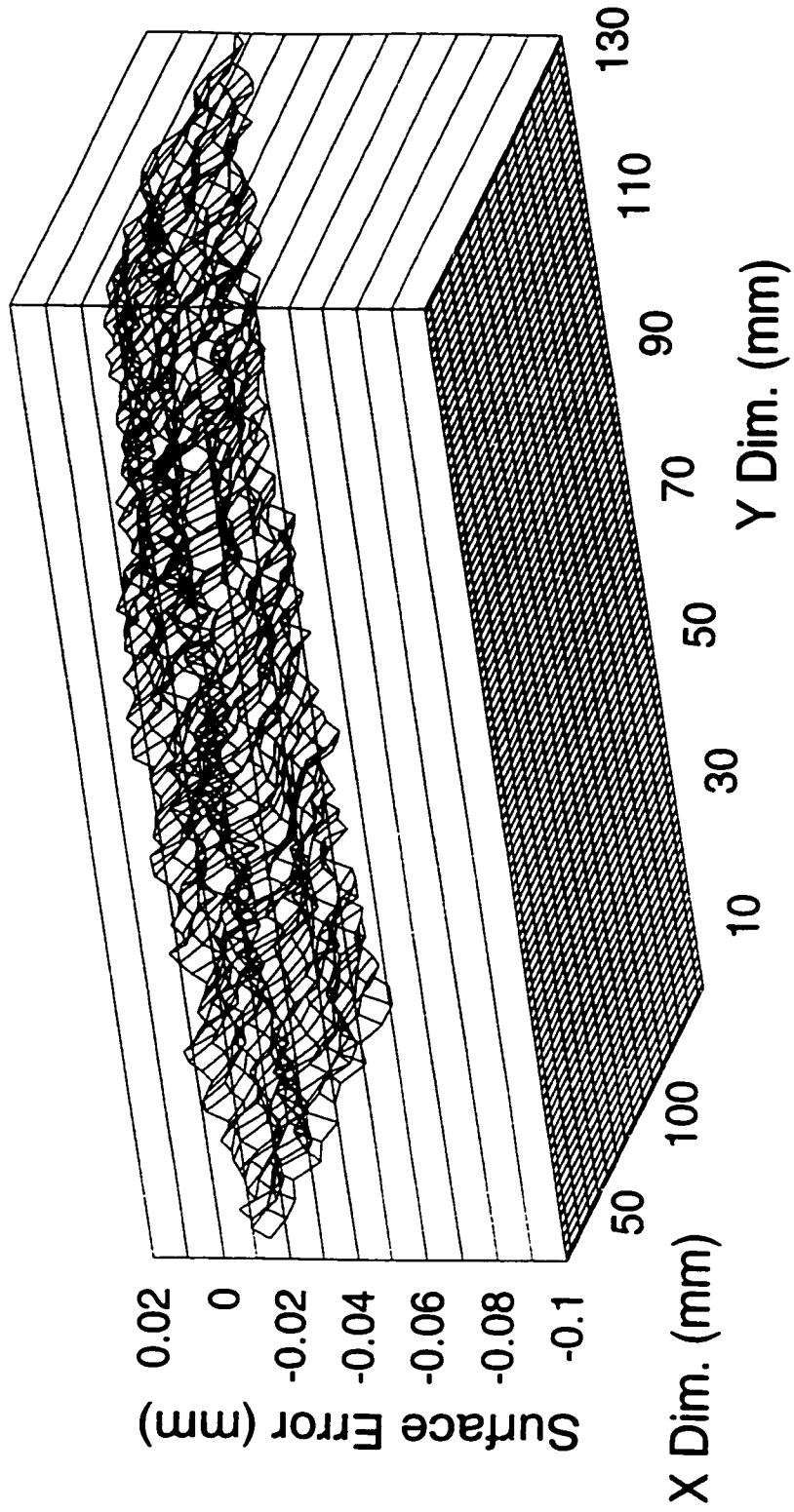

Figure 7.4 Errors in Machined Surface After Compensation With Off-Line Models

The on-line model was used to capture any unmodelled errors which may not be captured in the model trained previously with the off-line data. The cutting test was run once to allow the on-line parameters a chance to establish themselves before being used in the compensation strategy. Figure 7.5 shows the parameters updating with each sampling of the error.

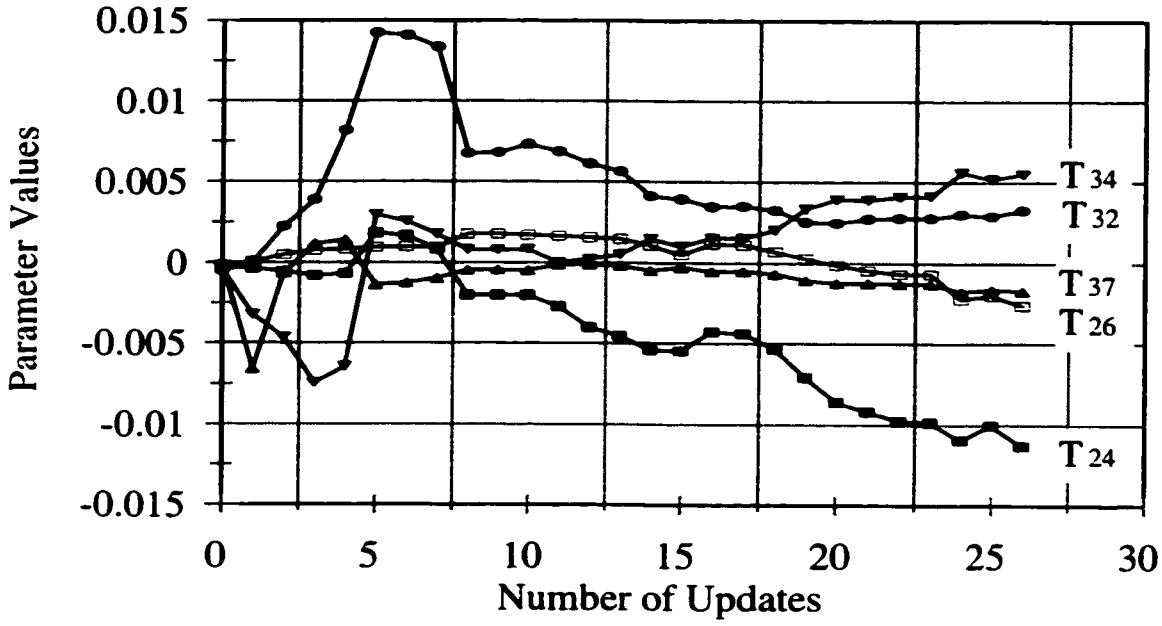

Figure 7.5 Parameter Update with On-Line Data

Figure 7.6 shows the errors remaining in the machined surface with both the off-line and on-line models being used. The RMSE of the final surface was reduced to 0.003 mm and the maximum error was reduced to 0.012 mm. The on-line model was updated every 15 minutes using data shown previously in Figures 5.19 and 5.20 in the experimental section.

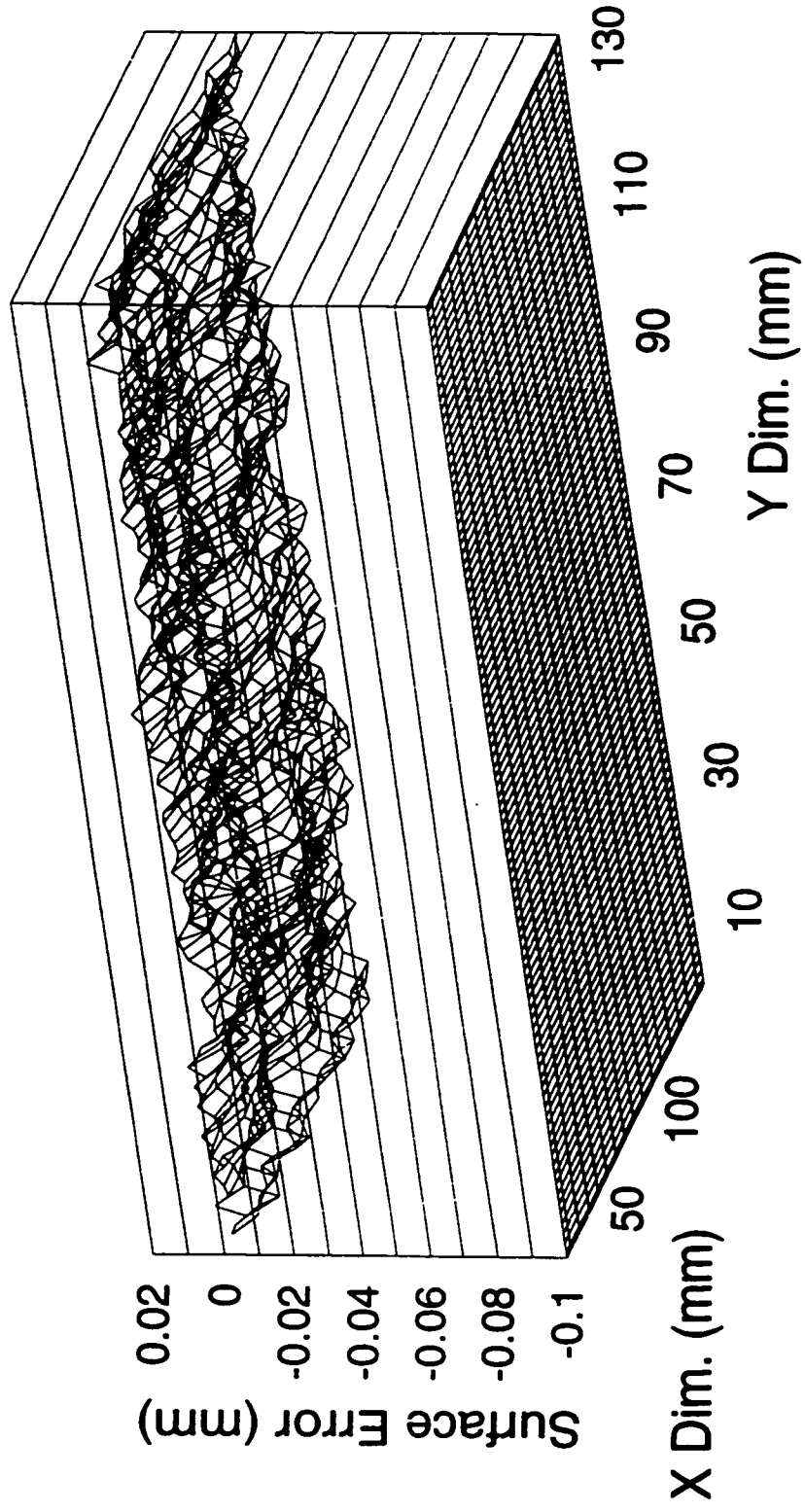

Figure 7.6 Errors in Machined Surface with Full Compensation Strategy

7.4 Summary

This chapter discussed the issues involved with integrating the two models, the off-line model and the on-line model, with the machine tools controller. The means of including the compensation values in the machine code was discussed along with the timing issues involved in providing up-to-date compensation values to the machine without compromising the machine's interpolation strategy. The results of realistic cutting tests were also presented, which showed a significant reduction in error with the use of the compensation strategy.

CHAPTER 8

CONCLUSIONS AND RECOMMENDATIONS

8.1 Introduction

The objective of this thesis was to improve the accuracy of a five-axis machine tool by using the underlying repeatability in the process. This was done by finding the parameters that caused the machine's accuracy to vary. The main influencing factor was found to be the change in the temperature distribution within the machine over time. Large heat sources and changes in the environment directly influenced the temperature distribution within the machine. This, combined with the material's coefficient of thermal expansion, resulted in significant deformation of the main structural and motion controlling components of the machine.

The errors in motion were within the manufacturer's stated accuracy. However, when the machine was run at high spindle speeds and feed rates, like those typically used in high speed machining, the errors went far beyond the tolerance limits specified by the manufacturer. Machine shops are familiar with this problem and have standard practices in place to ensure that these errors are not transferred onto the final part. Unfortunately, these procedures are time consuming and result in significant amounts of scrapped parts. In comparison, the compensation strategy proposed in this research would effectively maintain a stable reference frame by adjusting the machine code to account for any deformation in the machine's structure.

8.2 Conclusions

A kinematic model of a five-axis machine tool was formulated to represent the volumetric error in the work space as a function of the error in individual links and joints. This model was based on HTM which were formulated for every link and joint using small angle approximations. The kinematic model of the machine was applied to allocate the error measured in the work space to the error in the individual links and joints. This was done to aid the empirical modelling of the errors. The kinematic model was also used to calculate the axis motions which effectively eliminated the error in the work space.

Direct measurement of the error in the work space of the machine was done using a laser interferometer and reference surfaces. These measurements were related to the

temperature distribution in and around the machine. The temperature distribution in and around the machine was sampled using fifty thermocouples. A strategy for selecting the best location and number of thermocouples was developed. It involved placing an excess number of them on the structure and reducing their number based on the results of a correlation analysis, while keeping in mind the guidelines initially used for placing them.

The predictions used in the compensation strategy were based on empirical models which were identified using off-line and on-line error measurement techniques. The data used to identify the off-line empirical models came from measurements of the error in the work space. To facilitate modelling, the error variations measured in the work space were allocated to the individual links and joints in a systematic fashion using the kinematic model of the machine tool. By allocating the error to the region on the machine where it was generated, it was easier to include known physical relationships of the deformation process. The inclusion of these relationships saved time as it reduced the burden of identifying the relationship using the collected data.

Two different techniques were considered for identifying the errors in the machine. They were a neural network model and multiple linear regression model. The RMSE of the neural network technique and the multiple linear regression was 0.0025 mm and 0.0033 mm respectively on the same set of data. The neural network model predicted the error variations with a higher degree of accuracy than the multiple linear regression model. However, the multiple linear regression was chosen for use in the compensation strategy because of concerns with the performance of the neural network operating under conditions for which it was not explicitly trained. The neural network performed well when interpolating, but

poorly when extrapolating. This condition was observed during preliminary testing when the temperature went outside of the training range and the predicted error resulted in a work space error three times higher than that of the multiple linear regression technique. This condition is expected to occur in an industrial setting as well, since most machine shops have limited control over the room temperature. To guard against the need to extrapolate, the input values to the neural network model could be restricted within a set range; however, the usefulness of the model would then be limited during the conditions when it was most needed.

Preliminary testing of the empirical model showed a reduction of error was possible in both the position and orientation errors. The RMSE was reduced to less than 0.0033 mm for the translational motion and to less than 0.001 ° for the rotational motion of the test cases. These values closely match the resolution of the machine as stated by the manufacturer to be 0.0025 mm and 0.001 °.

Any relationships not captured in the off-line model of the errors, or variations which occurred after off-line measurements were made, were built into the compensation strategy through an on-line procedure. This procedure involved periodic process intermittent measurement of the errors in the work space using a touch trigger probe and a proximity sensor array. The on-line values could not be allocated in the same way as the off-line measurements. Thus, the compensating moves at each axis that minimize the error were applied. The on-line data was then used to recursively update a multiple linear regression model. This model was kept separate from the original off-line model since the on-line data could not be directly allocated to specific links and joints like the off-line data.

The implementation of the compensation strategy was done on a PC interfaced to the machine tool via an RS-232 serial communications port. Testing of the compensation strategy under realistic cutting conditions demonstrated that error on a machine surface could be reduced from an RMSE of 0.060 mm with a maximum error of 0.082 mm to an RMSE of 0.005 mm with a maximum error of 0.015 mm using the model identified off-line. When the on-line update of the compensation strategy was done every 15 minutes during the cutting test, the RMSE of the final surface was reduced to 0.004 mm.

8.3 Recommendations

One of the basic guidelines discussed in the literature stated that before applying a compensation strategy, every practical effort to eliminate the error must be made at the design stage. Significant errors are present due to this machine's design that could have been addressed by relatively simple design changes. For example, major heat sources could be isolated from the machine tool structure by using mounting components which have a lower heat transfer coefficient, such as a ceramic or epoxy composite. Also, some heat sources could be separated by a greater distance from the machine and more heat transfer fins could be added to reduce the build up of heat. Better use of the chilling unit already present in the machine could be made to cool not just the spindle bearing, but also the main spindle support arm. It would be interesting to make these changes to determine if the effectiveness of the compensation strategy improved, especially with regards to the rapid changes in error in the

spindle support arm.

The model of the errors was very dependent on the temperature distribution in the machine tool's structure. Therefore, the inclusion of thermal models which described this distribution would improve the model's ability to deal with rapidly changing conditions, like those associated with the thermal gradients in the spindle support arm. The compensation strategy's ability to capture these relationships would be enhanced if more elaborate thermal models could be included with the empirical models when predicting the error.

Further work could be done on developing a practical model update scheme for a five-axis machine tool based on the measurements made on the machined part. To do this, knowledge of the part's path must be combined with the errors measured on the part by a CMM and then interpreted to decide how to best command the five axes to compensate for the errors.

The issues associated with applying this compensation strategy on other machines should also be addressed. A minimum number of tests should be developed, using the knowledge already gained on this machine, to customize the empirical models for a new machine operating in a different setting.

REFERENCES

M. H. Attia, "Modelling of Thermal Deformation of Machine Tool Structures: Design and Control Issues", Mechanical Research Department, Ontario Hydro.

M. H. Attia and L. Kops, "Thermometric Design Considerations for Temperature Monitoring in Machine Tools and CMM Structures", Int. J. Adv. Manuf. Technol., vol. 8, pp. 311-319, 1993.

M. H. Attia and L. Kops, "System Approach to the Thermal Behaviour and Deformation of Machine Tool Structures in Response to the Effects of Fixed Joints", Trans. ASME, J. Eng. Ind., vol. 103, pp. 67-72, 1981.

M. H. Attia and L. Kops, "Calculation of Thermal Deformation of Machine Tools in Transient State, With the Effect of Structure Taken into Account", Annals CIRP, vol. 28, no.1, pp. 247-251, 1979.

A. Balsamo, D. Marques and S. Sartori, "A Method for Thermal Deformation Correction of CMMs", Annals of CIRP, vol. 39, no.1, pp. 557-560, 1990.

G. Belforte, B. Bona, E. Canuto, F. Donati, F. Ferraris, I. Gorini, S. Morei, M. Peisino and S. Sartori, "Coordinate Measuring Machines and Machine Tools Selfcalibration and Error Correction", Annals of CIRP, vol. 36, no. 1, pp 359-364.

J. A. Bosch, *Coordinate Measuring Machines and Systems*, Marcel Dekker, Inc. New York, 1995.

J. B. Bryan, "International Status of Thermal Error Research", Pass-out copy, CIRP, cooperative effort of STC "M" and STC "Q", 1990 .

J. B. Bryan, "The Abbe Principle Revisited: An updated Interpretation", Precision Engineering, Vol. 1, No. 3, 1979.

J. B. Bryan, "International Status of Thermal Error Research", Keynote Paper Annals CIRP, vol. 16, p. 203, 1968.

J. S. Chen, J. X. Yuan, J. Ni, and S. M. Wu, "Real-Time Compensation of Time-Variant Volumetric Error on a Machining Center", Sensors, Controls, and Quality Issues in Manufacturing, WAM ASME, pp. 241-253, 1991.

J. S. Chen, J. Yuan, J. Ni, and S. M. Wu, "Thermal Error Modeling for Volumetric Error Compensation", Sensors and Signal Processing for Manufacturing, WAM ASME, pp. 113-125, 1992.

R. Chiappulinin, L. Giannotti and A. Galbersan, "On-Line Correction Via Software of Thermal Errors in Numerically Controlled Machine Tools", CNR IMU, Milano, Italy, 1991.

H. Demuth and M. Beale, Neural Network Toolbox for Use with Matlab", The Math Works Inc., 1994.

J. Denavit, R. S. Hartenberg, "A Kinematic Notation for Lower-Pair Mechanisms Based on Matrices", J. Appl. Mech., June, pp. 215-221, 1955.

A. Donmez, "A General Methodology for Machine Tool Accuracy Enhancement: Theory, Application and Implementation", Ph. D. Dissertation, Purdue University, West Lafayette, Indiana, 1985.

U. Dorndorf, V. S. B. Kiridena and P. M. Ferreira, "Optimal Budgeting of Quasistatic Machine Tool Errors", Trans. of the ASME, vol.116, Feb. pp. 42-53, 1994.

P. Dufour and R. Groppetti, "Computer Aided Accuracy Improvement in Large NC Machine Tools", Proc. of 22nd Int. MTDR Conf., pp. 611-618, 1981.

K. F. Eman, B. T. Wu, and M. F. DeVries, "A Generalized Geometric Error Model for Multi-Axis Machines", Annals CIRP, vol. 36, no. 1, pp. 253-256, 1987.

Fadal, *Operators Manual*, North Hollywood, California, 1998

K. C. Fan, J. F. Lin and S. S. Lu, "Measurement and Compensation of Thermal Error on a Machining Center", Proceedings of the 29 Int. MATADOR Conference, April, pp. 261-268, 1992.

P. M. Ferreira and C. R. Liu, "An Analytical Quadratic Model for the Geometric Error of a Machine Tool", J. of Manuf. Sys., vol. 5, no. 1, pp. 51-63, 1986a.

P. M. Ferreira and C. R. Liu, "A Contribution to the Analysis and Compensation of the Geometric Error of a Machining Center", Annals CIRP, vol. 35, no. 1, pp. 259-262, 1986b.

J. A. Freeman and D. M. Skapura, "Neural Networks: Algorithms, Applications and Programming Techniques", Addison-Wesley, Reading Massachusetts, 1991.

M. Gull, "Advances in Acceptance Testing of Numerically Controller Machine Tools", Proceedings of the 28th Int. MATADOR Conference, April, pp. 497-504, 1992.

B. R. Hardwick, "Improving the Accuracy of CNC Machine Tools Using Software Compensation for Thermally Induced Errors", Proceedings of the 29 Int. MATADOR Conference, April, pp. 269-276, 1992.

Y. Hatamura, T. Nagao, M. Mitsuishi, G. Nakagawa, H. Sugishita and B. Kramer, "A Fundamental Structure for Intelligent Manufacturing and its Application to a Machining Center", Human Aspects in Computer Integrated Manufacturing, pp. 131-143, 1992.

Y. Hatamura, T. Nagao, M. Mitsuishi, K. Kato, S. Taguchi, T. Okumura, G. Nakagawa and H. Sugishita, "Development of an Intelligent Machining Center Incorporating Active Compensation for Thermal Distortion", Annals of the CIRP, vol. 42, no. 1, pp. 549-552, 1993.

S. Haykin, *Neural Networks A Comprehensive Foundation*, Macmillan College Publishing Company, New York, 1994.

C. P. Hemingray, "Some Aspects of the Accuracy Evaluation of Machine Tools", Proc. of 14th. Int. MTDR Conf., pp. 281-284, 1973.

Hewlett Packard, "Improve Machine Tool Productivity with Laser Calibration", 1990.

Hewlett Packard, "Machine Tool Calibration Using the HP 5528A Laser Measurement System", Application Note 325-2, 1990.

Hewlett Packard, "Manuals for HP 5527A Laser Measurement System", 1988.

G. E. Hinton, "How Neural Networks Learn from Experience", Scientific American, Sept. pp. 145-172, 1992.

R. J. Hocken, Technology of Machine Tools, Vol. 5: Machine Tool Accuracy. Lawrence Livermore Laboratory, University of California, Livermore, CA 1980.

J. Jedrzejewski and W. Modrzycki, "A New Approach to Modelling Thermal Behaviour of a Machine Tool Under Service Conditions", Annals CIRP, vol. 41, no. 1, pp. 455-458, 1992.

J. Jedrzejewski, J. Kaczmarek, Z. Kowal and Z. Winiarski, "Numerical Optimization of Thermal Behaviour of Machine Tools", Annals CIRP, vol. 39, no. 1, pp. 379-382, 1990.

V. S. B. Kiridena and P. M. Ferreira, "Kinematic Modeling of Quasistatic Errors of Three-Axis Machining Centers", Int. J. Mach. Tools Manufact., vol. 34, no. 1, pp. 85-100, 1994a.

V. S. B. Kiridena and P. M. Ferreira, "Parameter Estimation and Model Verification of First Order Quasistatic Error Models For Three-Axis Machining Centers", Int. J. Mach. Tools Manufact., vol. 34, no. 1, pp. 101-125, 1994b.

V. S. B. Kiridena and P. M. Ferreira, "Computational Approaches to Compensating Quasistatic Errors of Three-Axis Machining Centers", Int. J. Mach. Tools Manufact., vol. 34, no. 1, pp. 127-145, 1994c.

V. Kiridena and P. M. Ferreira, "Mapping the Effects of Positioning Errors on the Volumetric Accuracy of Five-Axis CNC Machine Tools", Int. J. Mach. Tools Manufact., vol. 33, no. 3, pp. 417-437, 1993.

V. S. B. Kiridena and P. M. Ferreira, "Modeling and Estimation of Quasistatic Machine-Tool Errors", Trans. NAMRI/SME, pp. 211-221, 1991.

L. Kops and R. Bouzaiene, "Thermal Deformation Control of Machine Tools: Modelling and Control of Thermoelastic Behavoiu of a Cantilever Beam with a Continuous Surface Heat Source", 1992.

B. V. Kreng, C. R. Liu and C. N. Chu, "A Compact Three-Dimensional Error Model of Machine Tools", WAM ASME, Control Issues in Manufacturing Processes, San Francisco, Ca., pp. 25-31, 1989.

W. J. Love and A. J. Scarr, Proc. 14th. Int. MTDR Conf., p. 307, 1973.

P. D. Lin, *Error Analysis, Measurement and Compensation for Multi-Axis Machines*, Ph.D. Dissertation, Northwestern University, 1989.

P. D. Lin and K. F. Ehmann, "Direct Volumetric Error Evaluation for Multi-Axis Machines", Int. J. Mach. Tools Manufact., vol. 33. no. 5, pp. 675-693, 1993.

R. P. Lippmann, "An Introduction to Computing with Neural Nets", IEEE ASSP Magazine, April, pp. 4-22, 1987

L. Ljung and T. Söderström, *Theory and Practice of Recursive Identification*, MIT Press, Cambridge, Massachusetts, 1987.

Maple, Symbolic Computation Group. University of Waterloo, Waterloo, Ontario, Canada, N2L 3L3.

P. A. McKeown, M. Weck, R. Bonse, "Reduction and Compensation of Thermal Errors in Machine Tools", Annals of CIRP, Keynote Paper, 1995.

T. Moriwaki, E. Shamoto and M. Kawano, "Prediction of Thermal Deformation of Machine Tool With Strain Sensor", ASME-WAM MED-Vol.6-1, pp.137-142, 1997.

T. Moriwaki, N. Sugimura and Y. Miao, "A Model Based Design of Kinematic Accuracy of Machine Tools", Human Aspects in Computer Integrated Manufacturing, Proc. of 8th Int. Prolamat Conf., pp. 673-684, 1992.

T. Moriwaki and C. Zhao, " Neural Network Approach to Identify Thermal Deformation of a Machining Center", Human Aspects in Computer Int. Manufact. pp. 685-697, 1992.

J. Mou, M. A. Donmez and S. Cetinkunt, "An Adaptive Error Correction Method Using Feature-Based Analysis Techniques for Machine Performance Improvement: Part I - Theory Derivation", ASME-WAM PED-vol. 68-2, pp.909-917, 1994a.

J. Mou, M. A. Donmez and S. Cetinkunt, "An Adaptive Error Correction Method Using Feature-Based Analysis Techniques for Machine Performance Improvement: Part II - Experimental Verification", ASME-WAM PED-vol. 68-2, pp.919-929, 1994b.

J. Mou and C. R. Liu, "A Methodology for Machine Tool Error Correction - An Adaptive Approach", WAM ASME New Orleans, pp.69-81, 1993

K. Okushima, Y. Kakino and A. Higashimoto, "Compensation of Thermal Displacement by Coordinate System Correction", Annals of the CIRP, vol. 24, no. 1, pp.327-331, 1975.

A. J. Otter, "Thermocouples and Surface Temperature Measurement", Chalk River, Ontario, 1968.

R. P. Paul, Robot Manipulators-Mathematics, Programming, and Control, MIT Press, Cambridge, Mass., 1982.

J. Riarh, "Inspect Your Machine Not Your Parts", Modern Machine Shop Magazine, July, 1994.

Z. Rujia, P. Qingjin, X. Qingyou and Y. Gongqi, "Study on the Thermal Behaviour of Machine Tools and its Improving Strategies", Proceedings of the 29 Int. MATADOR Conference. April, pp.287-290, 1992.

T. Sata, Y. Takeuchi, and N. Okubo, Proc. 18th Int. MTDR Conf., p. 93, 1977.

T. Sata, Y. Takeuchi, N. Sato, and N. Okubo, "Analysis of Thermal Deformation of Machine Tool Structure and its Application", Proc. of 14th Int. MTDR Conf., pp. 275-280, 1973.

R. Schultschik, "The Components of the Volumetric Accuracy", Annals of CIRP, vol. 25, no. 1, pp. 223-228, 1977.

A. H. Slocum, Precision Machine Design, Prentice Hall, Englewood Cliffs, New Jersey, 1992.

E. E. Sprow, "Step up to Five-Axis Programming", Manufacturing Engineering, Nov., pp. 55-60, 1993.

G. Spur and P. De Haas, "Thermal Behaviour of NC Machine Tools", Proc. of 14th Int. MTDR Conf., p. 267, 1973.

G. Spur and H. Fischer, "Thermal Behaviour of Machine Tools", Proc. of 10th Int. MTDR Conf., pp. 147-160, 1969.

N. Srinivasa and J. C. Ziegert. "Real-Time Learning of Thermal Errors in Machine Tools Using a Fuzzy Logic Based Neural Network", Manufacturing Sciences and Engineering ASME, PED-vol. 64, pp. 235-240, 1993.

N. Srinivasa, J. C. Ziegert and S. Smith, "Prediction of Positional Errors of a Three Axis Machine Tool Using Neural Network", Japan/USA Symposium on Flexible Automation ASME, vol. 1, pp. 203-209, 1992.

A. K. Srivastava, S. C. Veldhuis and M. A. Elbestawi, "Modelling Geometric and Thermal Errors in a Five-Axis CNC Machine Tool", Int. J. Mach. Tools Manufact., Vol. 35, No. 9, pp 1321-1337, 1995.

S. Takada, M. Obi, and T. Sata, J. of JSPE, vol. 40, no. 8, p. 678, 1974.

Y. Takeuchi, M. Sakamoto, and T. Sata, J. of JSPE, vol. 46, no. 11, p. 1576, 1980.

I. Tanabe, K. Takada and M. Tsutsumi, "Thermal Deformation of Machine Tool Structures using Epoxy Resin Concrete", Proceedings of the 26 Int. MTDR Conference, Sept, pp. 245-252, 1986.

R. W. Teltz, *Open Architecture Control for Intelligent Machining Systems*, Ph.D. Dissertation, McMaster University, Hamilton, Ontario, 1998.

J. Tlusty and F. F. Mutch, "Testing and Evaluating Thermal Deformations of Machine Tools", MTDR Conf. Proc. 14, pp. 285-297, 1973.

J. Tlusty and F. Koenigsberger, "New Concepts of Machine Tool Accuracy", Annals CIRP, vol. 19, pp. 261-273, 1971.

H. Trankle, *Effects of Position Errors in Five-Axis Milling Processes*, Ph. D. Dissertation, Stuttgart University, Federal Republic of Germany, 1980.

W. K. Veitschneggar and C. H. Wu, IEEE J. of Robotics and Automation, vol. RA-2/3, p. 339, 1986.

S. C. Veldhuis and M. A. Elbestawi, "Modelling and Compensation for Five-Axis Machine Tool Errors", ASME-WAM, Ped-vol. 68-2, 1994.

S. C. Veldhuis and M. A. Elbestawi, "A Strategy for the Compensation of Errors in Five-Axis Machining", Annals of CIRP, vol. 43, no. 1, pp , 1995.

R. Venugopal, *Thermal Effects on the Accuracy of Numerically Controlled Machine Tools*, Ph. D. Dissertation, Purdue University, West Lafayette, Indiana, 1985.

R. Venugopal and M. Barash, "Thermal Effects on the Accuracy of Numerically Controlled Machine Tools", Annals of the CIRP, vol. 35, no. 1, pp 255-258, 1986.

E. Weck, O. Schulze, F. Michels and R. Bonse, "Optimization of Machine Tool Performance and Accuracy", ASME-WAM, PED-Vol. 68-2, pp 895-908, 1994.

G. Zhang, R. Veale, T Charlton, B. Borchardt and R. Hocken, "Error Compensation of Coordinate Measuring Machines", Annals of CIRP, Vol.34/1, pp 445-448, 1985.

APPENDIX A

SIMULATION PARAMETERS

Table A.1 provides the various fixed link dimensions for the five-axis vertical machining centre used in the simulation study.

Machine Component	a mm	b mm	c mm
Spindle head	0.0	-400.0	-200.0
Vertical column	0.0	400.0	1200.0
Y-X carriage	0.0	0.0	-200.0
Main table	0.0	0.0	-200.0
θ_x-θ_z Support	0.0	0.0	-200.0
Part table	0.0	0.0	-400.0

Table A.1 Dimensions of the Simulated Machine Tool

The total errors for the fixed-links were calculated using the following equation:

$$\begin{bmatrix} \alpha(t) \\ \beta(t) \\ \gamma(t) \\ \Delta a(t) \\ \Delta b(t) \\ \Delta c(t) \end{bmatrix} = [0.3 + 0.7\ (1-e^{-t/\tau_L})] \begin{bmatrix} K_L\alpha \\ K_L\beta \\ K_L\gamma \\ K_L\Delta a \\ K_L\Delta b \\ K_L\Delta c \end{bmatrix} \quad \text{(A1)}$$

where the values of $K_L\Delta a$, $K_L\Delta b$, $K_L\Delta c$, $K_L\alpha$, $K_L\beta$, $K_L\gamma$ and τ_L are obtained from Table A.2.

Machine Component	$K_L\Delta a$ 10^{-3}mm	$K_L\Delta b$ 10^{-3}mm	$K_L\Delta c$ 10^{-3}mm	$K_L\alpha$ 10^{-6}rad	$K_L\beta$ 10^{-6}rad	$K_L\gamma$ 10^{-6}rad	τ_L hrs
Spindle head	12.7	-50.8	25.4	-10.0	-15.0	4.9	1.5
Vertical column	-12.7	25.4	-76.2	-24.0	-15.0	10.0	2.5
Y-X carriage	-50.8	-25.4	25.4	4.9	10.0	15.0	2.7
Main table	50.8	-38.1	25.4	10.0	-15.0	20.0	1.9
θ_x-θ_z Support	-12.7	9.6	-6.4	-10.0	-15.0	-20.0	1.2
Part table	-1.6	1.2	-0.8	-2.5	-3.3	-5.0	0.5

Table A.2 Error Constants for Fixed Links

The error terms in the moving axes are calculated using the following equation:

$$\begin{bmatrix} \alpha(x_i,t) \\ \beta(x_i,t) \\ \gamma(x_i,t) \\ \Delta x_i(x_i,t) \end{bmatrix} = [0.3\ x_i + 0.7\ x_{i\,\max}\ (1-e^{-t/\tau_T})] \begin{bmatrix} K_T\alpha \\ K_T\beta \\ K_T\gamma \\ K_T\Delta x_i \end{bmatrix} \qquad \text{(A2)}$$

where the values of $K_T\Delta x_i$, $K_T\alpha$, $K_T\beta$, $K_T\gamma$ and τ_T are obtained from Table A.3.

Axis x_i mm	Range $x_{i\,max}$ mm	$K_T\Delta x_i$ 10^{-6}mm/mm	$K_T\alpha$ 10^{-6}rad/mm	$K_T\beta$ 10^{-6}rad/mm	$K_T\gamma$ 10^{-6}rad/mm	τ_T hrs
X	254	40.0	0.142	0.094	0.189	2.8
Y	254	-60.0	0.213	0.220	-0.252	3.0
Z	-254	-5.0	-0.194	0.238	-0.083	3.0

Table A.3 Error Constants for the Translational Axes

The errors in the rotary axes are calculated using the following equation:

$$\begin{bmatrix} \alpha(t) \\ \beta(t) \\ \gamma(t) \\ \Delta x(t) \\ \Delta y(t) \\ \Delta z(t) \end{bmatrix} = [0.3\ \theta_i + 0.7\ \theta_{i\,\max}\ (1-e^{-t/\tau_R})] \begin{bmatrix} K_R\alpha \\ K_R\beta \\ K_R\gamma \\ K_R\Delta x \\ K_R\Delta y \\ K_R\Delta z \end{bmatrix} \qquad \text{(A3)}$$

where the values for $K_R\Delta x$, $K_R\Delta y$, $K_R\Delta z$, $K_R\alpha$, $K_R\beta$, $K_R\gamma$ and τ_R are obtained from Table A.4.

Axis θ_i rad	Max $\theta_{i\,max}$ rad	$K_R\Delta x$ 10^{-6}mm/rad	$K_R\Delta y$ 10^{-6}mm/rad	$K_R\Delta z$ 10^{-6}mm/rad	$K_R\alpha$ 10^{-6}rad/rad	$K_R\beta$ 10^{-6}rad/rad	$K_R\gamma$ 10^{-6}rad/rad	τ_R hrs
θx	π/4	32.3	-24.3	16.2	12.7	19.1	25.5	1.4
θz	π/4	8.1	-6.1	4.1	13.0	19.0	25.0	2.0

Table A.4 Error Constants for the Rotational Axes

APPENDIX B

THERMOCOUPLE CALIBRATION

The procedure for calibrating the thermocouples involved clamping two thermocouples together around a third thermocouple and placing the assembly in an ice bath. The temperature of the stirred ice bath was slowly raised using a hot plate, while recording the output of the thermocouples. The two outer thermocouples provided a reference output that could be compared to the output of the other thermocouple, which was to be installed. In this way if it failed while in use a new thermocouple could have its output scaled and shifted so that it would behave similarly when used as an input to the model. Calibrating the thermocouples to an exact reference was not critical given the empirical nature of the model used to relate the temperature distribution to the errors. The setup used for calibration is shown in Figure B.1.

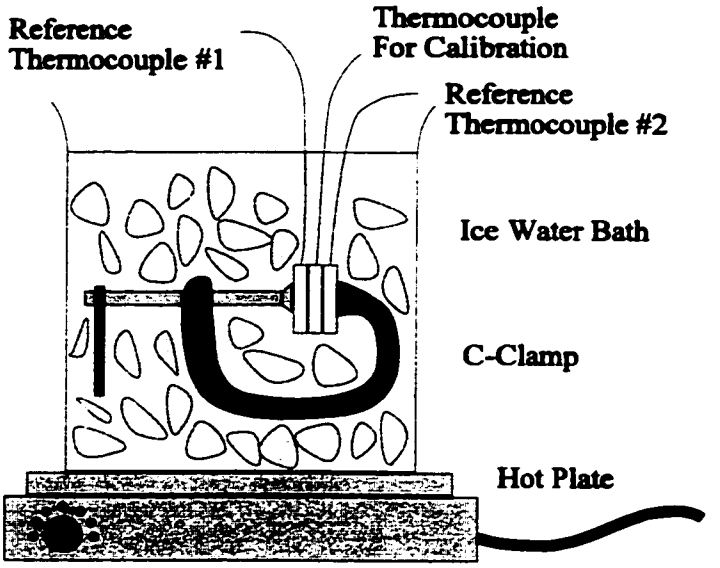

Figure B.1 Calibration Setup

The temperature range of interest was well within the linear range for the type E Chromel Constantan thermocouple wire used, as the slope adjustment factor was typically small. A typical value was only 1.000414. However, each thermocouple had its own characteristic offset, which for one thermocouple was measured as -0.20638°. Figure B.2 shows the calibration curve from which these constants were taken.

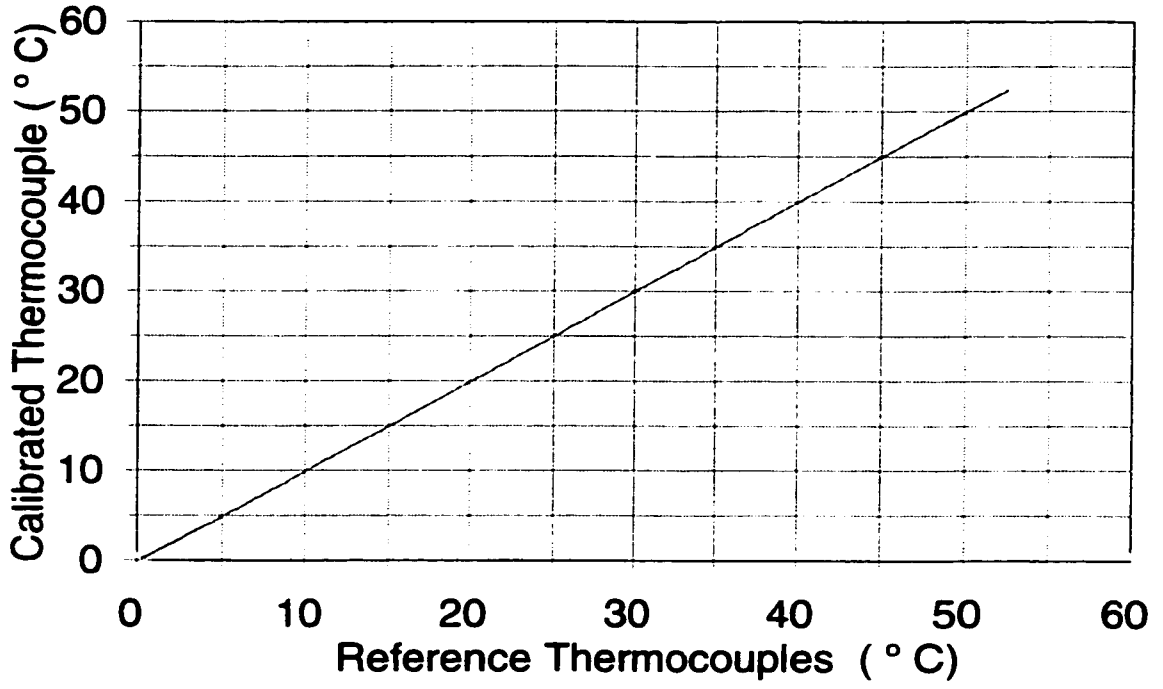

Figure B.2 Thermocouple Calibration Graph

APPENDIX C

PROXIMITY SENSOR CALIBRATION

The individual proximity sensors required calibration to relate their voltage output to real motion. The proximity sensors were calibrated with respect to the laser interferometer. The proximity sensor was mounted parallel to the laser interferometer optics on the machine. A sample plot for one of the proximity sensors is provided in Figure C.1.

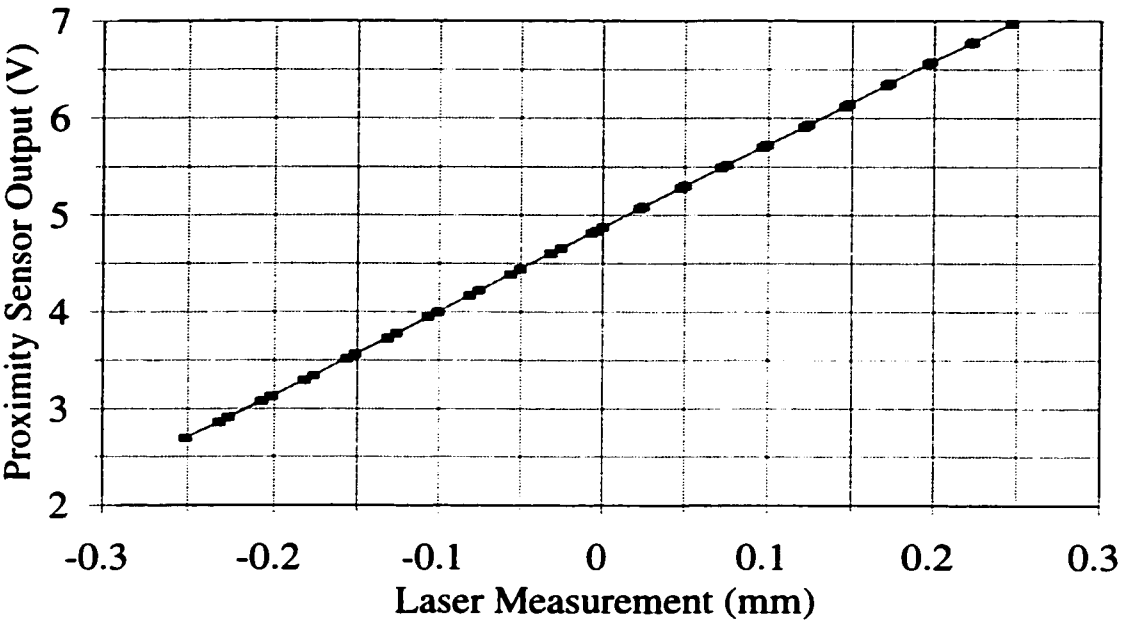

Figure C.1 Calibration of a Proximity Sensor

The proximity sensor array used for measuring the errors in the rotary table and on the parallel surfaces also required calibration. Calibration was required for the motion in the primary direction, as well as for perpendicular motion since the surfaces were not perfectly flat or square. Thus motion in one direction might cause error to be recorded in perpendicular directions. Tables C.1 and C.2 summarize the results of the A and B axis

systems of proximity sensors. Figures C.2 and C.3 show sample plots of the calibration data for Z and Y axis motion.

Axis and Motion	Sensor	Constant	Slope
A Axis X Motion	P1	5.1292	0.0104
	P2	5.2750	0.0481
	P3	4.9305	0.1306
	P4	5.3869	0.0185
	P5	4.1980	8.5811
A Axis Y Motion	P1	5.1095	8.4225
	P2	5.2712	8.5398
	P3	5.1215	0.0040
	P4	5.5147	0.0062
	P5	4.2214	-0.0496
A Axis Z Motion	P1	5.1609	-0.0044
	P2	5.3165	-0.0269
	P3	5.1204	8.4622
	P4	5.5392	8.7469
	P5	4.2362	0.0027

Table C.1 Calibration Data for the A Axis Reference Surface Measurements

Axis and Motion	Sensor	Constant	Slope
B Axis X Motion	P1	5.7087	0.3243
	P2	5.7002	0.3658
	P3	5.6850	8.7099
	P4	4.8001	8.6156
	P5	5.2896	0.0443
B Axis Y Motion	P1	5.7150	-0.0321
	P2	5.6976	-0.0361
	P3	5.6643	-0.0065
	P4	4.7992	-0.0113
	P5	5.2609	-8.3337
B Axis Z Motion	P1	5.6861	8.6192
	P2	5.6810	8.6111
	P3	5.6915	-0.0529
	P4	4.8268	-0.2458
	P5	5.2590	-0.0104

Table C.2 Calibration Data for the B Axis Reference Surface Measurements

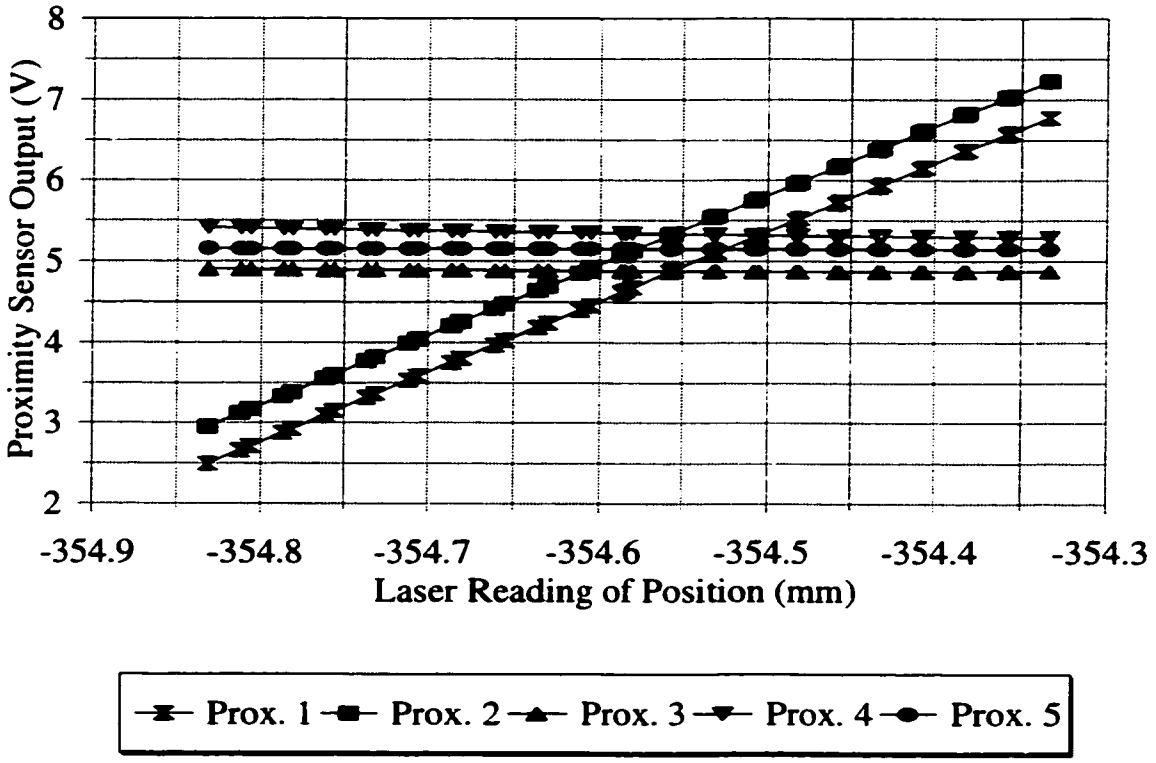

Figure C.2 A Axis Proximity Sensor Calibration for Z Motion

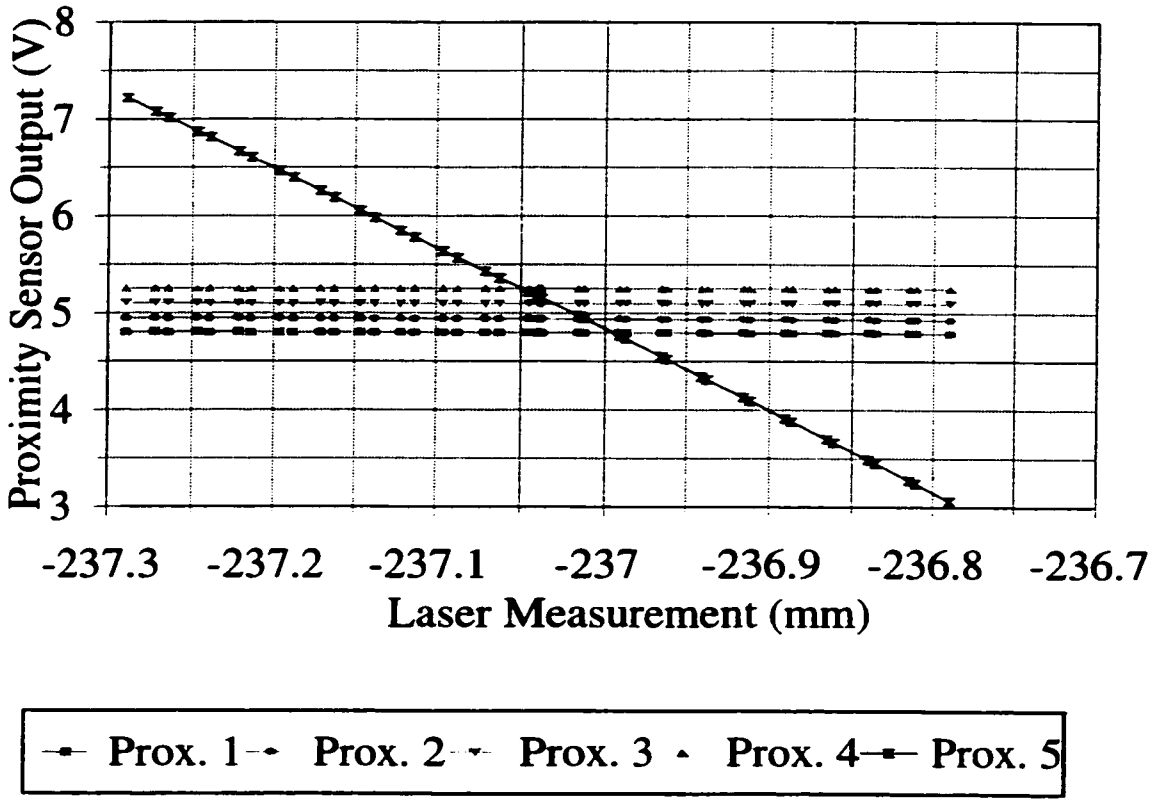

Figure C.3 B Axis Proximity Sensor Calibration for Y Motion

Although the surfaces used for calibration were not perfectly flat they were found to be repeatable. The stability of the reference surface was checked by using the laser interferometer to monitor important dimensional information on the reference surfaces while the tests were being conducted. The reference surfaces were not found to deflect significantly during the test. For the study of the thermal errors the first full motion was used as a template and any variation from this was recorded as a thermal error. The actual measurements are for the A and B axes are shown in Appendix D.

APPENDIX D

ERROR MEASUREMENT

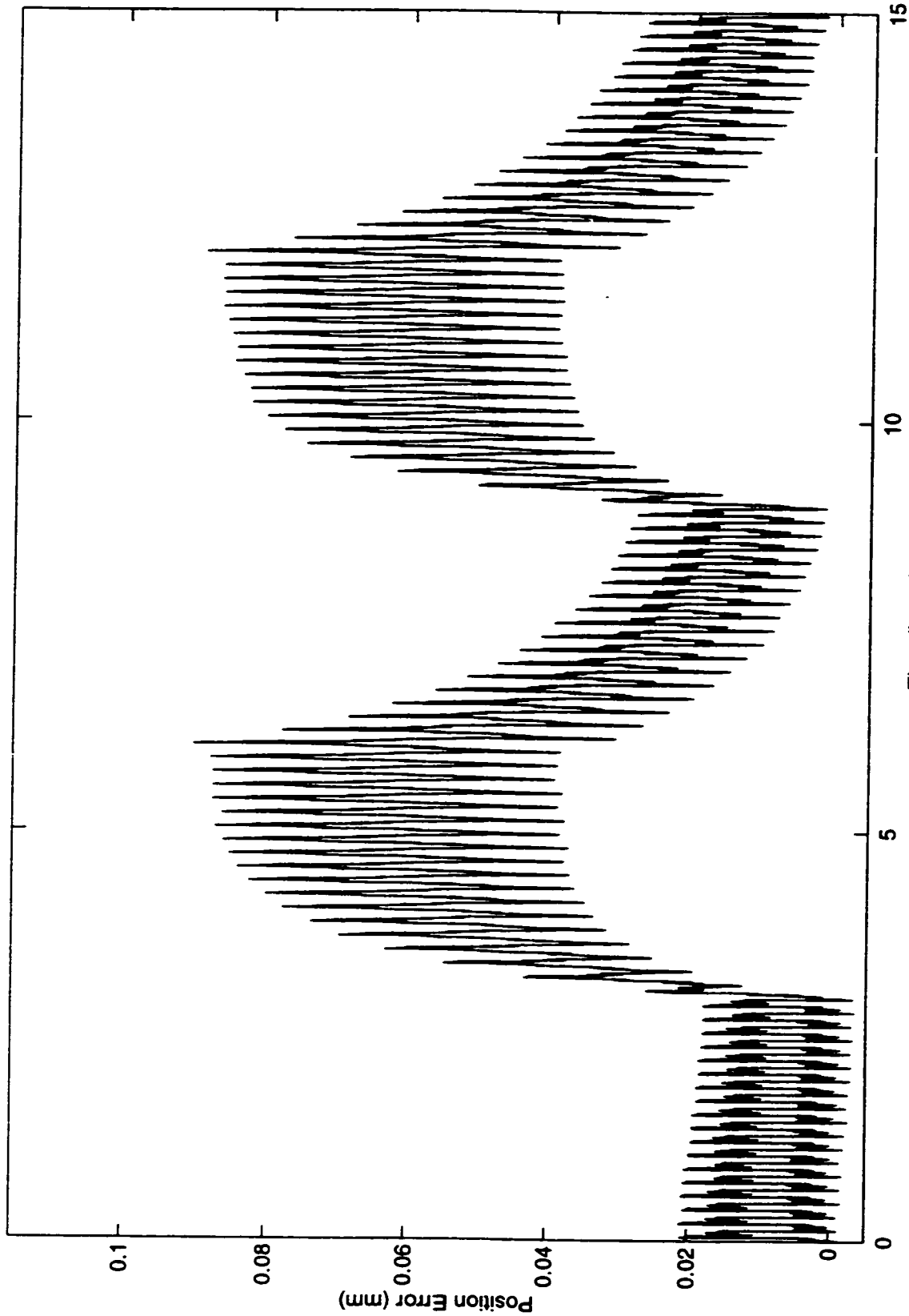

Figure D.1 X Axis Position Error

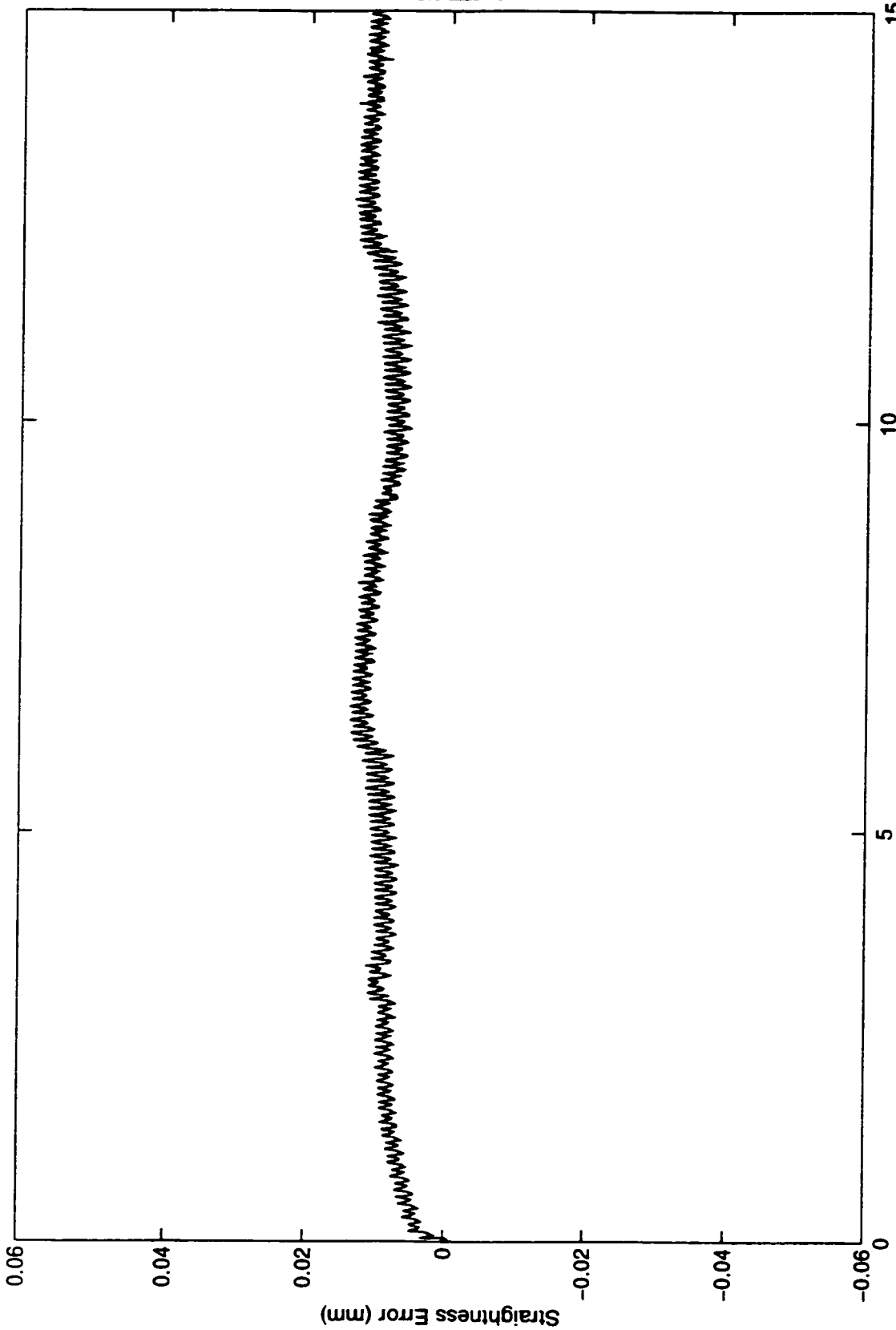

Figure D.2 X Axis Side to Side Straightness Error

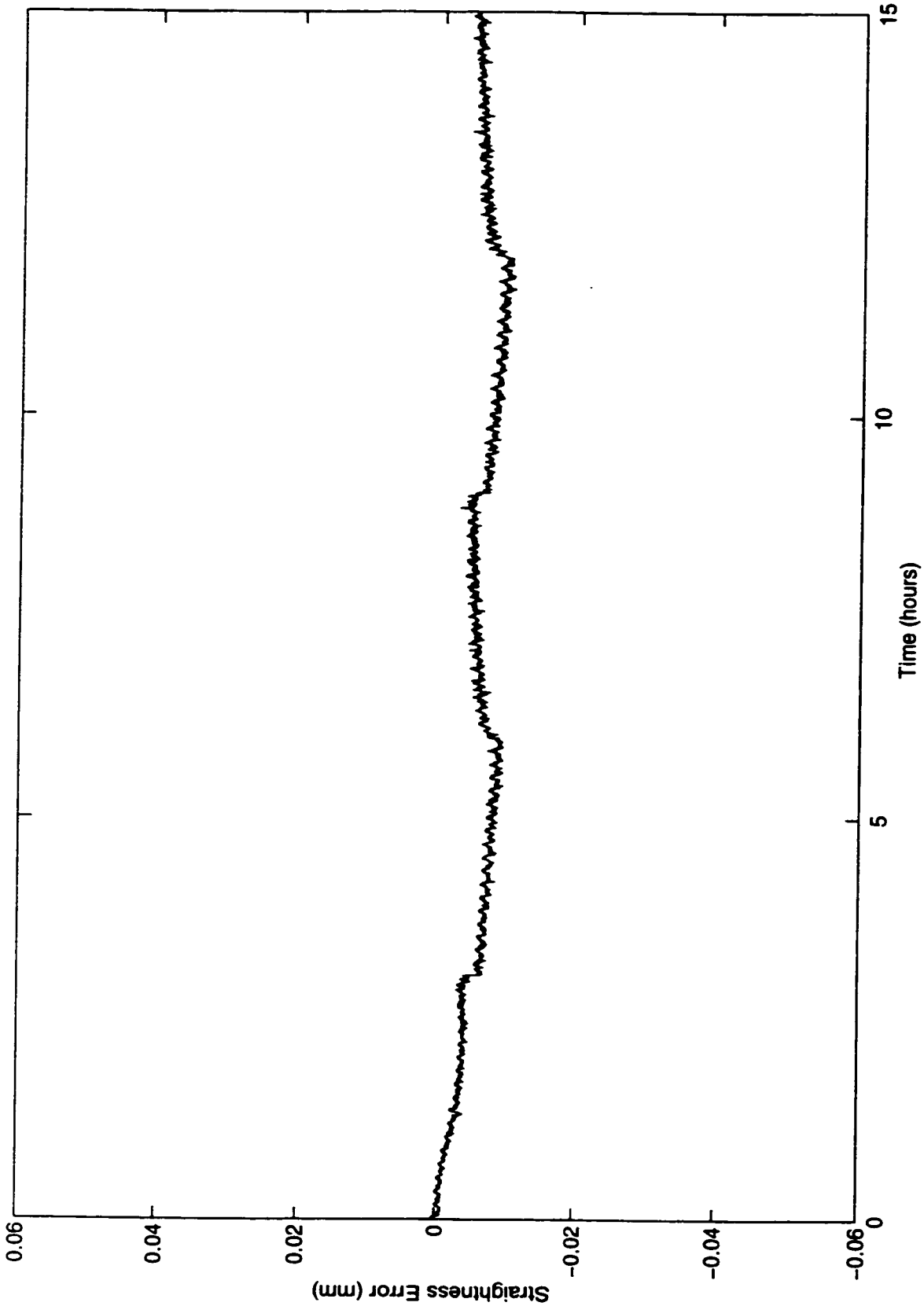

Figure D.3 X Axis Up and Down Straightness Error

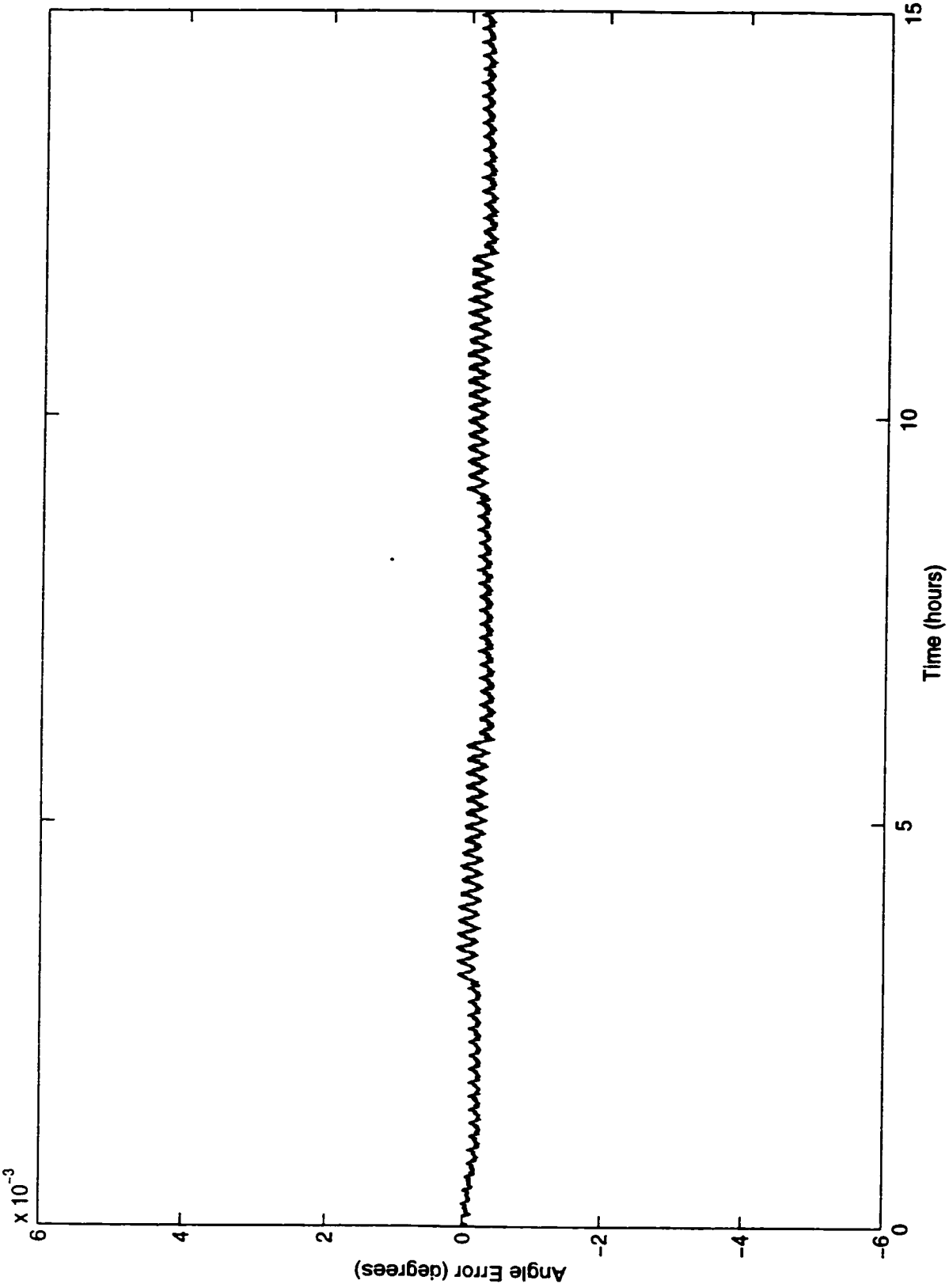

Figure D.4 X Axis Roll Angle Error

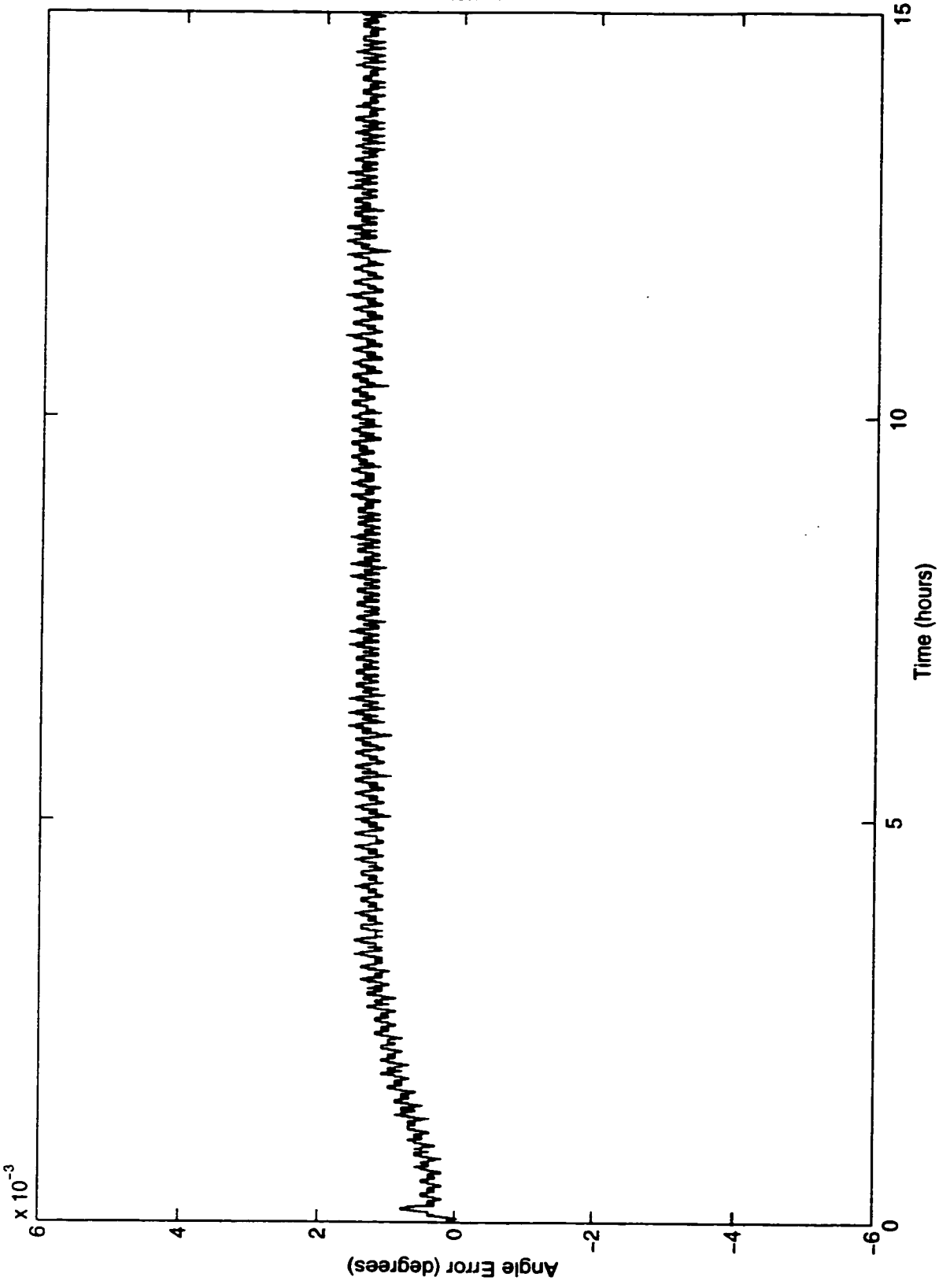

Figure D.5 X Axis Pitch Angle Error

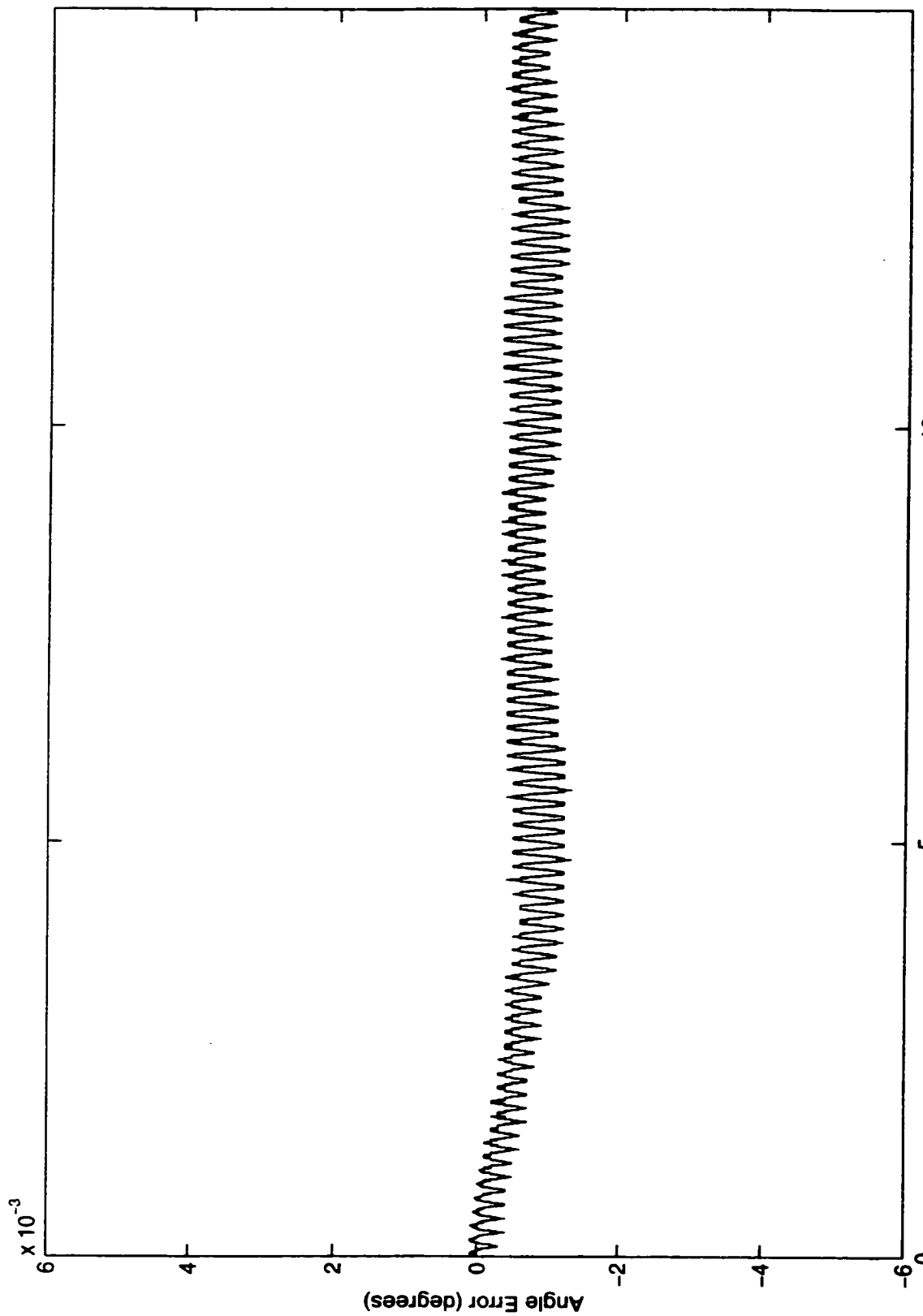

Figure D.6 X Axis Yaw Angle Error

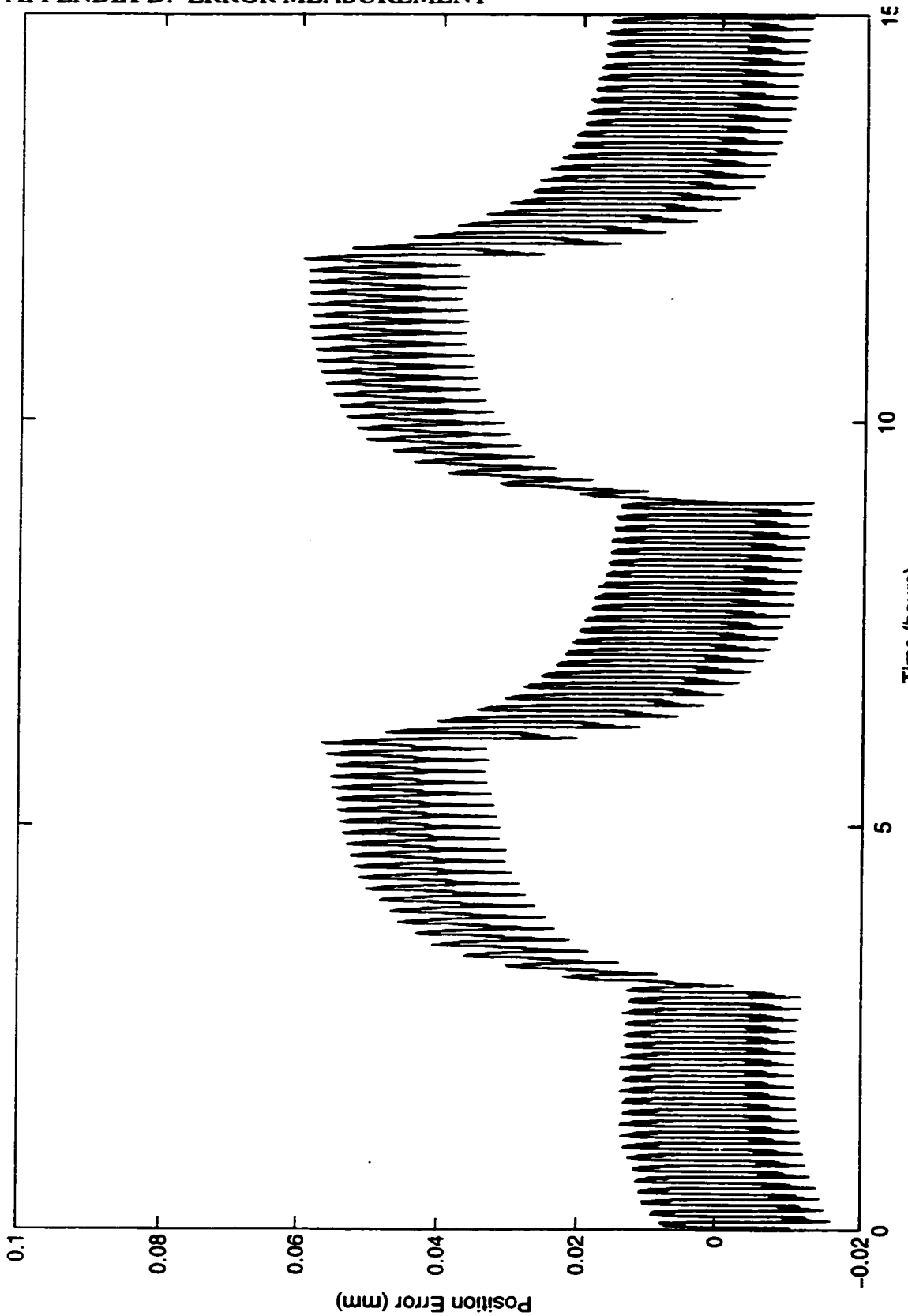

Figure D.7 Y Axis Position Error

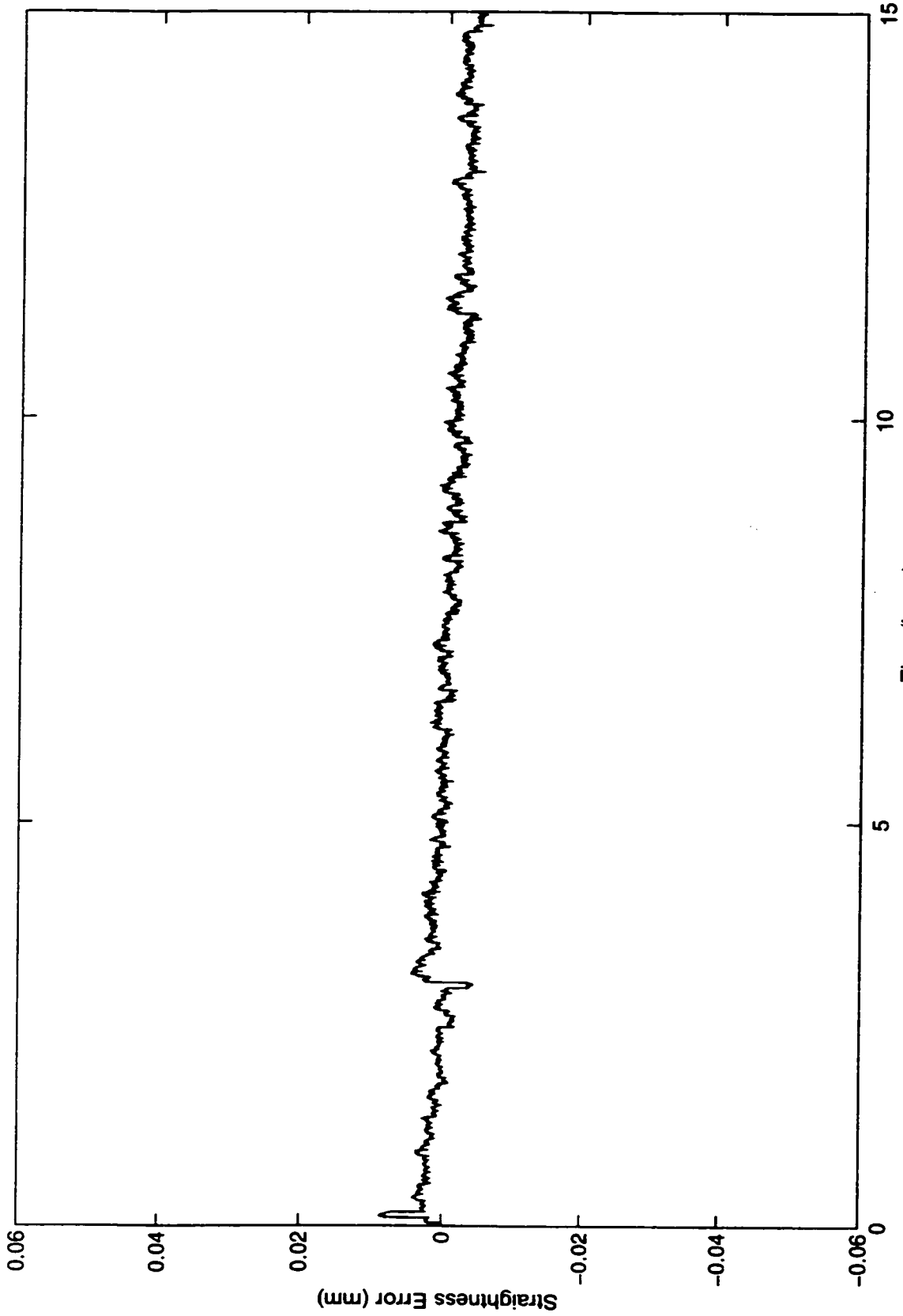

Figure D.8 Y Axis Side to Side Straightness Error

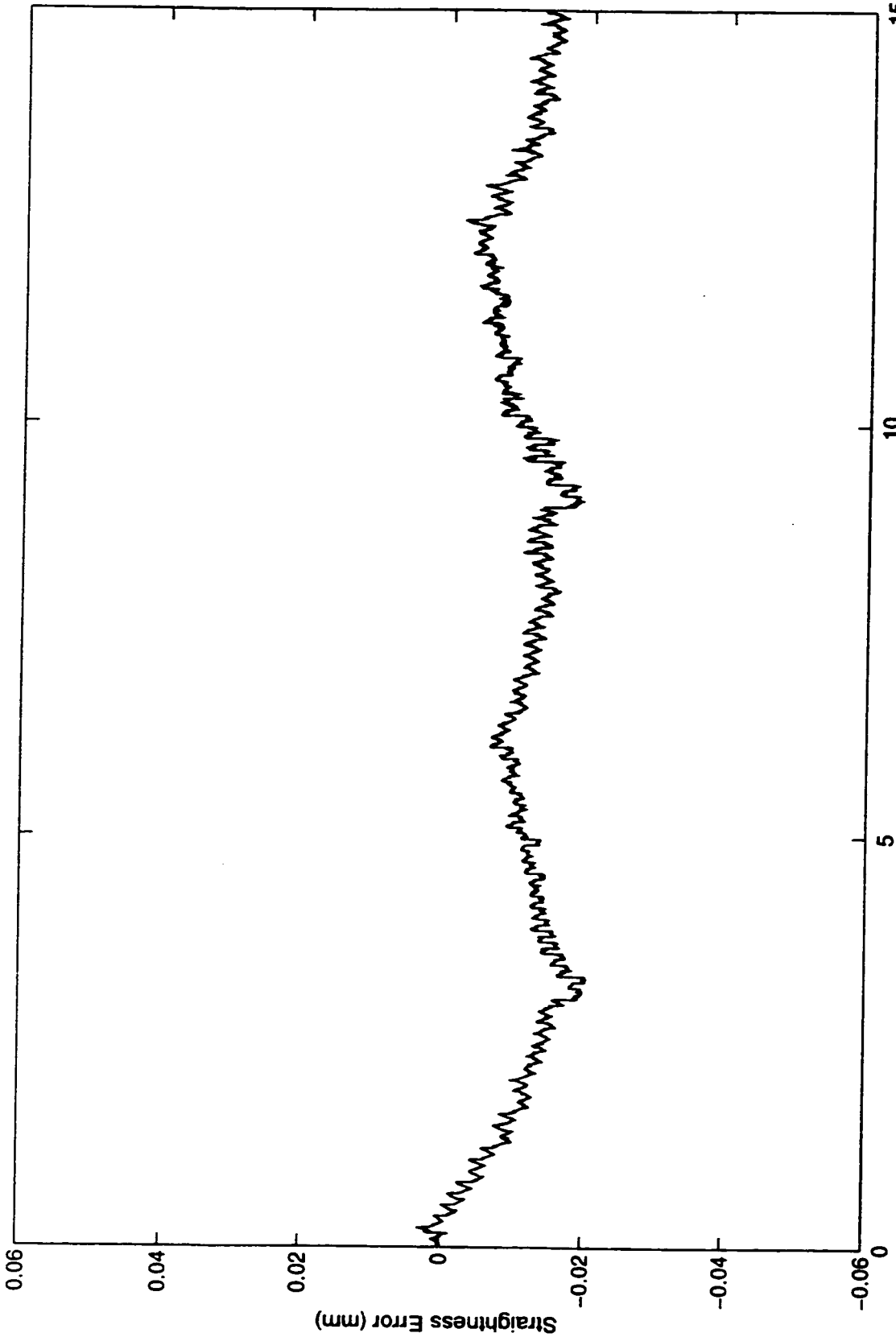

Figure D.9 Y Axis Up and Down Straightness Error

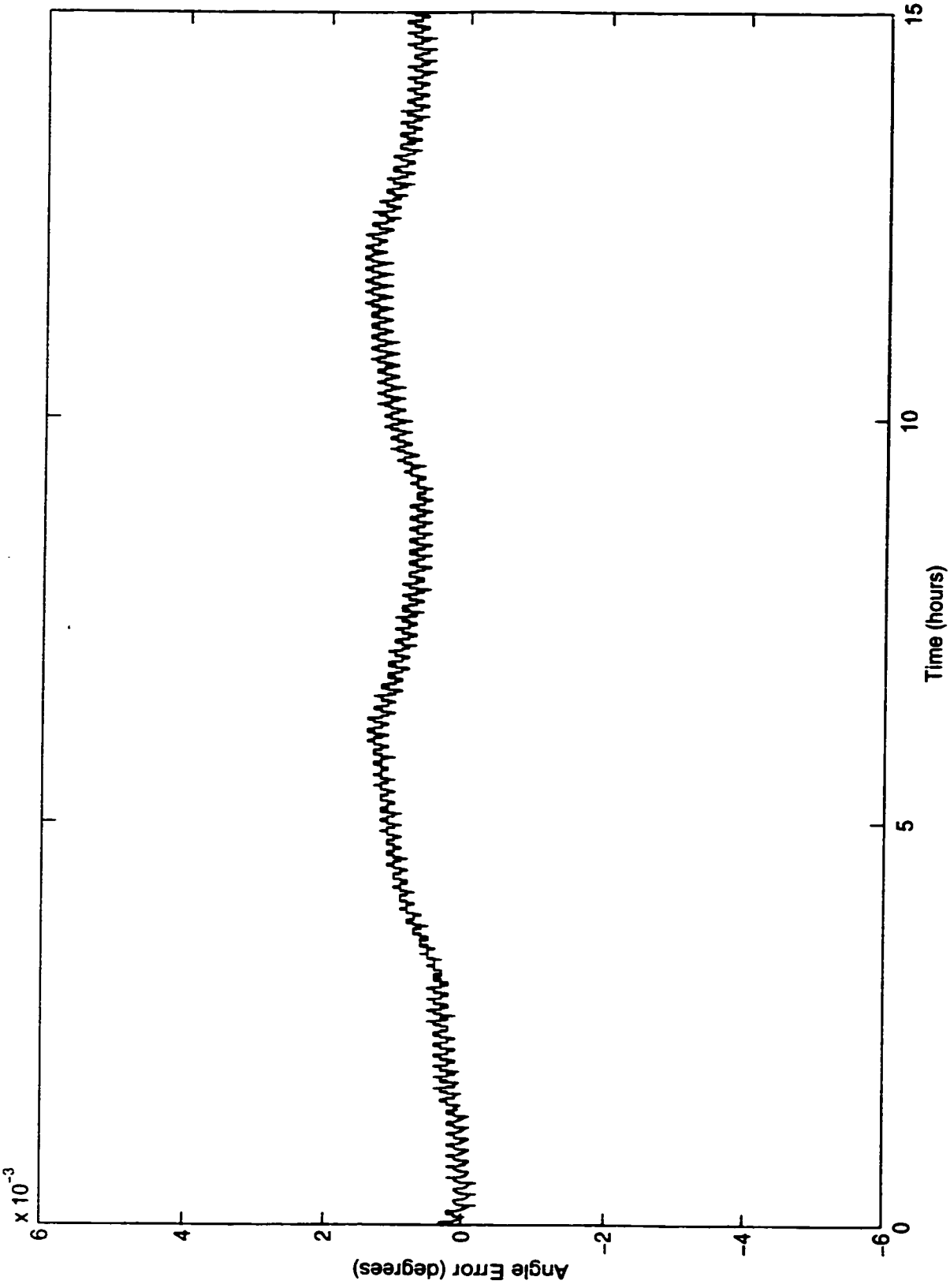

Figure D.10 Y Axis Pitch Angle Error

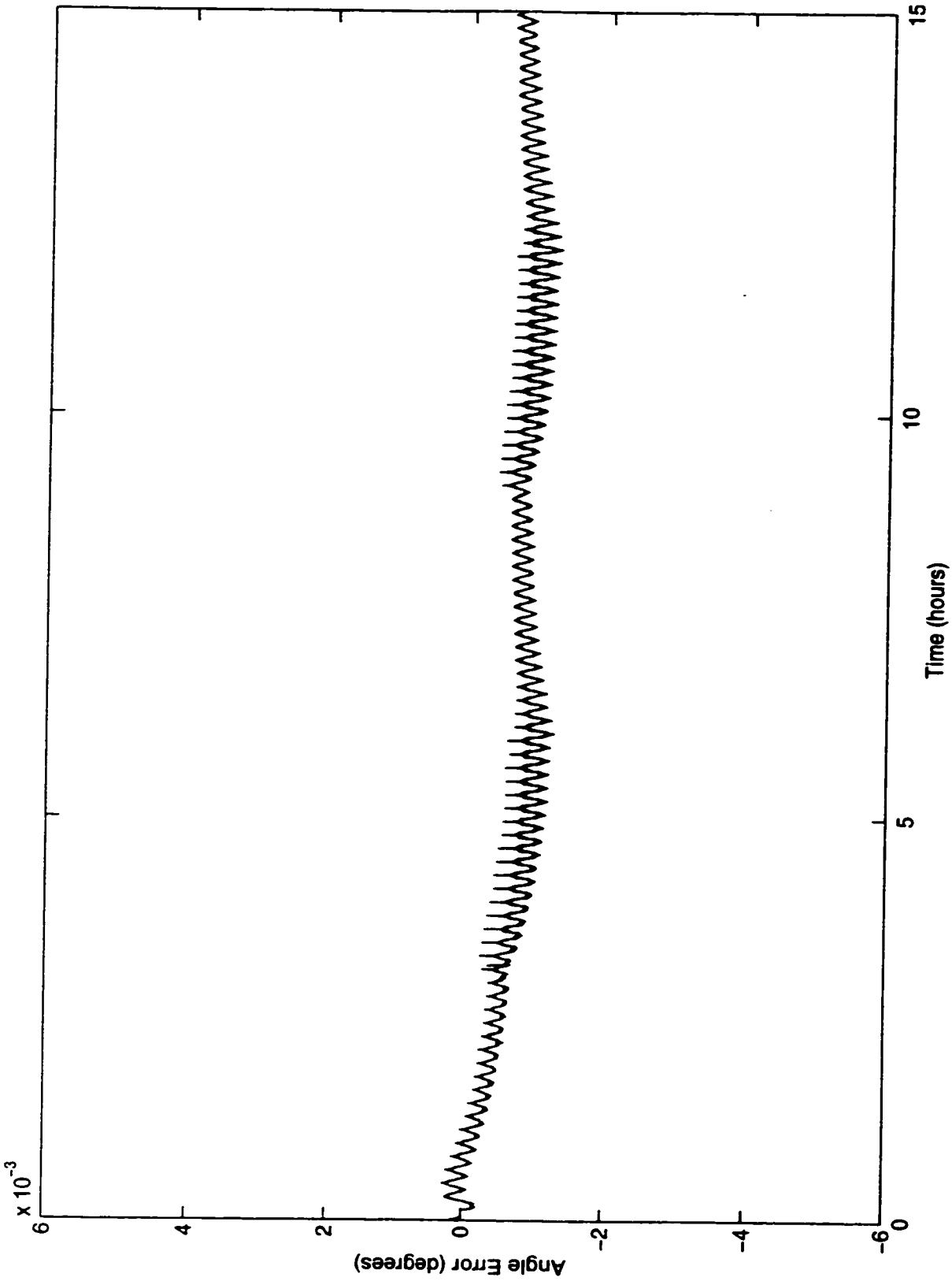

Figure D.11 Y Axis Roll Angle Error

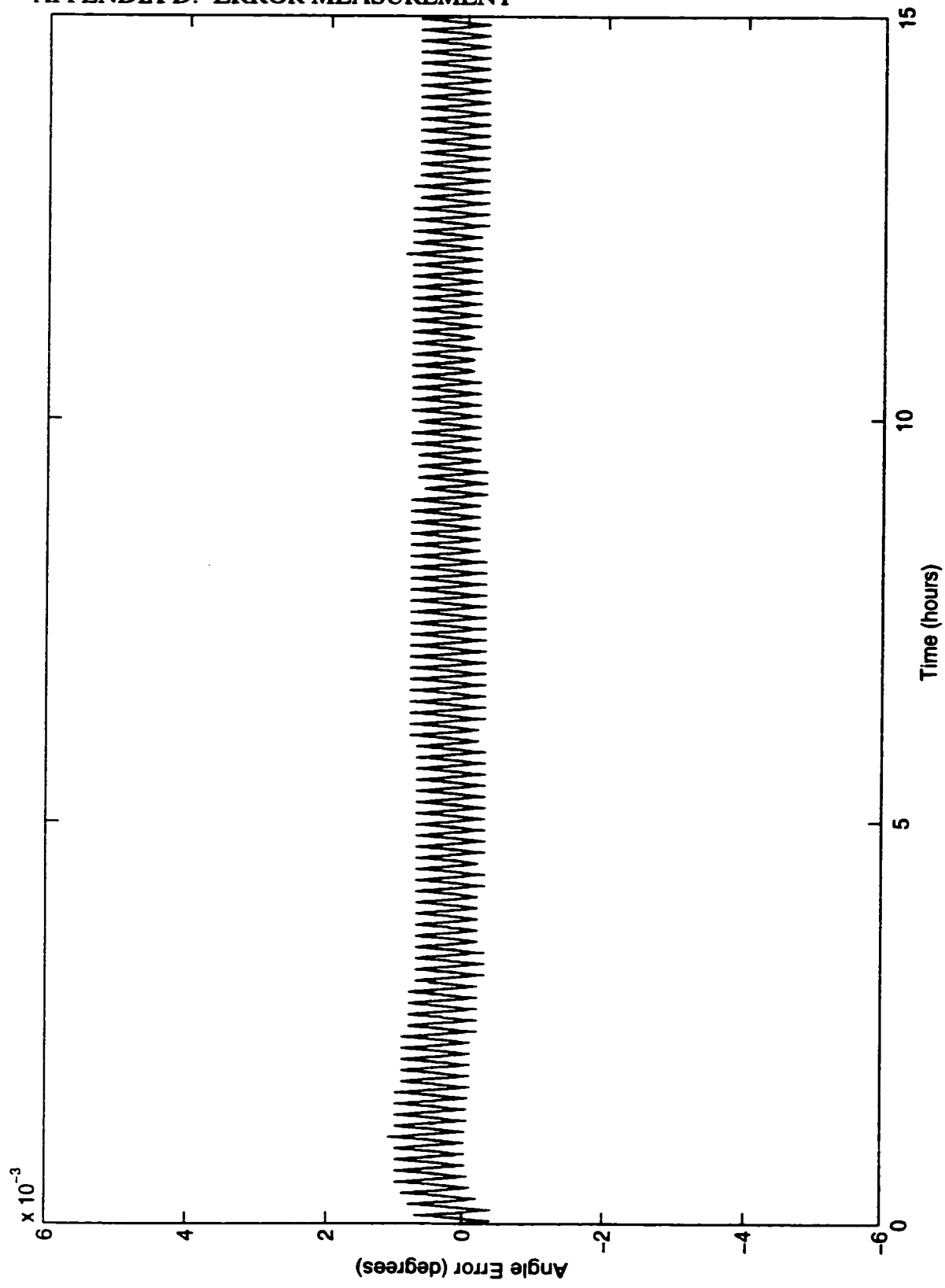

Figure D.12 Y Axis Yaw Angle Error

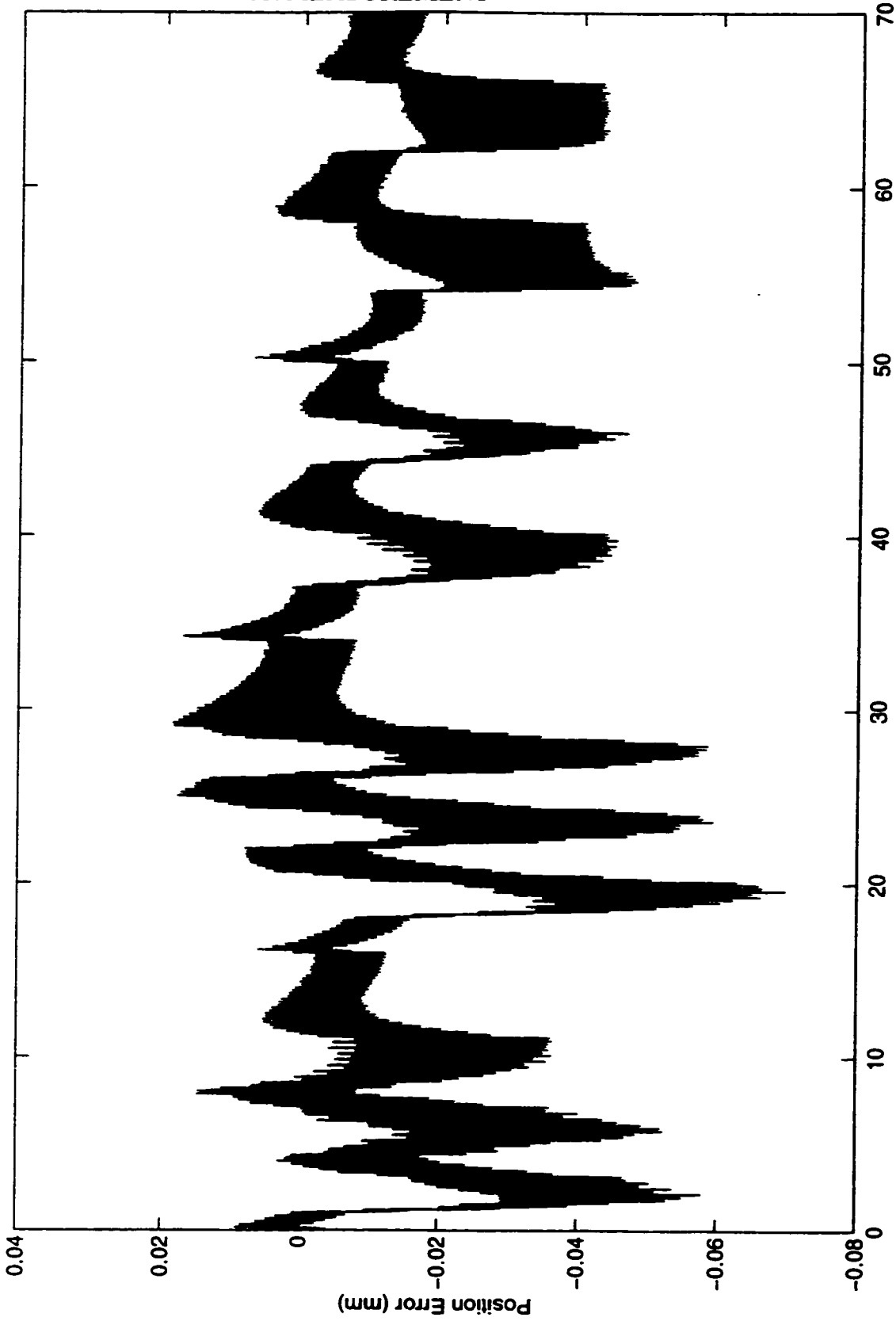

Figure D.13 Z Axis Position Error

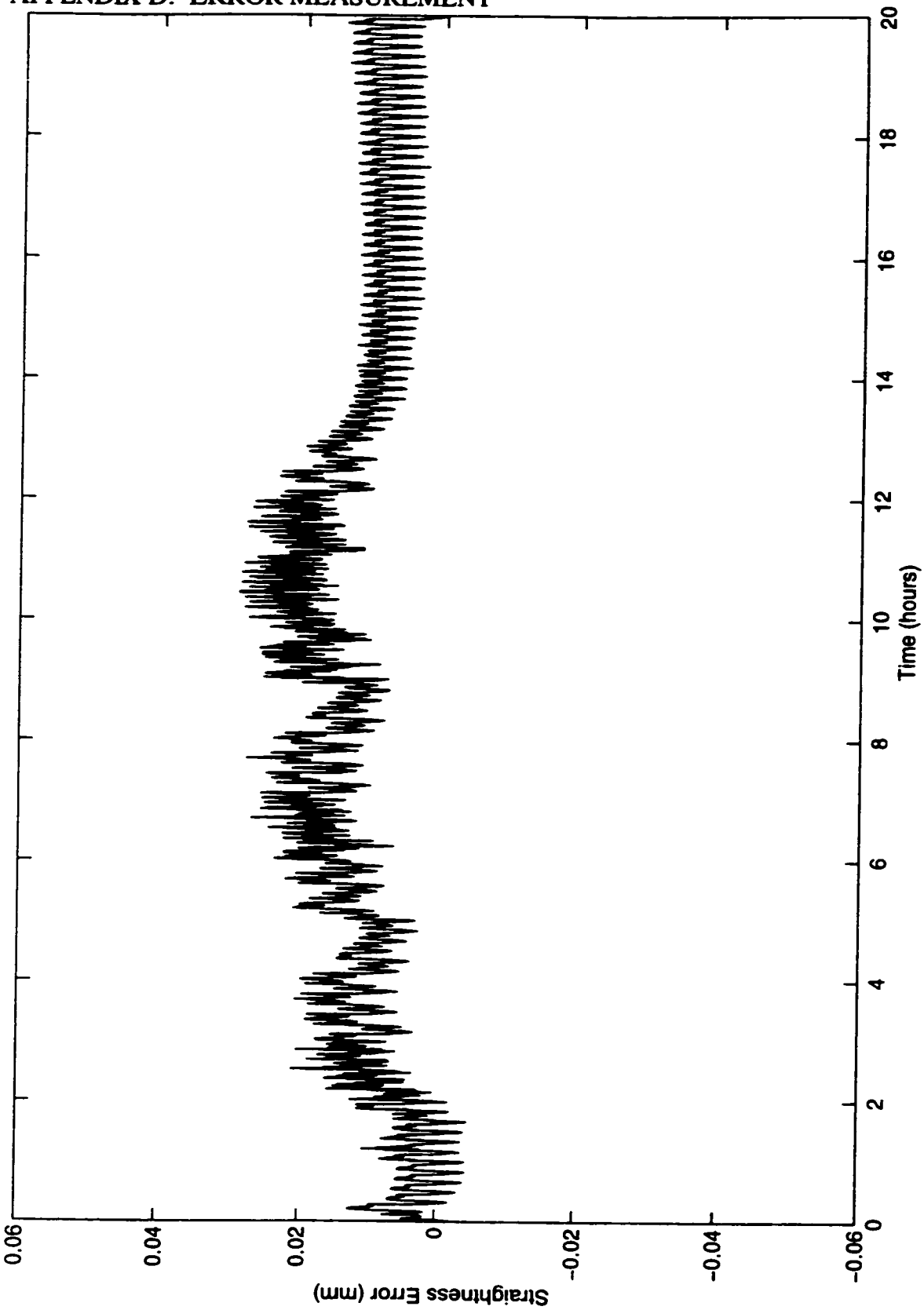

Figure D.14 Z Axis Side to Side Straightness Error

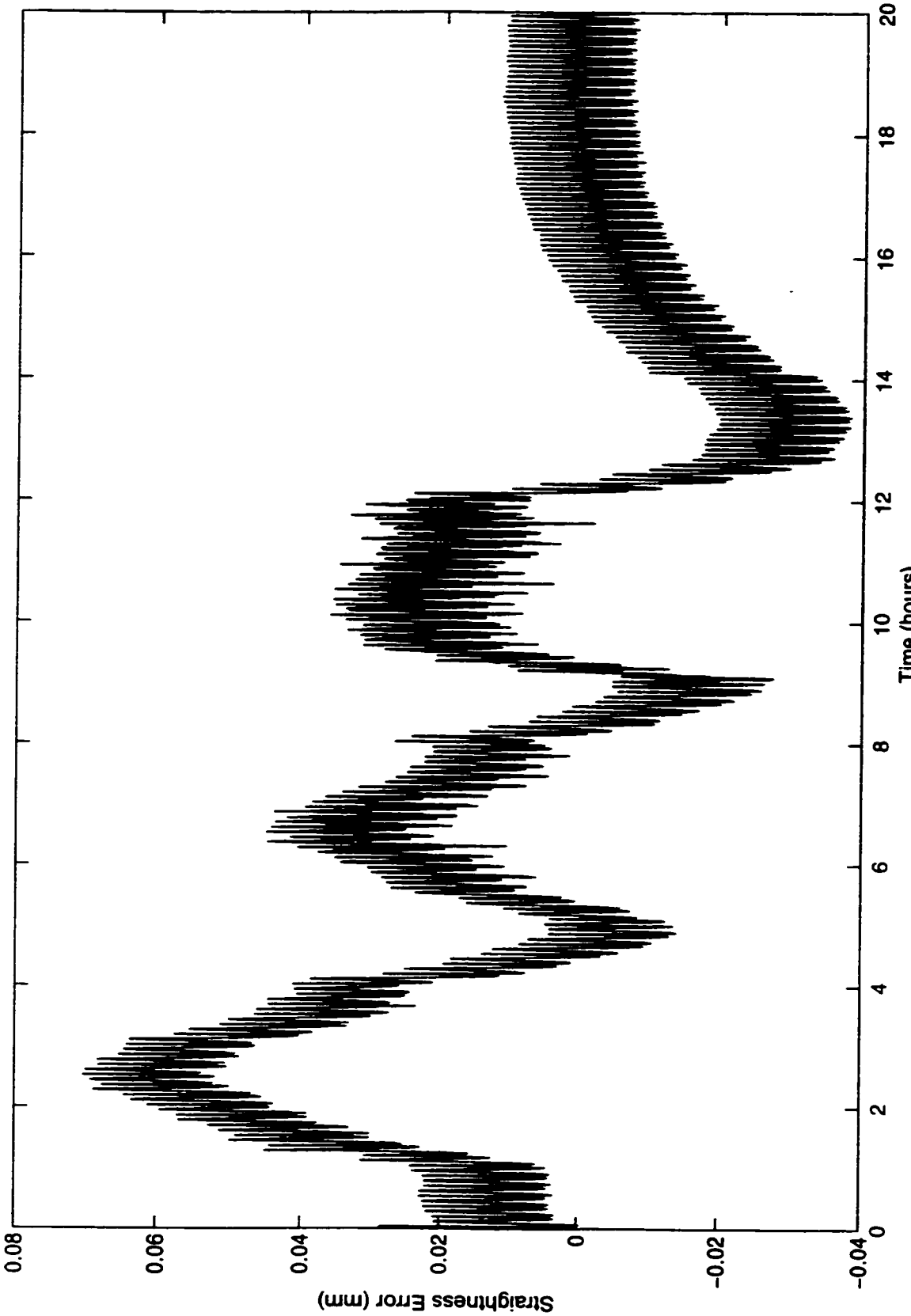

Figure D.15 Z Axis Back and Forth Straightness Error

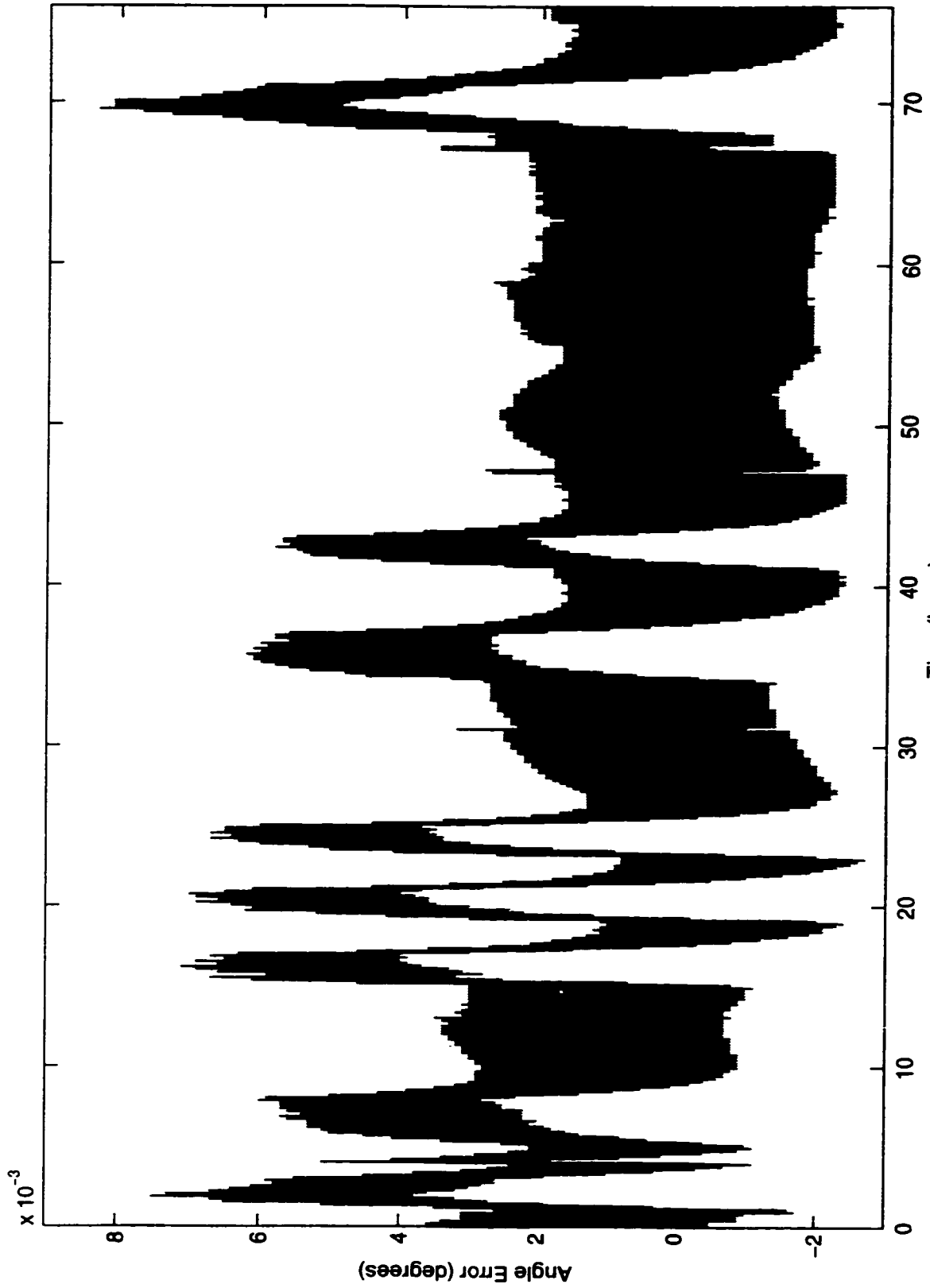

Figure D.16 Z Axis Pitch Angle Error

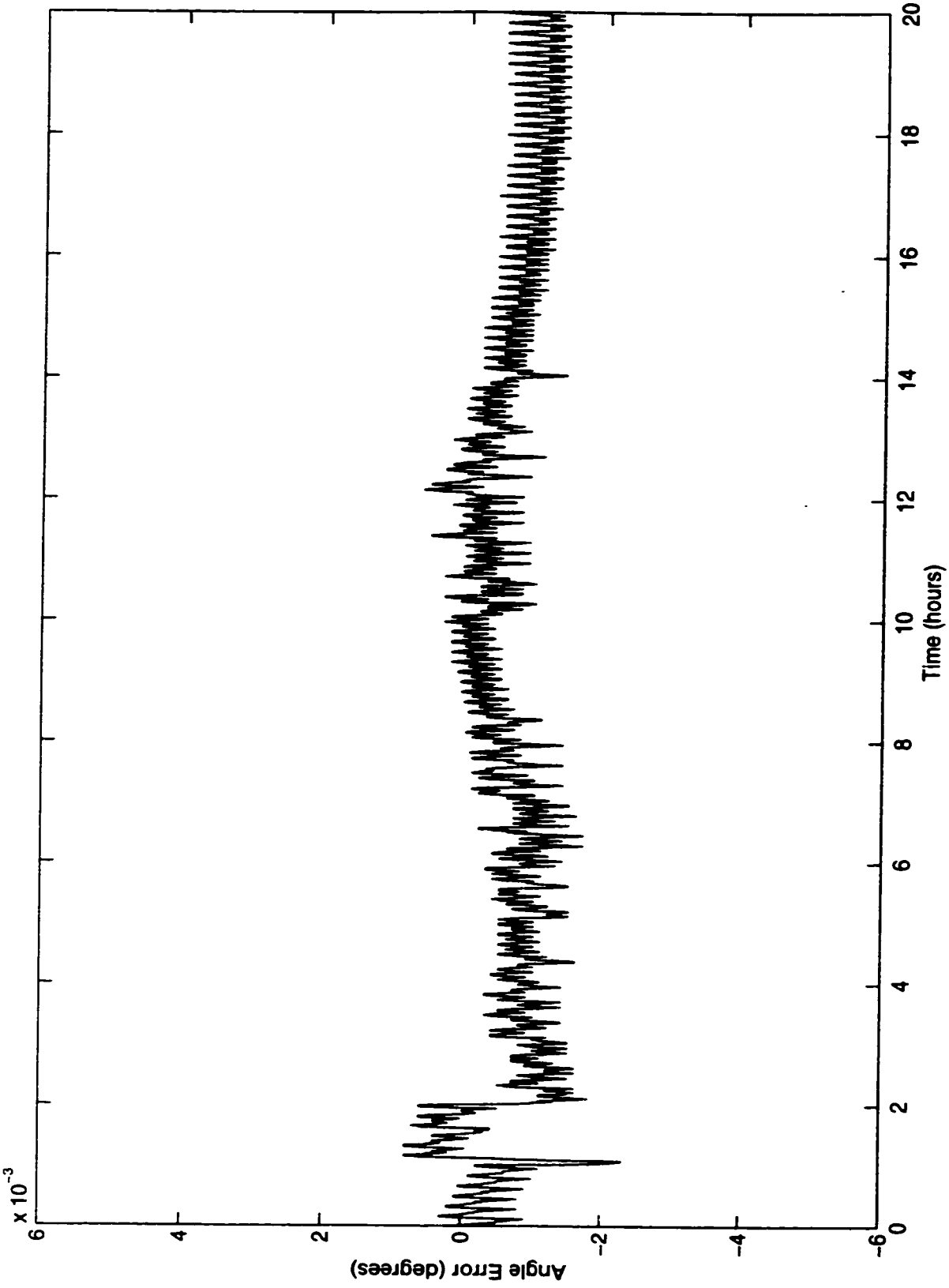

Figure D.17 Z Axis Yaw Angle Error

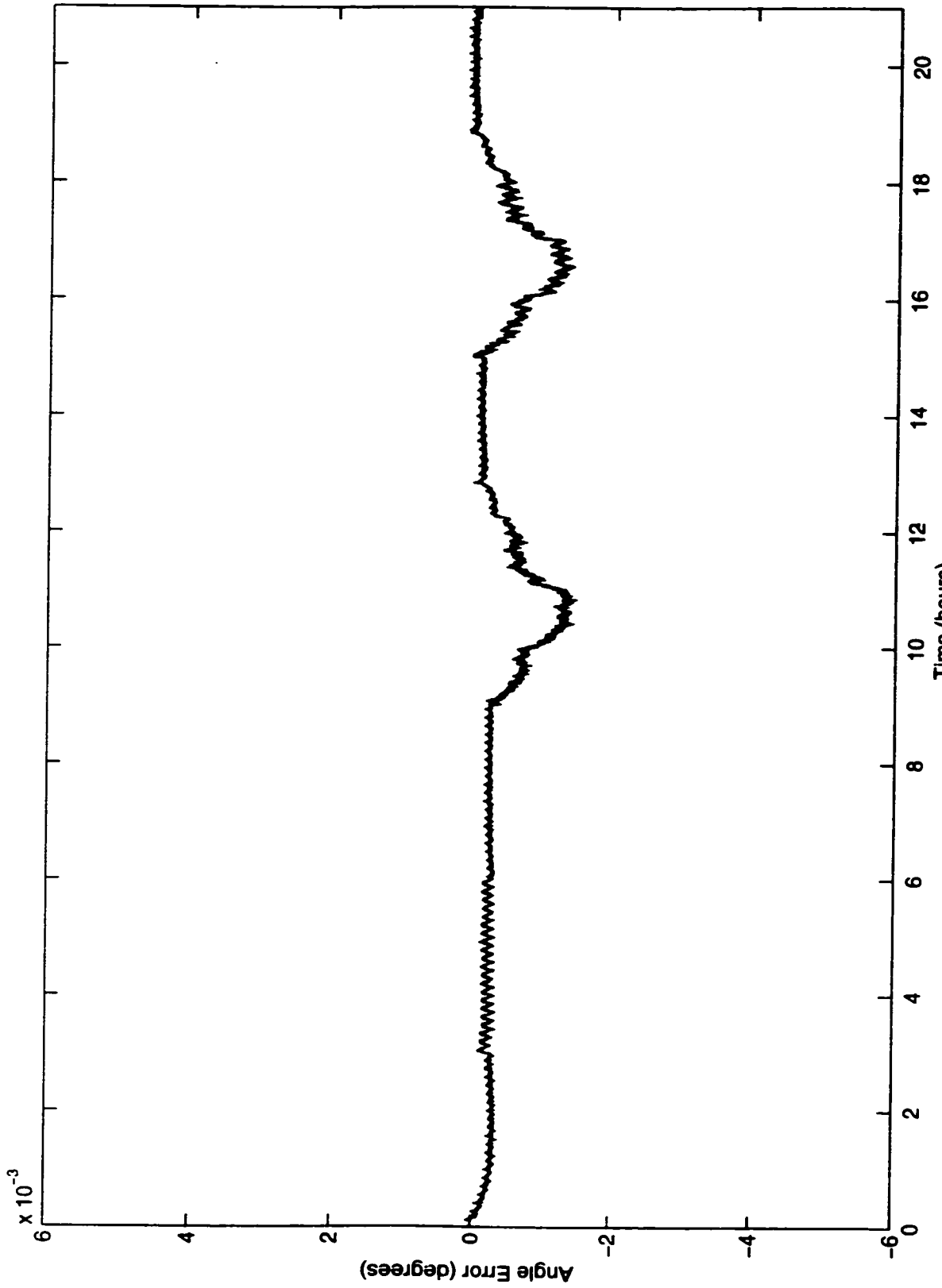

Figure D.18 Z Axis Roll Angle Error

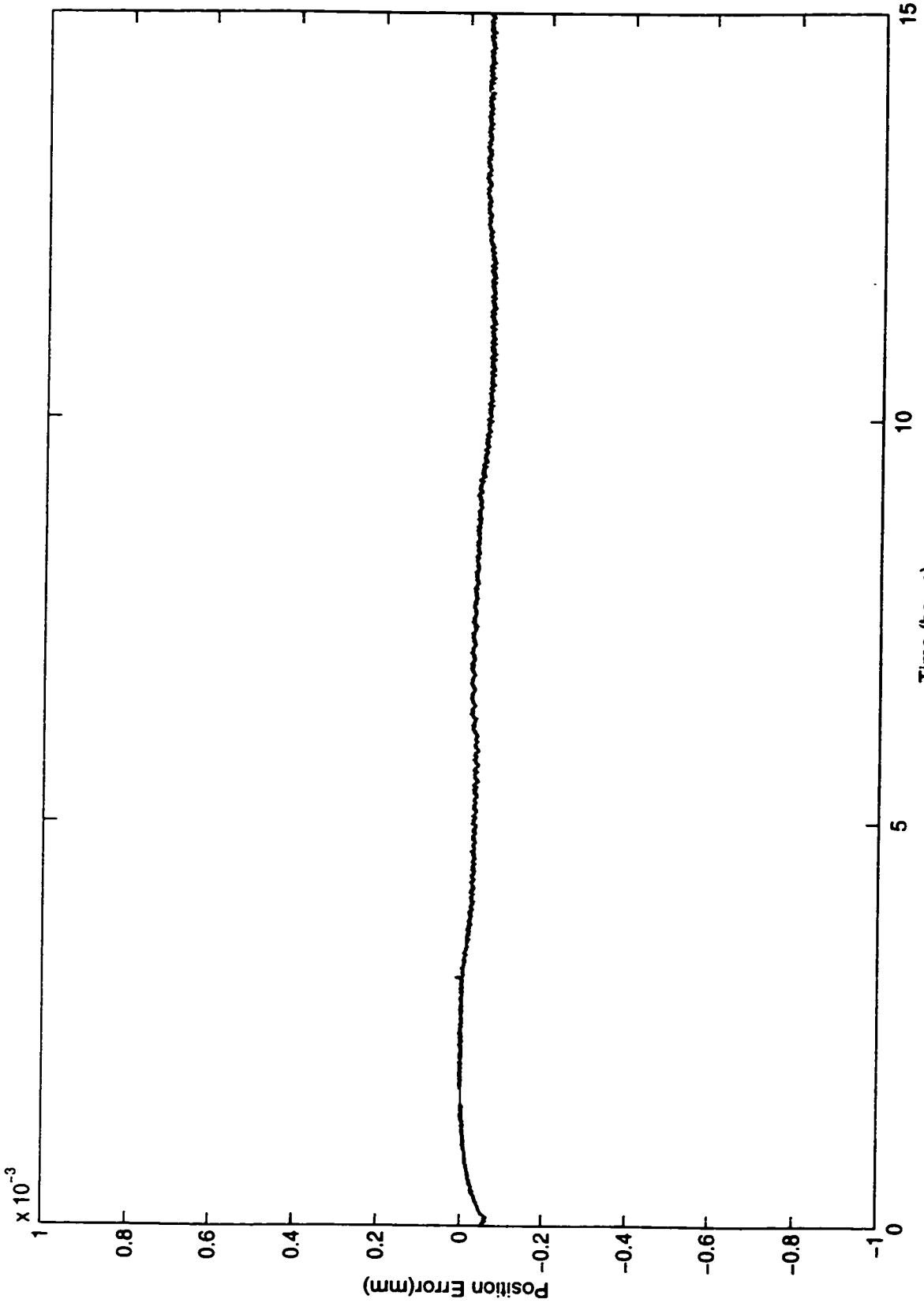

Figure D.19 A Axis X Centre of Rotation Motion

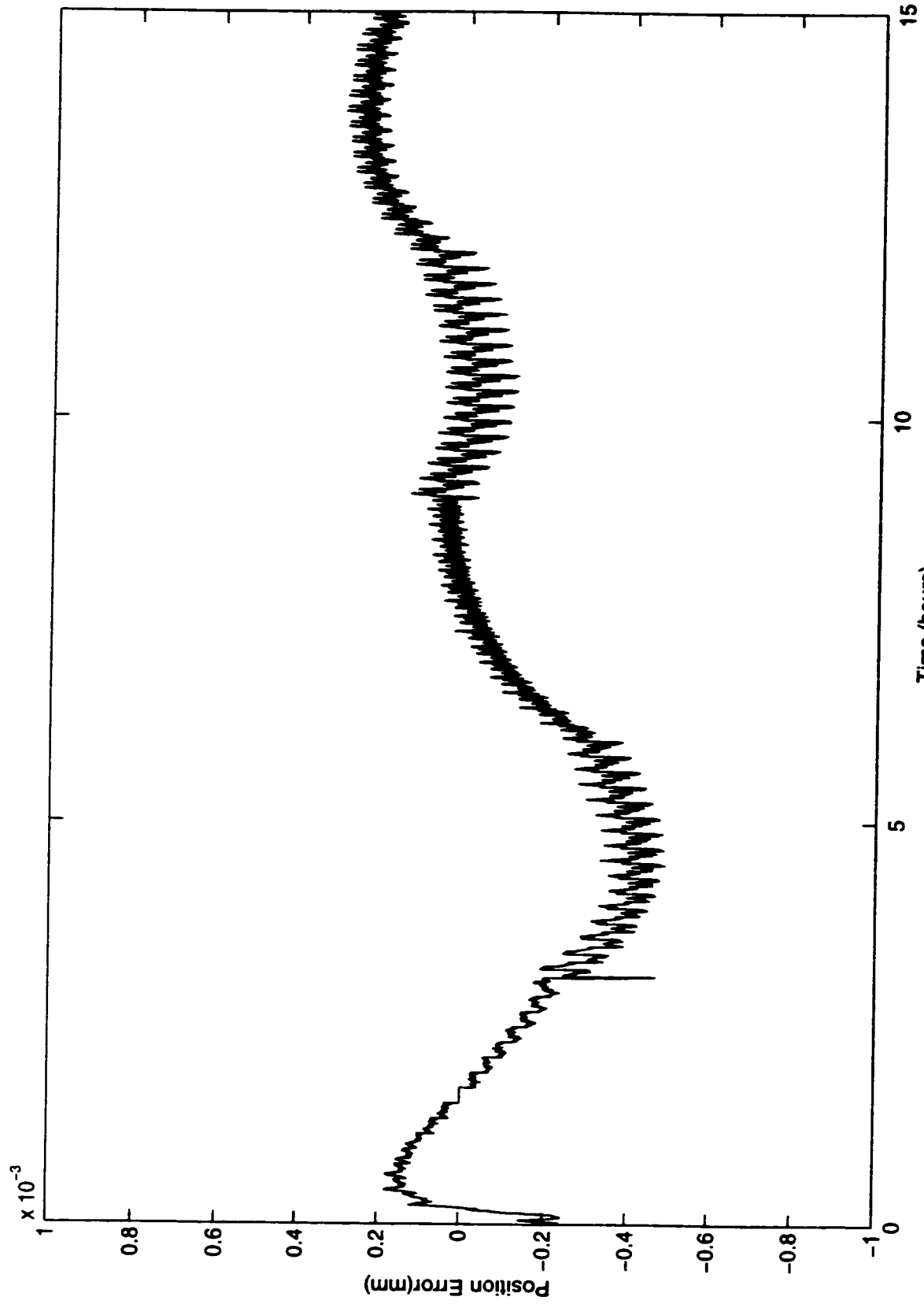

Figure D.20 A Axis Y Centre of Rotation Motion

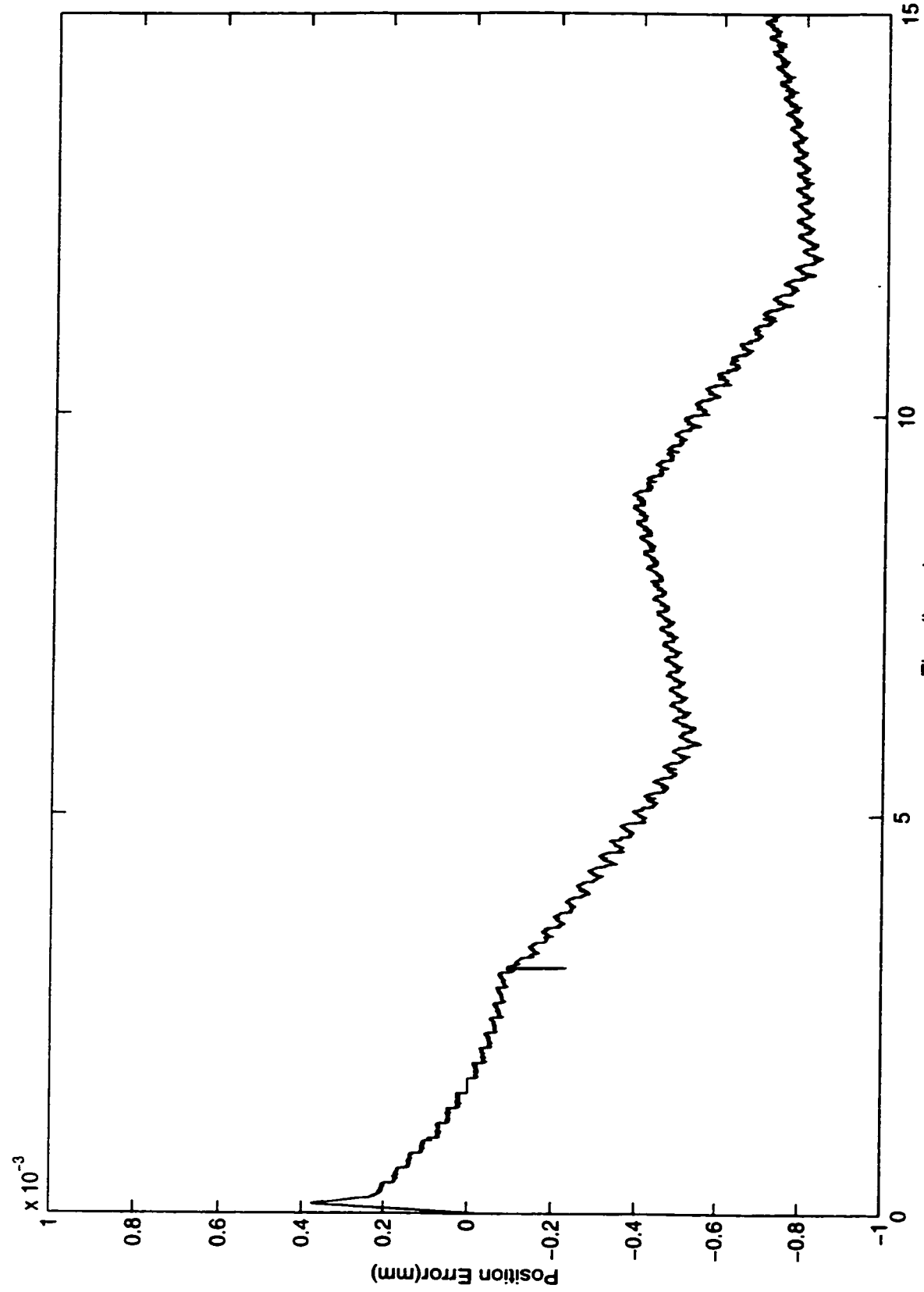

Figure D.21 A Axis Z Centre of Rotation Motion

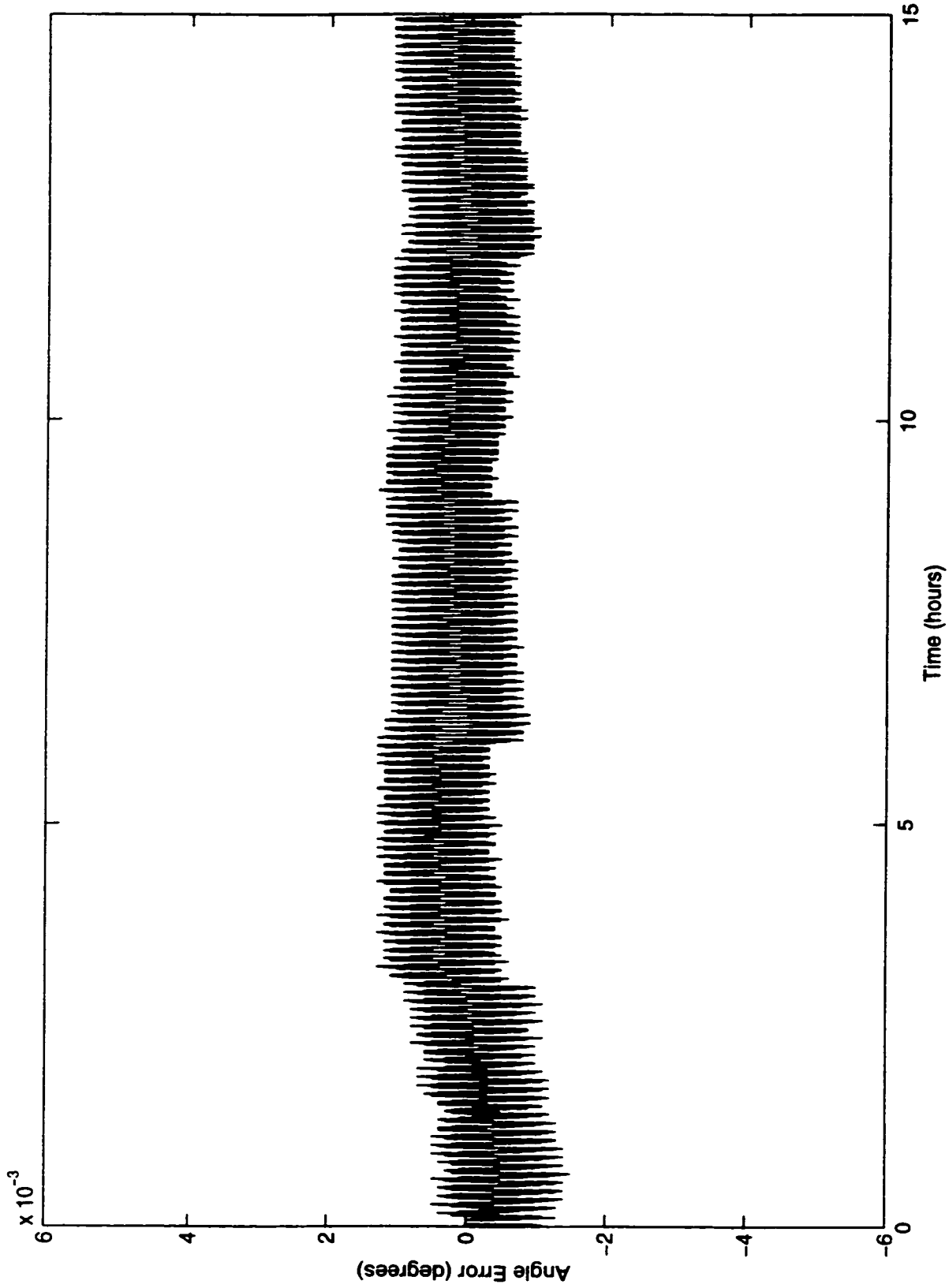

Figure D.22 A Axis Orientation Error

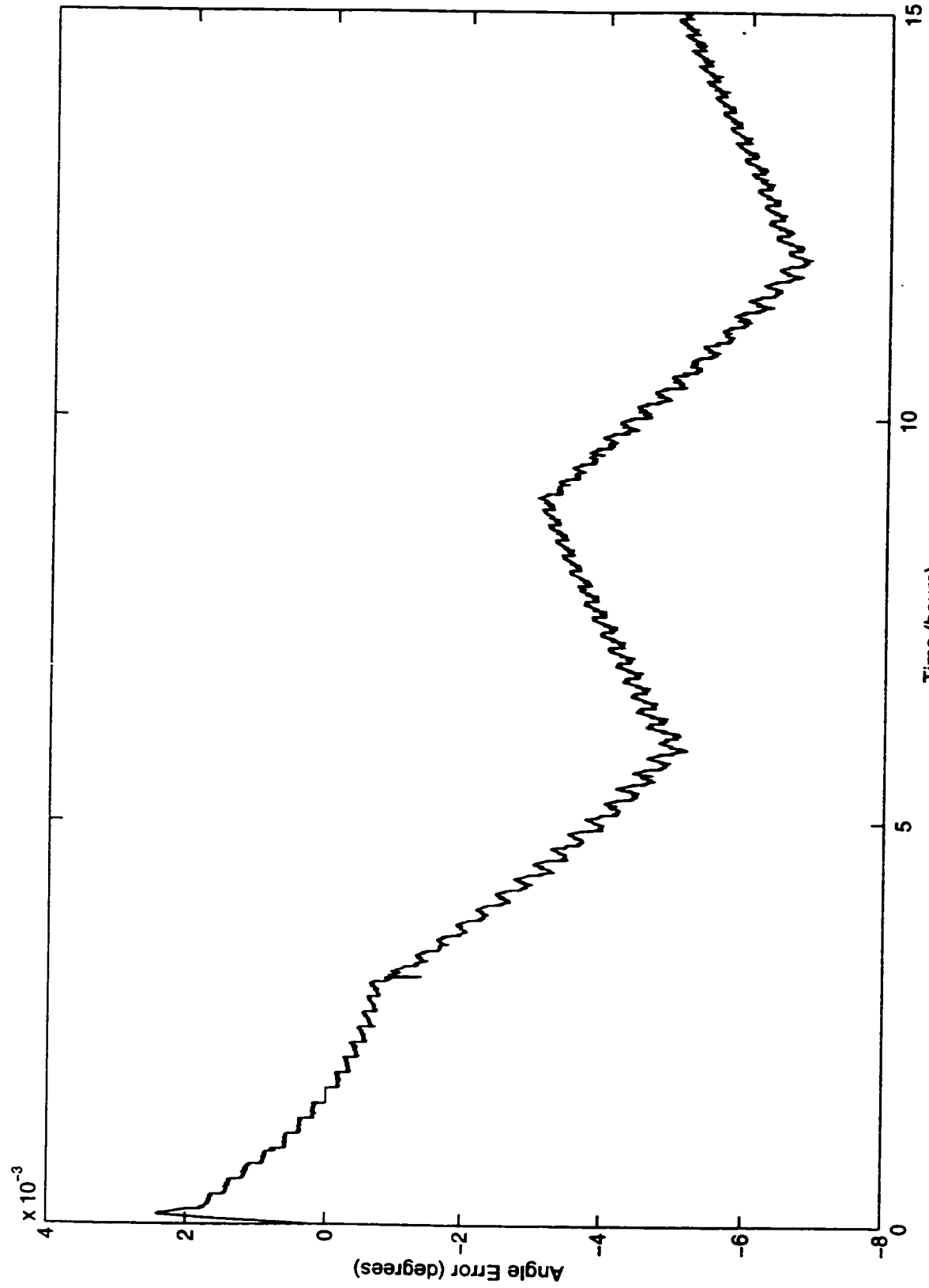

Figure D.23 A Axis θ_y Tilt Error

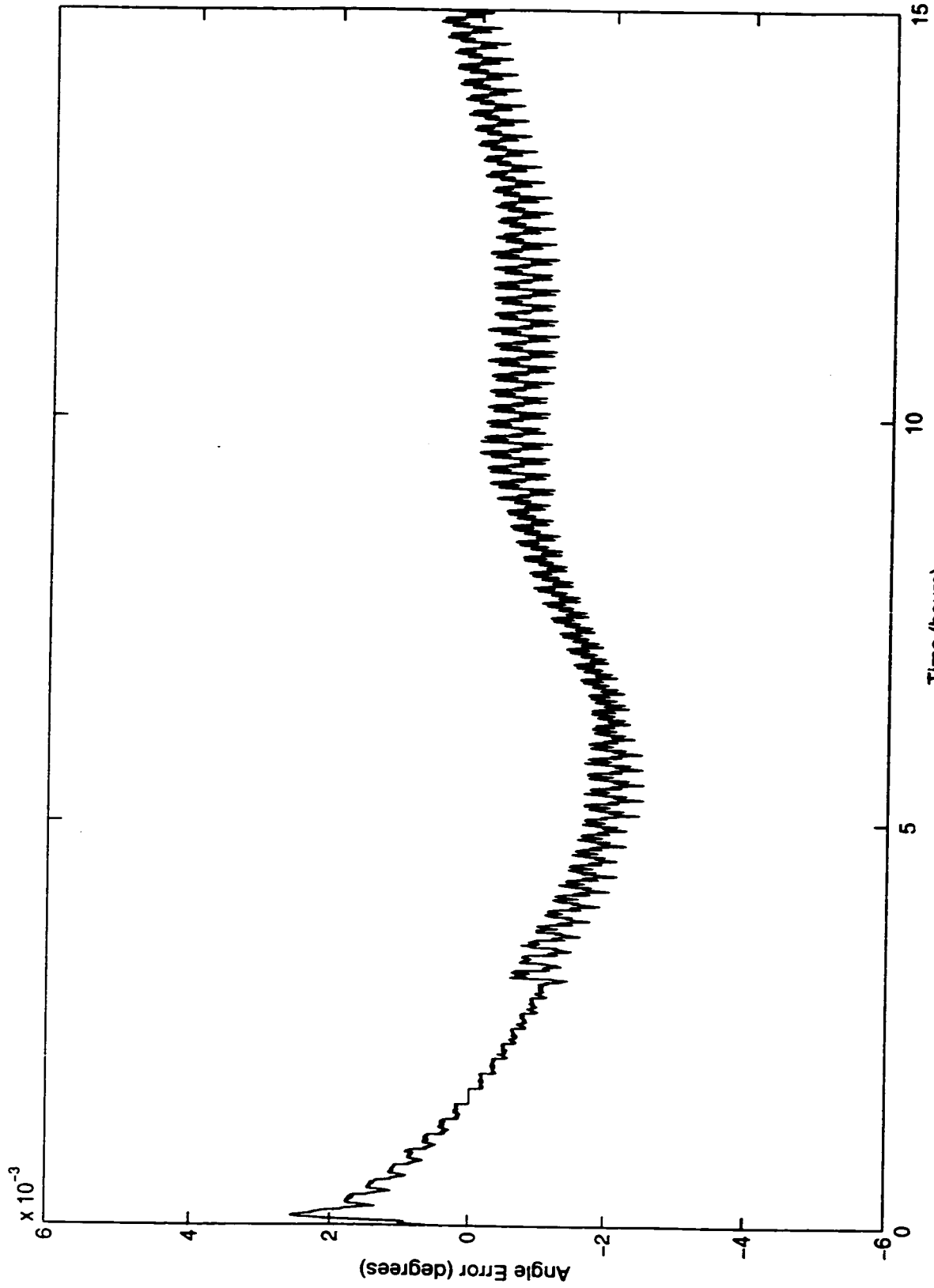

Figure D.24 A Axis θ_z Tilt Error

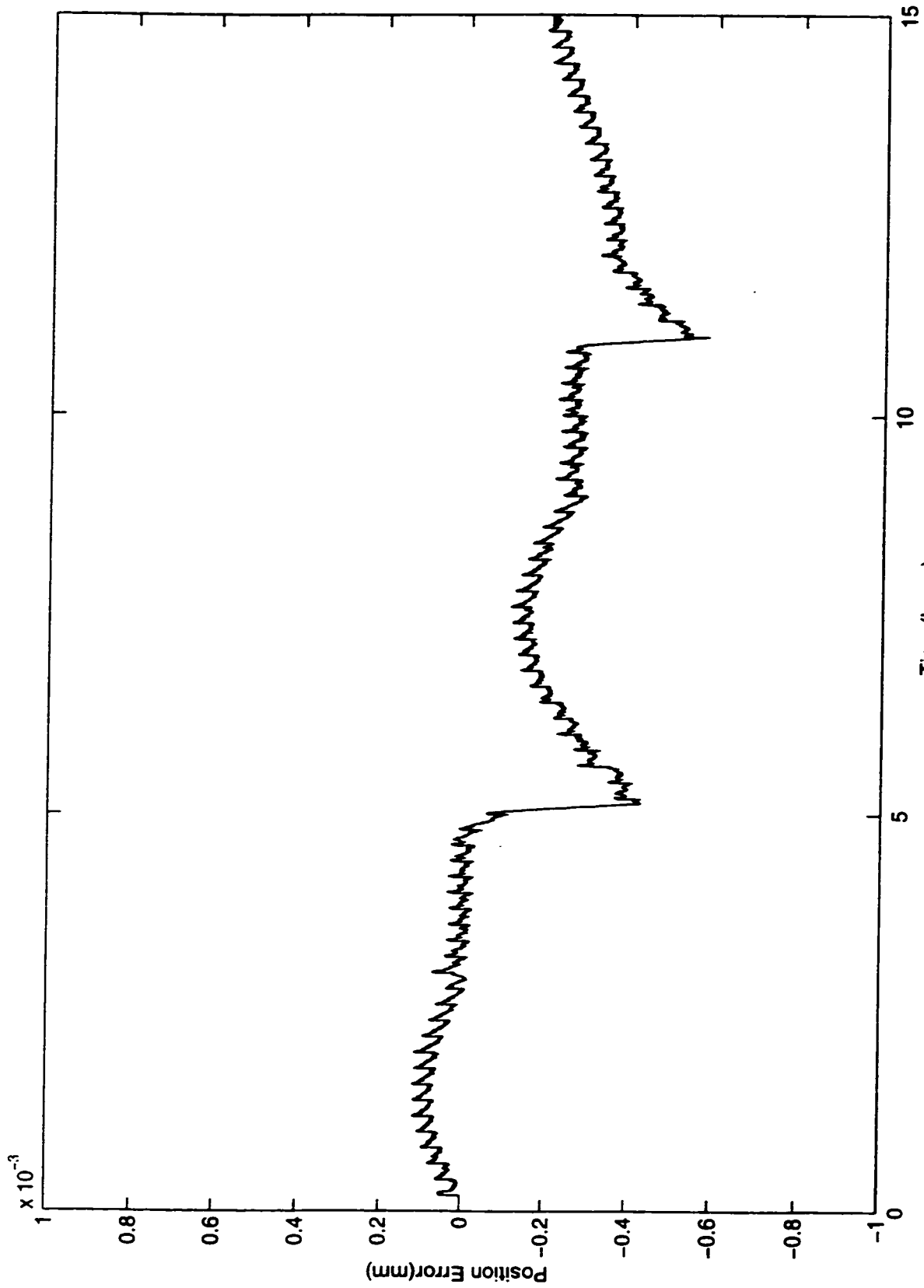

Figure D.25 B Axis X Centre of Rotation Motion

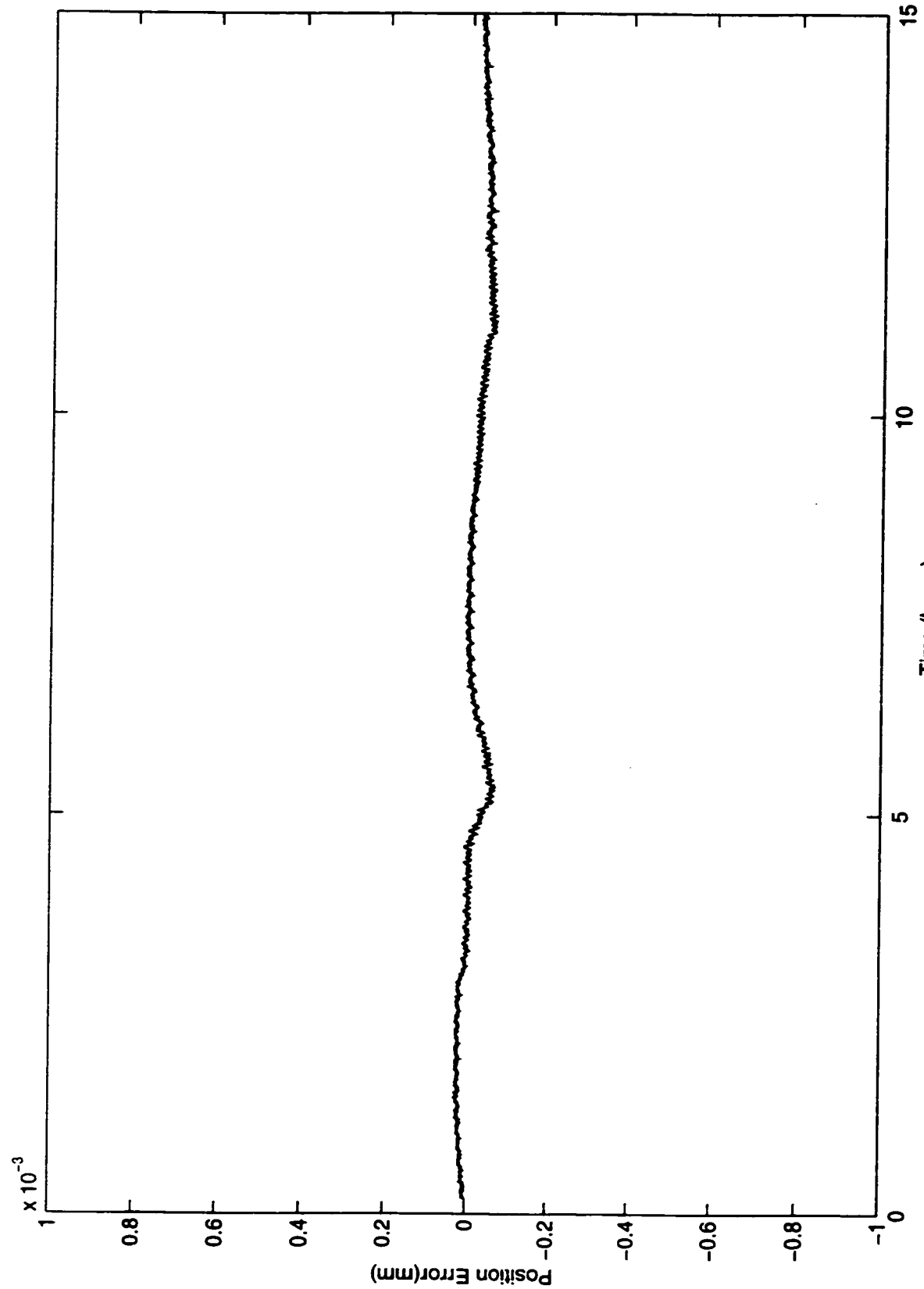

Figure D.26 B Axis Y Centre of Rotation Motion

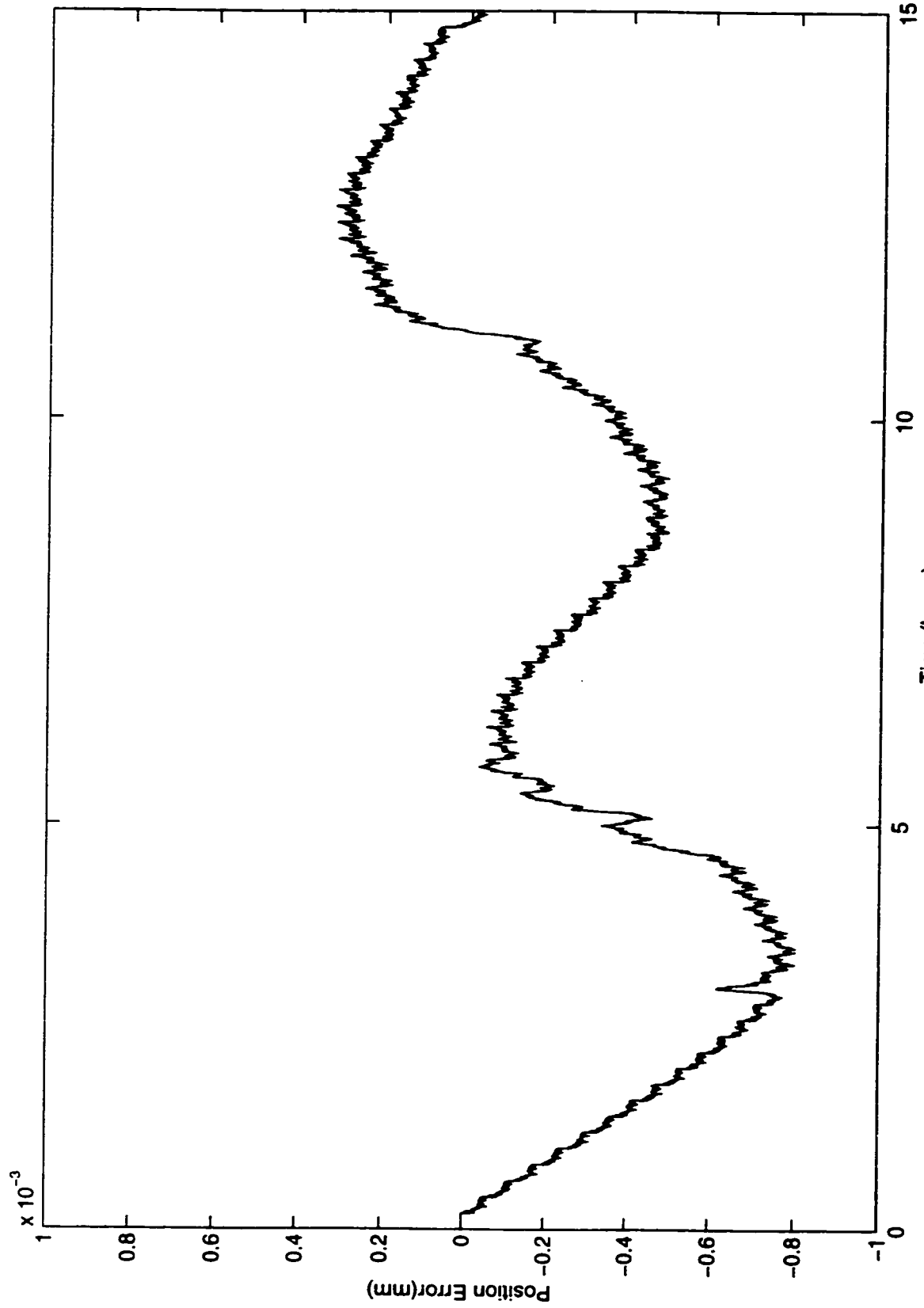

Figure D.27 B Axis Z Centre of Rotation Motion

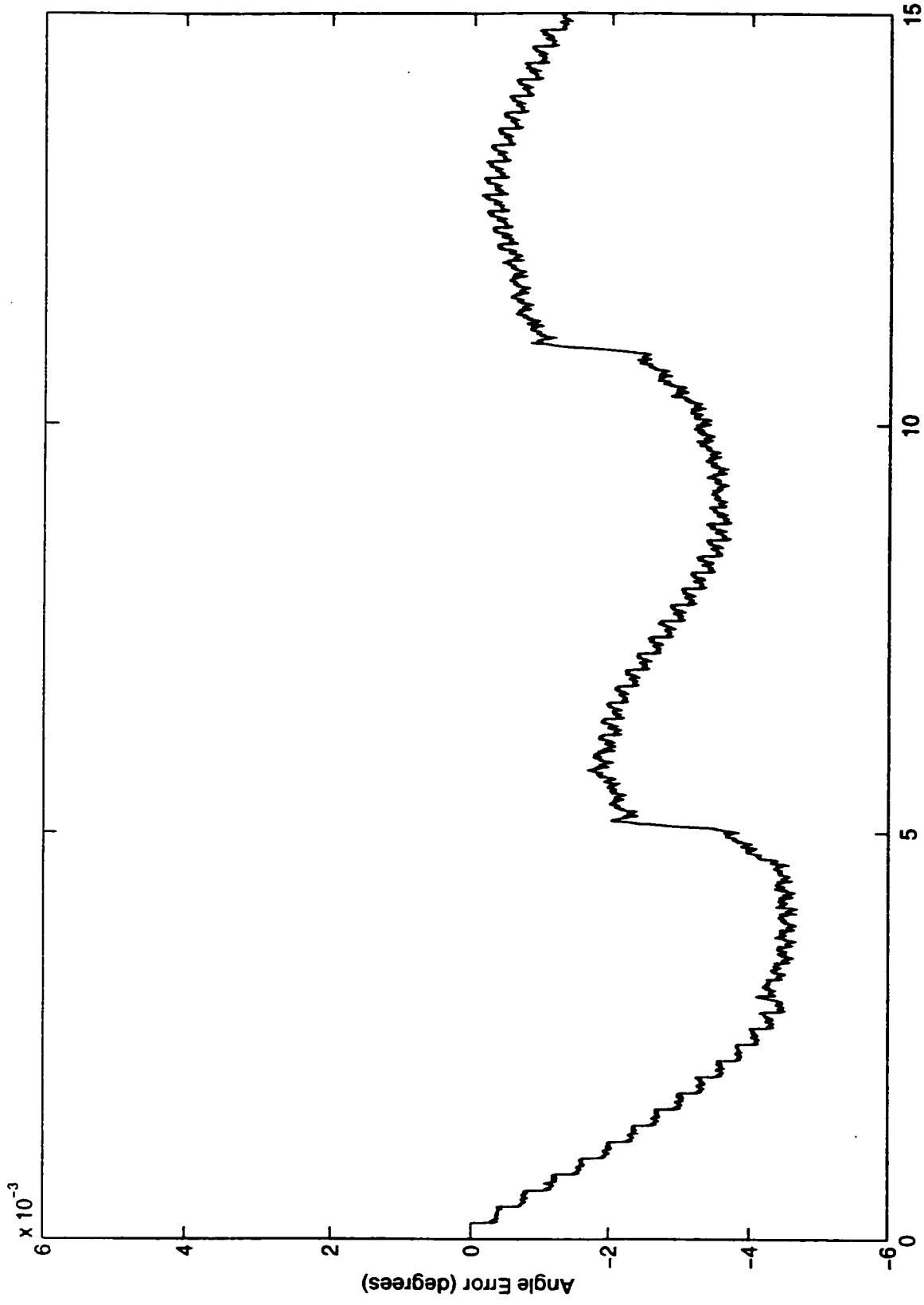

Figure D.28 B Axis θ_x Tilt Error

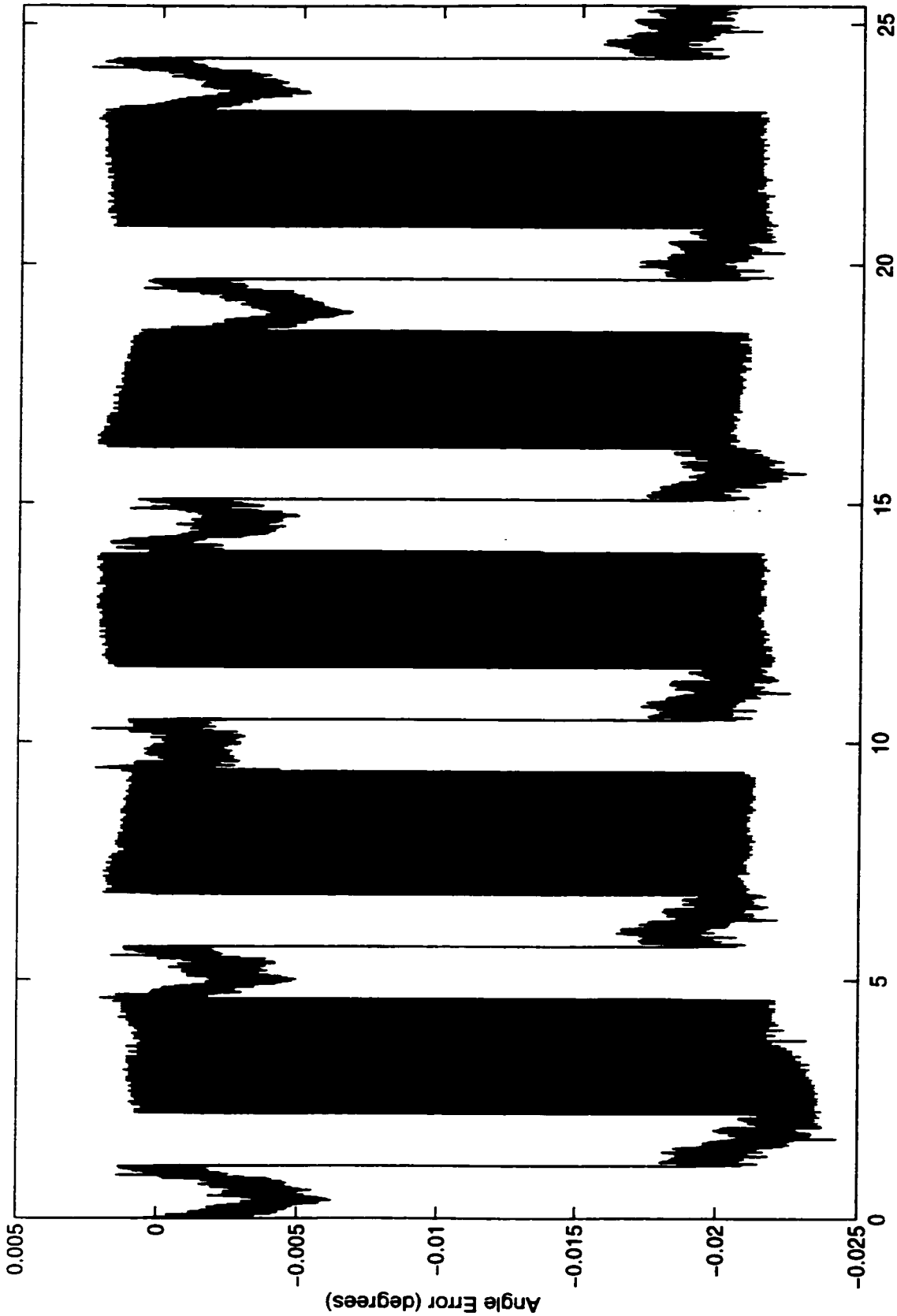

Figure D.29 B Axis Orientation Error

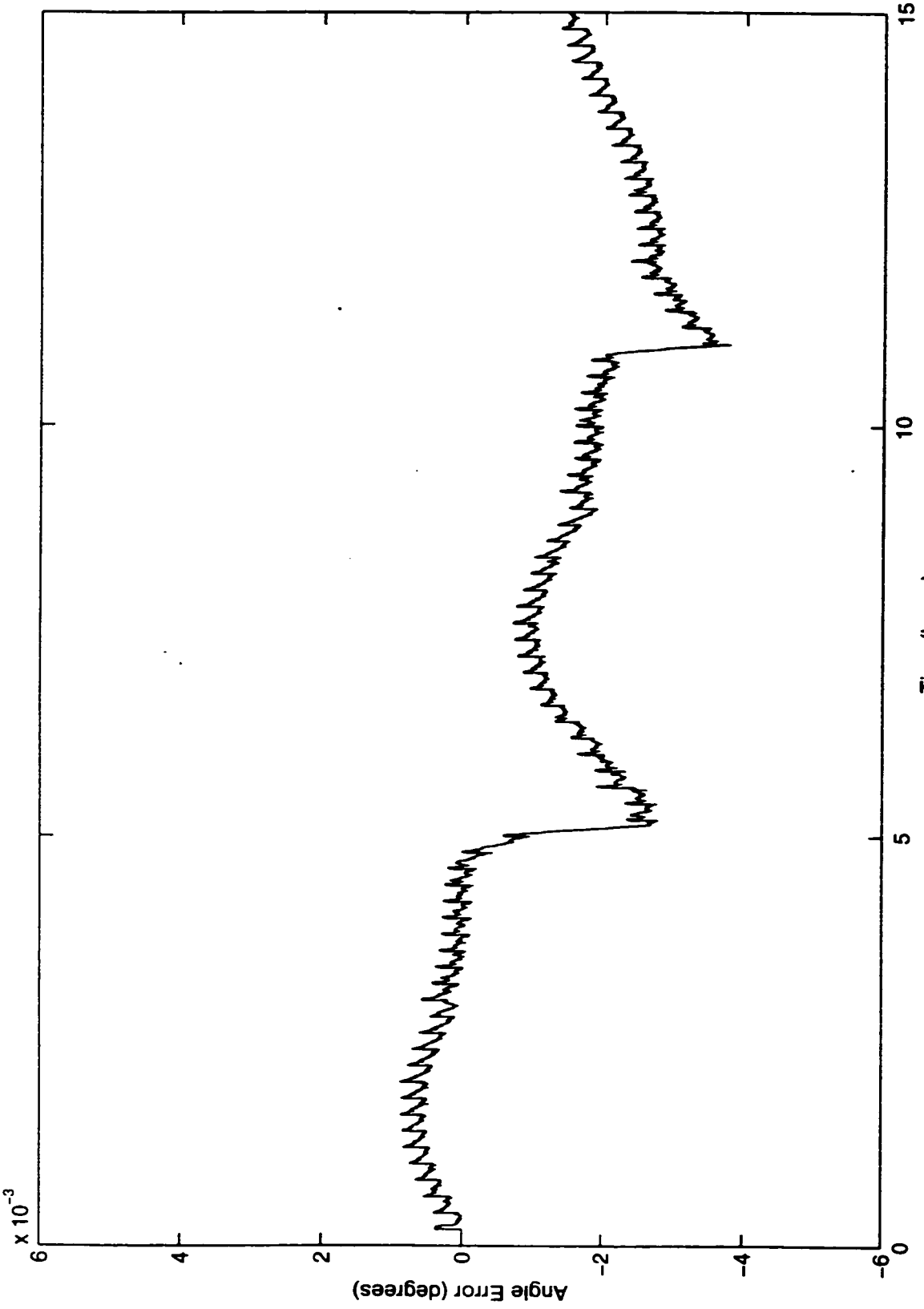

Figure D.30 B Axis θ_2 Tilt Error